Characterization of immune responses in the meninges

Dissertation

for the award of the degree

"Doctor rerum naturalium"

of the Georg-August-Universität Göttingen

within the doctoral program "Molecular Biology of Cells"

of the Georg-August University School of Science (GAUSS)

submitted by

Arianna Merlini

born in New York (U.S.A.)

Göttingen, 2021

Thesis committee

Prof. Dr. Alexander Flügel
Institute for Neuroimmunology and Multiple Sclerosis Research
University Medical Center Göttingen

Prof. Dr. Jochen Staiger
Center for Anatomy, Dept. of Neuroanatomy
University Medical Center Göttingen

Prof. Dr. Wolfgang Brück
Institute of Neuropathology
University Medical Center Göttingen

Members of the Examination Board

Referee: Prof. Dr. Alexander Flügel
Institute for Neuroimmunology and Multiple Sclerosis Research
University Medical Center Göttingen

2nd Referee: Prof. Dr. Jochen Staiger
Center for Anatomy, Dept. of Neuroanatomy
University Medical Center Göttingen

Further Members of the Examination Board

Prof. Dr. Wolfgang Brück
Institute of Neuropathology
University Medical Center Göttingen

Prof. Dr. Hannelore Ehrenreich
Clinical Neuroscience
Max Planck Institute of Experimental Medicine

Prof. Dr. Holger Reichardt
Dept. of Cellular and Molecular Immunology
University Medical Center Göttingen

Prof. Dr. Martin S. Weber
Institute of Neuropathology
University Medical Center Göttingen

Date of oral examination: 02.07.2021

TABLE OF CONTENTS

LIST OF FIGURES

LIST OF TABLES

LIST OF ABBREVIATIONS

AAV(s)	Adeno-associated virus(es)
AB	Arachnoid barrier layer
AG	Arachnoid granulations
APCs	Antigen presenting cells
AT	Arachnoid trabecula
BBB	Blood-brain barrier
brDura	Brain dura
brLepto	Brain leptomeninges
brPar	Brain parenchyma
bSYN/SYN	Beta-synuclein
CCL*x*	C-C chemokine ligand *x*
CCR*x*	C-C chemokine receptor *x*
cDNA	complementary DNA
CD*x*	Cluster of differentiation *x*
CFA	Complete Freund's Adjuvant
Cldn5	Claudin-5
CLN	Cervical lymph nodes
CNS	Central nervous system
COS	Confluence of sinuses
CSF	Cerebrospinal fluid
CXCL*x*	C-X-C chemokine ligand *x*
CXCR*x*	C-X-C chemokine receptor *x*
DB	Dura border layer
dcLNs	Deep cervical lymph nodes
EAE	Experimental autoimmune encephalomyelitis
EH	Eagle's Hepes Medium
eGFP	Enhanced green fluorescent protein
FACS	Fluorescence activated cell sorting
FCS	Fetal calf serum
FM	Freezing medium
GPEs	GP+E86 packaging cell
h	Hours
i.c.v.	Intracerebroventricular
i.t.	Intrathecal
i.v.	Intravenous
ICAM-1	Intercellular adhesion molecule-1
IFNγ	Interferon γ
IL-*x*(R)	Interleukin-*x* (Receptor)
ingLNs	Inguinal lymph nodes
ISF	Interstitial fluid
KDa	Kilodalton
LFA-1	Lymphocyte function-associated antigen-1

min	Minutes
MBP	Myelin basic protein
MFI	Median fluorescence intensity
MHCII	Major histocompatibility complex II
MOG	Myelin oligodendrocyte glycoprotein
MS	Multiple Sclerosis
n	number of animals/biological replicates
NFAT	Nuclear factor of activated T cells
NGS	Next-generation sequencing
NL	Nasal lymphatics
Ocln	Occludin
OVA	Ovalbumin
p.t.	Post-transfer
PBS	Phosphate-buffered saline
PLP	Proteolipid Protein
PSGL-1	P-selectin glycoprotein ligand-1
PSS	Petrosquamous sinus
qPCR	Quantitative polymerase chain reaction
RM	Re-stimulation medium
SA	Subarachnoid space
SD	Standard deviation
Sele	E-selectin
Selp	P-selectin
SEM	Standard error of mean
SSS	Superior sagittal sinus
TCGF	T cell growth factor medium
TM	Thawing medium
TCM	T cell medium
TCR	T cell receptor
TG	Transgenic
T_Hx cell	T helper *x* cell
TNFα	Tumor necrosis factor α
TPLSM	Two-photon laser scanning microscopy
TR	Transition zone
TS	Transverse sinus
VCAM-1	Vascular Cell Adhesion Molecule-1
VEGF-C/D	Vascular endothelial growth factor C/D
VEGFR-3	Vascular endothelial growth factor receptor 3
VLA-4	Very Late Antigen -4
WT	Wild type

x= varying numbers

SUMMARY

Multiple sclerosis (MS) is a chronic inflammatory disease of the central nervous system (CNS), which is characterized by plaque-like demyelination in both white and grey matter and diffuse neurodegeneration. A T cell-driven autoimmune response against CNS antigens is the initiating event in the MS pathogenesis, as demonstrated in the animal model of MS, experimental autoimmune encephalomyelitis (EAE). In EAE, CNS-reactive T cells reach the CNS through pial vessels and accumulate in the leptomeninges, from where they invade the CNS parenchyma. Also in human MS, the leptomeninges were shown to be a site of inflammation, and their involvement correlates with disease severity.

The role of the leptomeninges as a crucial checkpoint for the initiation of the disease has been therefore well documented. On the other hand, it remains unknown whether the outer meningeal layers, i.e. the dura mater, can contribute to the development of neuro-inflammation in EAE and be a site for T-cell trafficking to and from the CNS. Moreover, it has not been investigated whether CNS-invading T cells can also possibly leave the CNS via the dura. Recent studies proposed that the dura might represent an exit route for cells and solutes from the CNS, which could travel to the deep cervical lymph nodes via the dura lymphatics.

In this work we show that, unlike the leptomeninges, the dura is largely spared by the neuro-inflammatory process of EAE. We were able to identify several properties of the dura which may account for its marginal involvement. First, dura vessels were not permissive to T cell trafficking due to the lower expression of ligands that are necessary for the adhesion of effector CNS-reactive T cells. Further, activation of T cells in the dura during EAE was lower when compared to the leptomeninges and prevented the formation of a local inflammatory process. This was not due to intrinsic defects in T cells reaching the dura, nor to incompetence of the dura antigen presenting cells (APCs) in activating the T cells. In fact, when inflammation was induced in the dura, T cells readily accumulated there. Instead, the low activation of CNS-reactive T cells in the dura was due to the low availability of the cognate antigen: dura APCs failed to spontaneously present myelin or neuronal antigens to autoreactive T cells, while APCs of the leptomeninges or CNS parenchyma were able to spontaneously reactivate CNS-reactive T cells.

We also found that trafficking of CNS-reactive T cells through the lymphatic vessels of the dura and deep cervical lymph nodes is very limited during EAE. More importantly, we did not detect neither antigen drainage nor T cell activation in these structures. Consequently, depletion of the lymphatic system did not have any effect on EAE clinical course or immune cell

infiltration in the CNS. These data allowed us to conclude that the dura lymphatics and deep cervical lymph nodes play a marginal role, if any, in EAE development and severity.

In conclusion, this work highlights the uneven involvement of the meningeal compartments to the neuro-inflammatory process of EAE. Although the dura possesses all the cellular and anatomical components to mount an effective immune response, T cell trafficking and activation during EAE is functionally confined to the leptomeninges, where endothelial vessels are permissive to T cell adhesion and local APCs can process and present CNS antigens.

1 INTRODUCTION

1.1 Multiple sclerosis: evidence for a CD4-mediated autoimmune pathogenesis

Multiple sclerosis (MS) is a chronic inflammatory disease of the central nervous system (CNS), characterized by disseminated demyelinating lesions in both white and grey matter and a variable extent of axonal loss.[1,2] Lesions occur on the background of inflammation and consist of T lymphocytes, B lymphocytes, plasma cells and mainly mononuclear myeloid cells. Subpial demyelination in the cerebral cortex is a hallmark of MS pathology and leptomeningeal inflammatory infiltrates have also been described.[3-5]

Immunological studies suggest that a $CD4^+$ T cell-mediated autoimmunity against CNS antigens might be the primary event at the root of MS pathogenesis.[6,7] This assumption is substantiated by key observations in humans. First, CNS-reactive T cells can be identified in the immune repertoire of most individuals and are expanded and activated in MS patients.[8-11] These T cells are potentially pathogenic since they can induce an inflammatory CNS disease in humanized mice.[12] Second, genome-wide association studies in MS patients have highlighted a significant linkage with genes involved in adaptive immune responses and T cell signaling. In particular, the HLA-DR15 haplotype (a major histocompatibility class II molecule, which presents antigens to $CD4^+$ T cells) accounts for up to 60% of the genetic risk for MS.[10,13] Third, a significant proportion of successful disease-modifying treatments in MS targets either antigen presenting cells (APCs), hence, T cell activation, or T cell migration.[14]

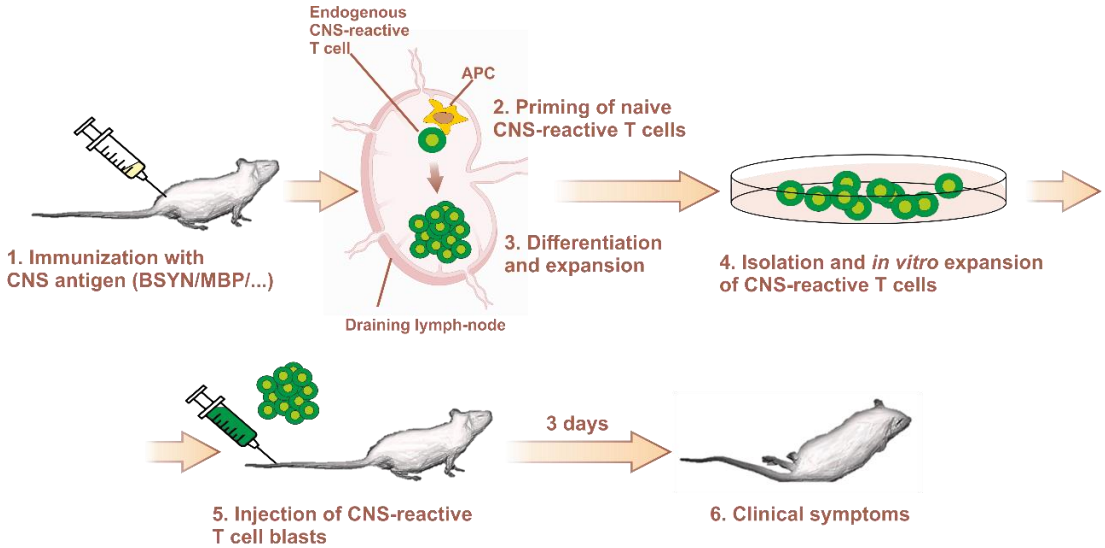

Figure 1: CNS-reactive T cells are sufficient to induce EAE. Upon immunization with a CNS antigen, the antigen is taken up by APCs in the lymph nodes draining the site of immunization. Endogenous naïve T cells reactive against the CNS antigen are primed, differentiate and expand within the draining lymph nodes. After around one week, the expanded CNS-reactive T cells can be isolated from the draining lymph nodes and amplified in culture. Injection of the CNS-reactive T cells causes neurological symptoms in the recipient rat.

Finally, auto-sensitization of rodents and primates, humans included,[15] with CNS components induces a paralytic neurological disorder, which is clinically similar to spontaneous MS. The neurological disease induced by such immunization protocols is named experimental autoimmune encephalomyelitis (EAE) and is a widely used model to investigate adaptive immunity and neuroinflammation. In this model, the sensitization protocol requires a strong immune adjuvant, such as Mycobacterium tuberculosis, to reliably induce disease. Adjuvants stimulate phagocytosis and antigen presentation by mononuclear cells, which result in the preferential activation and expansion of $CD4^+$ helper T cells.[16]

1.2 Passive-transfer EAE: a model to study the preclinical phase of MS

The formal proof that autoreactive T cells were sufficient to induce a MS-like disease came from the work of Ben Nun, Wekerle and Cohen in 1981.[17] By isolating and propagating T cell clones specific for the endogenous CNS protein myelin basic protein (MBP), they were able to trigger an acute, inflammatory, ascending paralysis in Lewis rats. Since then, this procedure has been used to induce autoimmunity against several CNS antigens (**Figure 1**).

A major advantage of such adoptive transfer models is that the T cells are already expanded and activated *in vitro*, and the outcome of EAE is not influenced by the immune activation in peripheral lymphoid tissues.

Another advantage of this approach is that antigen-specific T cells can be retrovirally engineered to express fluorescent proteins like green-fluorescent protein (GFP), which does not interfere with T cell function.[18,19] This technical advancement allows the easy tracking and characterization of the pathogenic T cells in the different peripheral and CNS compartments during all the various phases of EAE.

A handful of myelin components, such as MBP, myelin oligodendrocyte glycoprotein (MOG) and proteolipid protein (PLP) can induce EAE, although different animal models are susceptible to different antigens.[16] A common characteristic of these models is the predominant T cell infiltration in the myelin-rich white matter, in particular in the spinal cord. More recently, EAE has been successfully triggered also by T cells directed against a neuronal antigen, beta-synuclein (bSYN). EAE mediated by bSYN-reactive T cells (T_{bSYN} cells) is characterized by massive leptomeningeal and parenchymal infiltration of the gray matter of both brain and spinal cord and by atypical EAE symptoms such as hemiparesis and ataxia.[20]

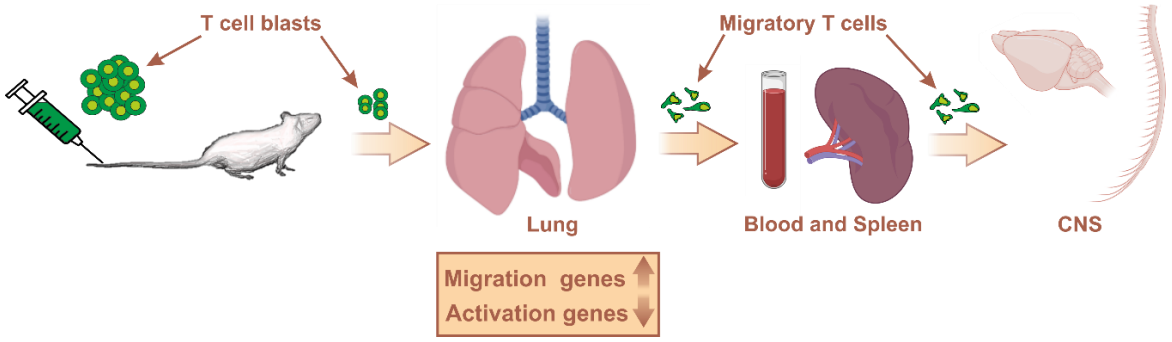

Figure 2: Route of CNS-reactive T cells upon intravenous injection.

1.3 Fate of autoreactive encephalitogenic T cells in EAE

In vivo imaging with two-photon laser-scanning microscopy, in combination with *ex vivo* flow cytometry, has been employed to dissect the fate of autoreactive T cells in the Lewis rat passive-transfer EAE model (**Figure 2**).[19,21,22]

Upon intravenous injection, autoreactive T cells accumulate mostly in the lung,[23] where they undergo transcriptional changes towards a migratory phenotype, which allows them to re-enter the circulation and infiltrate the leptomeningeal areas of the dorsal spinal cord (SC) between day 2 and 3 post transfer**.** Migratory T cells down-regulate activation markers and up-regulate adhesion molecules and chemokine receptors. Importantly, such migratory phenotype is not antigen restricted, since CNS-ignorant effector T cells undergo comparable phenotypical changes and are able to reach as well the CNS meninges, albeit in substantially lower numbers than autoreactive T cells.

The site of entry of encephalitogenic T cells into the CNS is still a matter of debate. So far, the following anatomical regions have been proposed:[24]

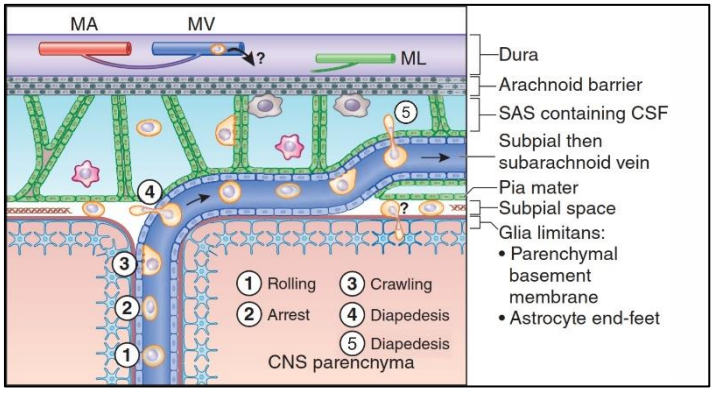

Figure 3: Putative sites of entry of encephalitogenic T cells. Leptomeningeal vessels. (modified from Engelhardt et al, Nat Immunol, 2017)

1) Leptomeningeal venules (**Figure 3).** This is the most established route for T cell access to the CNS. Myelin-reactive T cells have been observed entering the CNS through the

leptomeninges *in vivo* in mouse and rat models of EAE.[25,26] T cells enter the subarachnoid space from leptomeningeal venules in the SC, where they can either get reactivated by meningeal APCs and from there initiate CNS invasion[27] or detach and be washed away by the cerebrospinal fluid (CSF).[28] More recently, a similar route for T cell entry to the CNS has been demonstrated also for T_{bSYN} cells, which cause inflammatory lesions predominantly in the gray matter.[20] Also in pathological samples of MS patients, leptomeningeal inflammation is an early finding and has been shown to correlate with disability and gray matter damage.[4,29]

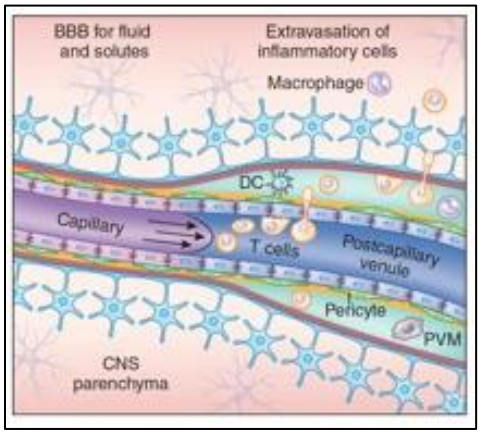

Figure 4: Putative sites of entry of encephalitogenic T cells. Parenchymal postcapillary venules. (modified from Engelhardt et al, Nat Immunol, 2017)

2) Post-capillary venules of CNS parenchyma (Figure 4). Encephalitogenic T cells may also enter the CNS parenchyma by breaching the blood-brain barrier (BBB) of subpial post-capillary venules.[30] In the perivascular space, T cells could then be re-activated by perivascular APCs before penetrating the CNS parenchyma.

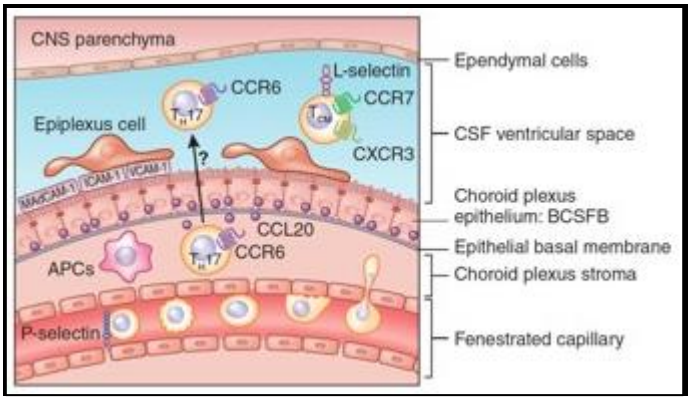

Figure 5: Putative sites of entry of encephalitogenic T cells. Choroid plexus. (modified from Engelhardt et al, Nat Immunol, 2017)

3) Choroid plexus (**Figure 5**)**.** T helper 17 (T_H17) cells, a subset of CD4 T cells, that express the chemokine receptor 6 (CCR6) might be able to cross the blood–CSF barrier in the choroid plexus, which expresses the CCR6 ligand Chemokine (C-C motif) ligand 20 (CCL20). From

the ventricular CSF, T cells should reach the subarachnoid space, attach to the pial surface, cross the leptomeninges and glia limitans and penetrate into the tissue parenchyma.[31]

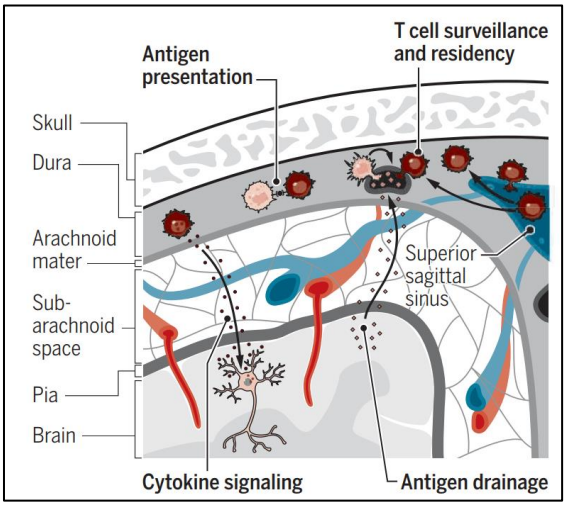

Figure 6: Putative sites of entry of encephalitogenic T cells. Dural sinuses. (modified from Rustenhoven J and Kipnis J, Science, 2019)

4) Dural sinuses (Figure 6). It has been recently hypothesized that CNS-reactive T cells extravasating into the dura from the dural sinuses, a process mediated by C-X-C chemokine receptor type 4 (CXCR4) and its ligand C-X-C motif chemokine ligand 12 (CXCL12), could encounter CNS antigens sampled by local APCs in the peri-sinus areas.[32] It is still unknown, if CNS-reactive T cells are indeed re-activated there and if they can then travel to the CNS parenchyma thorough the dura.

1.4 The multi-step process of T lymphocyte egress from the circulation

Regardless of the route of entry, T cells always have to breach an endothelial barrier to gain access to the CNS tissue. Interactions between T lymphocytes and the vessel endothelium follow a sequential process of adhesion and each of these steps is mediated by different molecules on both T cells and the endothelial cells.[33] In post-capillary venules, the hemodynamic effect of "margination" promotes the localization of leukocytes in proximity to the vascular wall.[34] This positioning facilitates the initial capture of circulating T cells by the vessel endothelium, which expresses members of the selectin family that bind to P-selectin glycoprotein ligand 1 (PSGL-1) on leukocytes.[35] Once captured, T cells roll along the vascular endothelium, significantly slowing their velocity. On the endothelium, rolling T cells may encounter chemokines which activate G protein-coupled receptors on T cells, inducing an "inside-out" activation of T cell integrins.[36,37] Integrins can bind to a variety of ligands on the endothelial surface, in particular, it has been shown that the very late antigen 4 (VLA-4, $\alpha_4\beta_1$-

integrin) mediates T cell arrest on leptomeningeal vessels via its interaction with endothelial vascular cell adhesion molecule 1, VCAM-1.[25] Following firm adhesion to the endothelium, attached leukocytes undergo a morphological change, which results in a slow, amoeboid movement, termed crawling, that scans the intraluminal surface of the vessel endothelium.

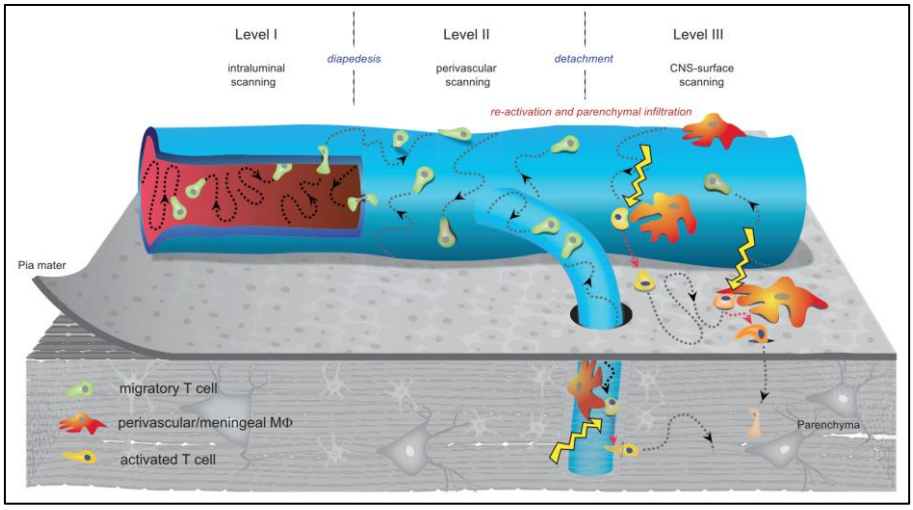

Figure 7: Invasion steps of autoreactive T cells into the CNS. Adapted from Bartholomäus et al, Nature, 2009

Notably, *in vivo* imaging of leptomeningeal venules during the initiation phase of EAE **(Figure 7)** showed that intraluminal encephalitogenic T cells crawl preferentially against the direction of blood flow and that this process is largely dependent on $\alpha_4\beta_1$ integrins.[25] Crawling T cells on the endothelial surface can either detach and be washed away by the blood flow, or breach the endothelial barrier and extravasate. After extravasation in the subarachnoid space, T cells scan the abluminal vascular surface. There, T cells can encounter meningeal APCs, which present CNS antigens to the autoreactive T cells and activate them.[27,38] Activated T cells produce cytokines that stimulate the endothelial cells to upregulate adhesion molecules and parenchymal cells to produce chemokines. This process ultimately results in the recruitment of other immune cells to the site of T cell activation. *In vivo* imaging studies in EAE describe a continuous trafficking of T cells between the leptomeninges and the CSF, where integrins VLA-4 and lymphocyte function-associated antigen 1 (LFA-1, $\alpha_L\beta_2$ integrin) prevent T cell detachment and chemokine signaling via CCR5 and CXCR3 enforces T cell adhesiveness onto the leptomeningeal surface.[28] As the clinical disease develops and neuroinflammation spreads, activated T cells can be found migrating further through the meninges and parenchyma.[27]

1.5 The immunological relevance of CNS meninges

As seen in the previous chapter, the CNS meninges represent a site for meaningful interactions between encephalitogenic T cells, CNS structures and CNS resident immune cells during EAE. Indeed, meningeal inflammation has been repeatedly implicated in MS pathogenesis and disease progression.[4,29,39,40]

In this paragraph, we will briefly discuss the anatomy of this immunologically relevant compartment, with a special focus on the cranial meninges and on the dura mater.

1.5.1 Pia mater, arachnoidea and the dura-arachnoidea barrier

The pia mater is the innermost meningeal layer and is in direct contact with the CNS parenchyma. The pia is comprised of one-two cell layers that are connected together by desmosomes and gap junctions.[41] The pia mater coats veins and arteries in the subarachnoid space and a sheath of pial cells follows the arteries in the parenchyma, creating the subpial space, which separates the pial layer from the glia limitans. On the other hand, pial venules lose their pial sheath once they penetrate the CNS parenchyma. The pia mater serves as both a metabolic and cellular barrier as it processes neurotransmitters,[42] is permeable to solutes smaller than 200 Å and immune cells, while it is impermeable to erythrocytes.[43] On the surface of the pia mater, phagocytic cells positive for the class-II major histocompatibility complex ($MHCII^{+)}$ are detected.[25] Thanks to high throughput flow cytometry, the identity of such cells has recently become clearer: leptomeninges harbor border associated macrophages,[44] both $MHCII^{+}$ and $MHCII^{-}$, dendritic cells and, to a lesser extent, microglia-like cells, B cells and monocyte-derived $Ly6C^{+}$ cells. Among those, conventional dendritic cells, specifically type 2 $CD11b^{+}$ $CD172a^{+}$ cells, are postulated to be the most efficient at reactivating CNS-reactive T cells.[44-46]

The arachnoid mater lies between the pia mater and the dura mater and the CSF flows between its layers. The arachnoid mater can be grossly divided into the parietal arachnoid, which is tightly apposed to the dura, and leptomeningeal trabeculae that connect the pial surface and vessels to the parietal arachnoidea.

The parietal arachnoid is regarded as the true barrier between the dura mater and the subarachnoid space. The ultrastructural composition of this barrier has been investigated in humans by W. Schachenmayr and R. L. Friede.[47] They describe a tight layer of cells, the interface layer (**Figure 8A**), which they state is devoid of connective tissue fibers and comprises the innermost portion of the dura mater (the dural border cells) and the outermost

layer of the arachnoid (the arachnoid barrier layer). Such "dura-arachnoid interface layer" has been reported in several publications, with inhomogeneous definitions.[48,49] Regardless of the nomenclature, this structure is comprised of an outer portion with loosely packed cells, also called the border layer by later publications,[41] and a proper arachnoid barrier layer, which contains closely apposed cells, with very narrow intercellular spaces and characteristic tight junctions (**Figure 8B**), desmosomes, that connect the barrier layer cells to the trabecular cells, vimentin filaments and possibly a basement membrane, although the existence of the latter has not been consistently reported.[41,50-52] Similar to the BBB, the arachnoid barrier layer expresses efflux pumps.[53] The permeability of the arachnoid-dura barrier has not been systematically investigated. Balin et al[54] and, more recently, Roth et al[55] suggest that such barrier may be more permeable than the BBB, since molecules up to 40KDa can pass from the dura through the arachnoid barrier when administered either intravenously[54] or directly onto the dura mater.[55]

The leptomeninges are well-known sites of immunological pathology. During acute meningitis, especially of bacterial origin, the leptomeninges are massively inflamed and inflammation can spread to the underlying tissue (meningoencephalitis).[56] In the case of fulminant meningitis, leptomeningeal inflammation rapidly exacerbates, causing potentially fatal intracranial hypertension.[57]

In the case of recurrent meningitis, leptomeninges become cyclically inflamed[58] due to a variety of causes. Anatomical skull defects or immunodeficiency can cause recurrent bacterial invasion of the CNS, while reactivation of latent viruses, in particular herpesviridae, can rarely manifest with benign lymphocytic meningitis. Aseptic drug-induced recurrent meningitis is also a rare and poorly understood complication of some treatments, such as non-inflammatory steroids and monoclonal or polyclonal immunoglobulins.[59,60]

Several systemic autoimmune disorders can present with leptomeningeal involvement: Lupus erythematosus and Sjögren's syndrome are at risk of drug-induced aseptic meningitis, which likely has an autoimmune basis.[59] Sarcoidosis and Behçet's disease can be associated with both pachymeningits and leptomeningitis and are frequently localized in the base of the skull.[58] Systemic vasculitides and primary CNS vasculitis can both affect the leptomeningeal vessels.[61] Finally, the Vogt-Koyanagi-Harada syndrome, a T-cell-mediated autoimmune disease directed against melanocyte antigens, is characterized by recurrent uveitis and meningitis.[62]

In multiple sclerosis, leptomeningeal inflammation is an early event and it is often topographically associated with subpial demyelinating lesions.[3,4] In some cases, meningeal infiltrates organize in ectopic lymphoid follicles, which could sustain intrathecal B cell

maturation.[29] The presence of such follicles strongly correlates with disability progression and disease severity.[40]

It is worth noting that recently also MOG-associated diseases[63-65] and, very rarely, neuromyelitis optica spectrum disorders have been reported in association with meningitis.[66]

1.5.2 Dura mater

The transition from the border layer to the dura proper is marked by the appearance of abundant extracellular matrix, with microfibrils, collagen and elastic fibers (**Figure 8**).

Electron scanning microscopy of the human dura shows a variety of fiber dispositions, ranging from linear and tight strata in the outmost layers, to whorl-like structures in the vascular layer and disorganized bundles in the innermost tiers.[67]

The cranial dura mater has its own vascular supply, largely independent from the brain, coming from branches of external carotid artery, vertebral artery and rarely from the internal carotid artery.[68,69] The middle meningeal artery is the main vessel of the dura mater, from which primary and secondary anastomotic arteries are generated to give rise to arteriovenous shunts and a rich capillary and anastomotic network. Some branches of the dural arteries can contribute to the bone vascularization and form arteriovenous shunts. In humans, venous drainage of the dura occurs through satellite veins, which typically accompany the arteries in pairs (two veins per one artery) and flow into the venous sinuses and in epithelialized blood lacunae surrounding the sinuses.[69] Venous sinuses also drain the intrathecal space via arachnoid villi, [70] the brain parenchyma through the bridging veins and part of the skull diploe.[71]

The dura mater vasculature is permeable to molecules up to 40 KDa MW.[72] Electrical stimuli, neuropeptides and neurotransmitters, in particular histamine, can induce vasodilation.[73,74] Given the relative leakiness of the dura vasculature, the impermeable arachnoid barrier may play a crucial role to prevent the entry of circulating factors (and potentially also cells) into the CSF.

The dura is richly innervated, with a prominent afferent network of Aβ, Aδ and C fibers that relay to the trigeminal, vagus, hypoglossal and C1-C3 spinal nerves.[75-77] Sympathetic fibers, from the superior cervical ganglion, and sparse parasympathetic fibers, from the sphenopalatine ganglion, exert a variety of actions on dura resident cells and vessels through a plethora of neurotransmitters, such as acetylcholine, calcitonin gene-related peptide, histamine, neurokinin A, neuropeptide Y, P substance, serotonin, vasoactive intestinal peptide, most of which possess vasoactive properties.[78,79] Dura autonomic responses are directly linked to cortical activity, as exemplified by migraine: cortical spreading depression, the initial event in migraine with aura, activates trigeminovascular afferents and evokes a brainstem reflex, through the superior salivatory nucleus, that travels via parasympathetic fibers from the sphenopalatine ganglion to the dura and causes long-lasting blood-flow enhancement within the middle meningeal artery and plasma protein leakage within the dura mater, in part by a neurokinin-1-receptor mechanism.[80] The functional coupling of the cranial dura to brain metabolic activity also results in neurogenic neuroinflammation, another putative pathogenic mechanism in migraine.

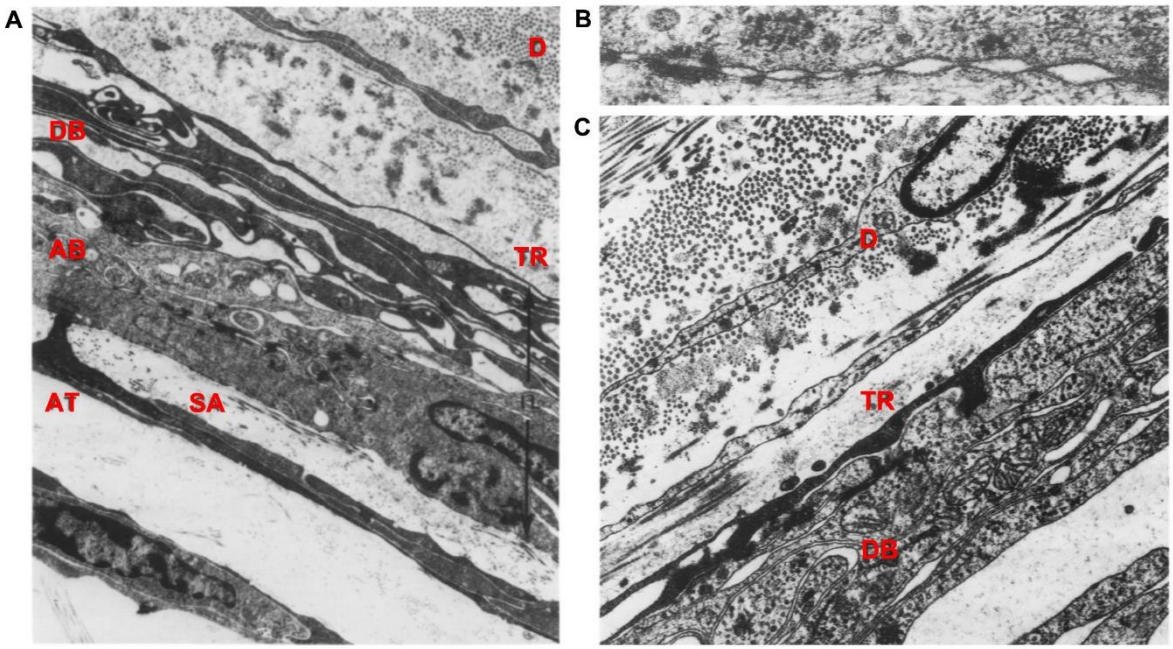

Figure 8: Structure of the dura mater-arachnoid barrier. A, Electron microscopy scans from human cranial meninges showing the interface layer composed of the arachnoidea barrier layer (AB), the dura border cell layer (DB). In the AB tight cell disposition with no extracellular matrix can be observed, with some cells connecting with an arachnoidea trabecula (AT) in the subarachnoid space (SA). The DB is instead composed of loosely packed cells with amorphous extracellular material interspersed among them. On top of the DB, the transition zone (TR) precedes the characteristic collagen fibers of the dura proper (D). B, A higher magnification of the arachnoid barrier layer, showing the characteristic tight junctions. C, Example of the lax cellular disposition of the DB, with rare cell junctions, as well as of the dense collagen and elastin fiber network of the dura. Modified from Schachenmayr and Friede, Am J Pathol, 1978

The cellular composition of the dural tissue has only recently been systematically addressed.[32,81] Besides the vascular and nerve cells that pertain to the dural vascular and innervation system, it is known that the dura mater contains fibroblasts, rare osteoblasts and telocytes,[82] and populations of multipotent cells with the ability to give rise to both nerve and mesenchymal precursors.[83]

The dura also contains a varied population of immune cells.[81] McMenamin and colleagues described $MHCII^+$, $CD68^+$, $CD11b^+$ cells in all the layers of the rat dura meninges.[84,85] Those cells seem to either follow a perivascular distribution or spread along collagen fibers. Notably, the dura is particularly rich in mast cells, which have been implicated in migraine pathogenesis, due to their interaction with dural nerve fibers and ability to secrete vasoactive mediators,[86,87]and have been postulated to aid T cell extravasation during EAE.[88] Recently, innate type-2 lymphoid cells have been described in the dura, lining along the dural sinuses, and they might play a protective role in traumatic CNS injury.[89] Dendritic cells, B cells and T cells have also been described in the non-inflamed dura mater.[90,91]

The distribution of immune cells in the dura appears inhomogeneous, with the majority aligning along the big vascular conduits of the sagittal and transversal sinuses. This led to the recent speculation that immune cells may encounter antigens and pathogens there.[32,92] Notably, dura immune cell infiltration and pathogen colonization have been described in animal models of trypanosomiasis,[93] borreliosis[94] and systemic candidiasis.[92] In fact, IgA^+ plasma cells located in perisinusal areas expand during *C albicans* infection, and similarly to IgA+ cells in the mucosae, may serve a barrier function to contain the spread of infection, possibly also to the CNS.[92]

T cells have also been described in perisinusal areas, in close contact with APCs, leading to the speculation that dural APCs may sample CNS antigens and, therefore, similarly to leptomeningeal APCs, activate CNS-autoreactive T cells.[32]

Despite this, the dura mater is rarely a primary or prominent site of immune pathology in clinical practice. Selective inflammation of the dura (i.e. pachymeningitis) can be rarely observed in systemic granulomatoses, vasculitides and IgG4-related diseases, although it has been described as a possible manifestation of almost every systemic autoimmune disorder.[95,96] Infectious agents, in particular spirochaete, mycobacteria and fungi, can also cause chronic pachymeningitis.[97] In those cases, in contrast with (lepto)meningitis, the CSF is frequently negative for the pathogenic agent.[97]

Up to this day, the evidence regarding a potential involvement of the dura in human multiple sclerosis pathogenesis is limited to one magnetic resonance report, which describes dura mater

vascular gadolinium enhancement in patients with multiple sclerosis.[98] The significance and specificity of this observation to multiple sclerosis is at present not determined.

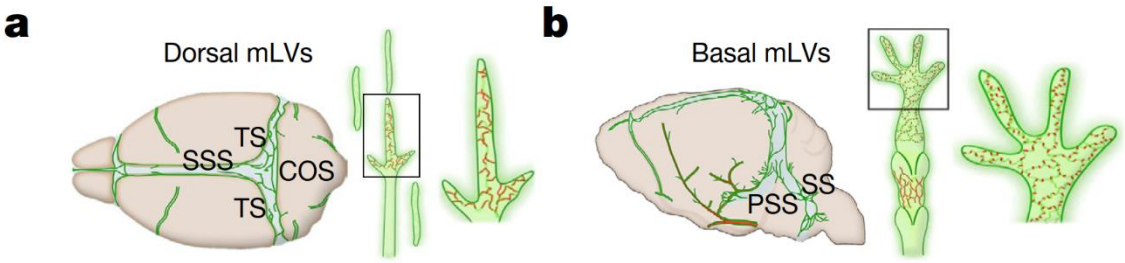

Figure 9: Anatomical location of the dural lymphatic vessels. (a) Lymphatic vessels in the cranial vault run along the superior sagittal sinus (SSS), sinus confluence (COS) and transverse sinus (TS), are discontinuous and have an immature morphology with zipper-like junctions, unsuited for the take-up of antigens. (b) Lymphatic vessels of the cranial base have larger diameter, run along the squamous sinus (SS) and petrosquamous sinus (PSS) and have protruding (oak-leaf shaped) branches with button-like junctions and valves, more suited for solute drainage. Adapted from Ahn et al, Nature, 2019.

Lymphatic vessels in the dura mater have been repeatedly described, with the first report dating back to the XVIII century.[99-106] In more recent times, the dura lymphatic network has been described in anatomical detail by Aspelund et al and, more recently, by Ahn et al (**Figure 9**),[107,108] who showed that it is mostly developed in the cranial base, where lymphatics run down along the transverse sinus, the petrosquamous and sigmoid sinus, the retroglenoid vein, the rostral rhinal vein, and the major branches of the middle and anterior meningeal arteries. In the cranial vault, the lymphatic network is much more rudimentary, with few vessels along the superior sagittal sinus, and the middle meningeal artery.[108] Lymphatic vessels exit the skull along the pterygopalatine artery, the jugular veins, the cranial nerves and the cribriform plate.

The lymphatic vessel system of the dura is characteristically dependent, both in its embryogenesis as well as in its maintenance, on steady vascular endothelial growth factor C (VEGF-C) signaling,[109] presumably provided by neighboring arterial smooth muscle cells. Blockade of VEGF-C signaling pathway induces rapid regression of the dura lymphatic network.

In conclusion, the dura possesses a varied immune cell repertoire, which, together with the presence of lymphatic vessels, defines the dura as an immunologically competent tissue, fully capable of mounting an immune response. In that respect, the dura resembles more closely other peripheral “barrier” tissues (e.g. the skin or the gut) rather than the leptomeninges or the CNS parenchyma.[110] In contrast to the dura, both leptomeninges and CNS parenchyma have a relatively monotonous immune cell repertoire: the leptomeninges are seeded almost exclusively with border associated macrophages and rare lymphocytes and dendritic cells,

while in the parenchyma microglia are the dominant immune cell.[44,81] Furthermore, lymphatic vessels are absent from both leptomeninges and CNS parenchyma.

1.6 Exit routes from the CNS to the periphery for solutes and cells

The CNS has been historically considered "immune privileged". This definition was initially ascribed to the inability of the CNS to reject allogeneic grafts implanted intraparenchymally.[111-114] On the other hand, when grafts where implanted both in a peripheral tissue as well as the CNS, rejection occurred swiftly.

Medawar ascribed this disparity of behavior to the absence of lymphatic vessels in the CNS. Consequently, the CNS could "submit to but not elicit an immune response".[114]

Soon it was noted that such immune privilege was not absolute and overall confined to the parenchyma. Indeed, grafts injected into the ventricles or that came into contact with the subarachnoid space could elicit an immune response without the need of peripheral immunization.[115,116] Further, the recent re-appraisal of the dural lymphatic vessels has sparked numerous immunological speculations on the possibility for CNS-derived cells and solutes to exit the CNS, potentially via the dural lymphatic vessels, to modulate peripheral immune responses.

In this paragraph, we will briefly summarize the current evidence regarding the drainage of cells and solutes from the CNS to peripheral secondary lymphoid organs.

An initial suggestion for an exit route for cells, or, at least, antigens, from the CNS, comes from the observation that myeloid cells bearing myelin antigens have been detected in the cervical lymph nodes of EAE monkeys and MS patients[117] and surgical removal of CNS-draining lymph nodes ameliorates EAE disease severity.[118-120] However, these findings do not provide meaningful proof for a cellular exit route from the CNS.

In non-inflammatory conditions, dendritic cells or T cells injected intracerebroventricularly have been retrieved in deep cervical lymph nodes (dcLNs), whilst no cells could be detected upon intraparenchymal injection.[121,122] On the other hand, upon lesion of the entorhinal cortex, intraparenchymally-injected T cells might drain to deep cervical lymph nodes, possibly through the cribriform plate.[123] Finally, upon ligation of the afferent lymphatic of the dcLNs, Louveau et al. describe an increase in the number of T cells in the dura, indirectly suggesting an afferent trafficking path for those cells through the dural lymphatics.[122,124] Similarly, Ahn and colleagues describe T and B cells within the lumen of the lymphatic vessels of the base of the skull.[108]

While the evidence of a trafficking pathway for immune cells outside of the CNS is still scarce, a drainage route from the CNS to periphery is established for solutes.

Two extracellular fluids are associated with the CNS: the CSF and the interstitial fluid (ISF). The CSF, in humans, drains directly into the venous sinuses via arachnoid villi and granulations[125] and a further proportion of CSF drains to regional lymph nodes. In particular, the lymphatic drainage of CSF via the cribriform plate of the ethmoid bone has been demonstrated in humans.[126] A drainage from the CSF to the dcLNs, in humans, has so far not been demonstrated. However, it has been implicated by the observation of increased iron deposits in the dcLNs of patients who died from intracerebral hemorrhage[127] and by the detection of CNS-derived proteins in the dcLNs of patients with neurological diseases characterized by parenchymal destruction.[117,128] The routes of lymphatic drainage that have been demonstrated in animal models are dural lymphatics, especially at the level of the cranial base, and lymphatics associated with cranial and spinal nerves (**Figure 10**).[107,108,129]

In peripheral organs, ISF, produced by capillary filtration or by cell metabolism, is generally drained by lymphatic vessels. Although the density of lymph vessels typically correlates with tissue metabolic rate, the CNS, which has characteristically high metabolic activity, does not have lymphatic vessels. On that note, the CSF might exert a lymphatic function through its exchange with brain ISF.[130]

Two-photon studies have shown that CSF from the subarachnoid space moves rapidly into the brain along a paravascular pathway surrounding cerebral arteries, mixes with ISF and is drained along cerebral veins.[131] Such transit is facilitated by arterial pulsation and astrocytes via aquaporin-4.[132] This paravascular CSF–ISF exchange, termed the "glymphatic system",[133] plays a role in amyloid beta clearance and its functioning may be impaired during aging.[131]

Another model for drainage of ISF implies that solutes are directly drained along basement membranes in the walls of capillaries and then of arterioles and arteries.[134,135] From there, they leave the CNS through the base of the skull and reach the cervical lymph nodes. Also in this

system, the driving force for ISF drainage may be arterial pulsations, as predicted by mathematical models.[136,137]

It is at present unclear if and how a unifying model could combine these systems of CSF drainage, namely the dural/epineurial lymphatics, the glymphatic system and the para-arterial route. Such model would be of relevance, since in the recent years disturbances of CSF drainage have been detected or postulated in different pathological conditions.

In stroke, glymphatic inflow of CSF into the parenchyma appears to be the primary determinant of brain edema in the first hours after ischemia.[138] The role of the dural lymphatic system in ischemic stroke is at present unclear: one study shows improved stroke outcomes upon blockade of drainage to the deep cervical lymph nodes, potentially via dampening of the immune response,[139] while other reports state that depletion of the dura lymphatic vessels results in increased disease severity.[140,141] A similar protective role for the lymphatic system has been postulated for traumatic brain injury[142] and subarachnoid hemorrhage.[143-145] Here, the dural lymphatic system may aid in controlling intracranial pressure and in eliminating toxic waste products generated by parenchymal damage and disruption of the BBB.

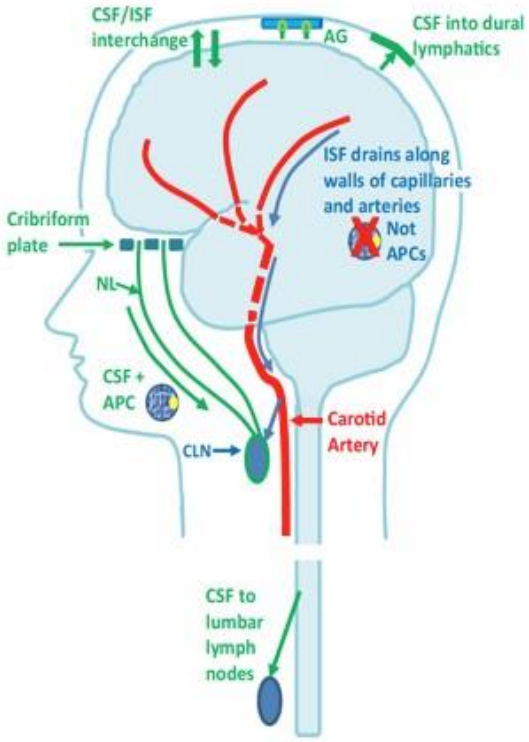

Figure 10: Possible routes for CSF and ISF drainage outside of the CNS (Engelhardt B et al, Acta Neuropath, 2016). CSF drains into the venous sinuses through arachnoid granulations (AG). CSF drainage can also occur via nasal lymphatics (NL) and dural lymphatics, which are connected to the cervical lymph nodes (CLN). APCs coming from the CSF (CSF+ APC) may also use this route. CSF interchanges with the ISF by entering the surface of the brain along a paravascular pathway surrounding brain arteries (glymphatic system). ISF from the brain parenchyma may drain along basement membranes of cerebral capillaries and arteries (blue arrows) to the CLN. This intramural perivascular drainage pathway is not permissive to the traffic of APCs.

In neurodegenerative diseases, impairment of the glymphatic and para-arterial system have been repeatedly described in normotensive hydrocephalus and Alzheimer's disease.[146] Similarly, ablation of the lymphatic system aggravates pathology in animal models of Alzheimer's disease.[147] A recent study reported that also patients with Parkinson's disease might present impairment of meningeal lymphatic drainage.[148]

The role of the lymphatic system in multiple sclerosis and its animal model EAE, as already mentioned, is at the moment unclear. Louveau and colleagues showed that ablation of the dural

lymphatics improved disease course.[122] The authors speculate that such amelioration could be motivated by reduced antigen presentation in the deep cervical lymph nodes of CNS-derived antigens. However, at present it is unclear how such lymphatic stations may contribute to the priming and reactivation of T cells in EAE.

2 AIMS AND OBJECTIVE

The aim of this project is to study the involvement of the dura mater meninges in the inflammatory process of EAE. To this end, we investigate:

1) If and how CNS-reactive T cells accumulate in the dura during EAE and if dura vessels can represent a site of entry for autoreactive T cells to the CNS.
2) The immunological properties of the dura tissue during steady state and if the dura can be a site for the reactivation of autoreactive T cell during EAE.
3) If T cells or CNS antigens can exit the CNS via the dura lymphatics and deep cervical lymph nodes and if this drainage system plays any role in T cell recruitment to the CNS and EAE initiation.

3 MATERIALS AND METHODS

3.1 Materials

3.1.1 Media and buffers

Buffers were prepared with water purified with a Milli-Q purification system (Merck, Germany).

Phosphate-buffered saline (10x PBS)	8.1 mM	Na_2HPO_4 (Roth, Germany)
	1.47 mM	$Na_2H_2PO_4$ (Roth, Germany)
	137 mM	NaCl (Roth, Germany)
	2.68 mM	KCl (Roth, Germany)
		adjusted to pH 7.2 – 7.4 with HCl (Roth, Germany)
Ammonium-chloride-potassium buffer (ACK)	0.15 mol / l	NH_4Cl (Roth, Germany)
	1 mmol / l	$KHCO_3$ (Roth, Germany)
	0.1 mmol / l	Na_2xEDTA (Roth, Germany)
		Adjusted to pH 7.2 – 7.4 with HCl (Roth, Germany)
Dulbecco´s Modified Eagle Medium (DMEM)	13.4 g / l	DMEM Powder (Thermo Fisher Scientific, USA)
	3.72 g / l	$NaHCO_3$ (Roth, Germany)
Eagle´s HEPES medium (EH)	75 %	DMEM
	25 %	HEPES 1M (Thermo Fisher Scientific, USA)
T cell medium (TCM)	950 ml	DMEM
	4 µl	β-mercaptoethanol (Roth, Germany)
	10 ml	Penicillin / Streptomycin (Thermo Fisher Scientific, USA)
	10 ml	Sodium pyruvate (Thermo Fisher Scientific, USA)
	10 ml	L-asparagine monohydrate

		(Sigma-Aldrich, Germany)
	10 ml	L-glutamine
		(PAN Biotech, Germany)
	10 ml	Non-essential amino acids
		(Thermo Fisher Scientific, USA)
Re-stimulation medium (RM)	99 %	TCM
	1 %	Rat serum (in-house production)
T cell growth factor medium (TCGF)	88 %	TCM
	10 %	Horse serum (Merck, Germany)
	2 %	IL-2 containing supernatant
FACS buffer	2 mM	Na_2xEDTA (Roth, Germany)
	0.5 %	Albumin Fraction V
		(Roth, Germany)
		in 1x PBS
Freezing medium (FM)	80 %	Horse serum (Merck, Germany)
	10 %	TCM
	10 %	DMSO (Roth, Germany)
Thawing medium (TM)	90 %	EH
	10 %	Fetal calf serum (Merck, Germany)
Digestion buffer (endothelial cells)	15 ml	EH
	0.4 u / ml	Liberase (Roche, Switzerland)
	120 / ml	DNase I (Roche, Switzerland)
Digestion buffer (leukocytes)	0.15%	Collagenase II (Sigma)
	60 u / ml	DNase I (Roche, Switzerland)
Isotonic Percoll (Isopercoll)	90 %	Percoll (GE Healthcare, USA)
	10 %	10x PBS

3.1.2 Reagents, chemicals and sera

Albumin Fraction V	Roth, Germany
Agarose, Low Melt	Roth, Germany
APC beads (BD Calibrite)	BD Biosciences, USA
β-Mercaptoethanol	Roth, Germany
Collagenase from C histolyticum	Merck, Germany
Chloroform	Roth, Germany
Dextran fluorescein (70, 2000KDa)	Thermo Fisher Scientific, USA
Dextran Texas-Red (3, 70KDa)	Thermo Fisher Scientific, USA
Dextran Tetramethylrhodamine (2000KDa)	Thermo Fisher Scientific, USA
Diethyl ether	Roth, Germany
Dimethyl sulfoxide (DMSO)	Roth, Germany
DMEM powder	Thermo Fisher Scientific, USA
DNase	Roche, Switzerland
DPBS (10x) without $CaCl_2$ and $MgCl_2$	Thermo Fisher Scientific, USA
EDTA	Roth, Germany
Fetal calf serum (FCS)	Merck, Germany
Glycogen	Roche, Switzerland
G-418 sulfate solution	Capricorn Scientific, Germany
HEPES	Thermo Fisher Scientific, USA
Horse serum	Merck, Germany
Hydrochloric acid (HCl)	Roth, Germany
Incomplete Freund´s Adjuvant (IFA)	BD Biosciences, USA
Recombinant Rat Interferon γ	Peprotech, USA
Isofluorane	Abbott, USA
Isopropanol	Roth, Germany
Isotonic saline solution (NaCl, 0.9 %)	B. Braun, Germany
Liberase	Roche, Switzerland
Lymphocyte separation medium 1077 (LSM1077)	PromoCell, Germany
Ketamine	Medistar, Germany
M tuberculosis	BD Biosciences, USA
Paraformaldehyde (PFA)	Roth, Germany
Puromycin	Thermo Fisher Scientific, USA
Recombinant rat TNF a	Peprotech, USA

TRI Reagent	Merck, Germany
Trypsin-EDTA solution (10x)	Merck, Germany
qPCR Mastermix	Eurogentec, Belgium
Xylazine	Ecuphar, Belgium
Nuclease-free water	Thermo Fischer Scientific, USA

3.1.3 Antigens and adjuvants

Myelin basic protein (MBP) Isolated from guinea pig brains	In-house production
Ovalbumin (OVA) from chicken egg white	Merck, Germany
Ovalbumin 323-339 peptide (OVA, ISQAVHAAHAEINEAGR)	Peptide facility, Charitè Hospital, Berlin
Rat beta synuclein 93-111 peptide (bSYN, LKPEEVAQEAAEEPLIEPL)	Peptide facility, Charitè Hospital, Berlin
Complete Freund´s Adjuvant (CFA, stock)	40 mg *M. tuberculosis* H37Ra (BD Biosciences, USA) 10 ml Incomplete Freund´s Adjuvant (IFA) (BD Biosciences, USA)

3.1.4 Antibodies

Table 1: Primary and secondary antibodies used in this study

Antibody	**Fluorophore**	**Clone**	**Dilution**	**Brand**
Mouse IgG1anti-rat CD8a	PE	OX-8	1:200	BioLegend, USA
Mouse IgG1 anti-rat RT1B	FITC	OX-6	1:200	BD Biosciences, USA
Mouse IgG1 anti-rat αβTCR	AF647	R73	1:200	BioLegend, USA
Mouse IgG2a anti-rat CD11b/c	PE	OX-42	1:200	BioLegend, USA
Mouse IgG2a anti-rat CD11b/c	AF647	OX-42	1:200	BioLegend, USA
Mouse IgG1 anti-rat CD45RA	PE	OX-33	1:200	BioLegend, USA
Mouse IgG1 anti-rat CD31	PE	TLD-3A12	1:100	BD Biosciences, USA
Mouse IgG1 anti-rat CD4	PE/Cy7	W3/25	1:200	BioLegend, USA
Mouse IgG1 anti-rat CD45	PerCP	OX-1	1:200	BioLegend, USA
Mouse IgG1 anti-rat CD45	AF647	OX-1	1:200	BioLegend, USA
Mouse IgG1 anti-rat CD25	-	OX-39	1:150	Bio-Rad, USA

Mouse IgG1 anti-rat CD134	-	OX-40	1:150	Bio-Rad, USA
Mouse IgG1κ isotype control	-	MOPC 31C	1:150	Sigma-Aldrich, USA
Mouse anti-rat-CD43	-	W3/13	1:200	BioRad, USA
Mouse anti-rat CD68	-	ED1	1:200	BioRad, USA
Rabbit anti-Lyve1	-	-	1:300	Origene, Germany
Goat anti-mouse IgG (H+L)	AF647	Polyclonal	1:200	Jackson IR, USA
Goat anti-mouse IgG (H+L)	AF647	-	1:200	Invitrogen, USA
Goat anti-rabbit IgG	AF647	-	1:500	Invitrogen, USA

3.1.5 List of Primers

Table 2: List of TaqMan primers used in this study

Gene (*Abbreviation*)	**Forward primer (5´-3´)**	**Reverse primer (5´-3´)**	**Probe (FAM-5´-3´-TAMRA)**
β-actin (*Actb*)	GTACAACCTCCTTGCAGCTCCT	TTGTCGACGACGAGCGC	CGCCACCAGTTCGCCATGGT
Interferon gamma (*Ifng*)	AACAGTAAAGCAAAAAAGGATGCATT	TTCATTGACAGCTTTGTGCTGG	CGCCAAGTTCGAGGTGAACAACCC
Interleukin-17A (*Il17a*)	GAGTCCCCGGAGAATTCCAT	GAGTACCGCTGCCTTCACTGT	ATGTGCCTGATGCTGTT
Vascular cell adhesion protein-1 (*Vcam1*)	ACATGAGGGTGCTCCTGTGA	GGTGGCATTTCCCGAGAGGA	TGTGCCAGCGAGGGTCTACCAGCTCCT
Fibronectin (Fn1)	TGATCTTTGAGGAACATGGCTTT	GCAGGTATGGTCTTGGCCTAAG	AACCACGCCACCCACTGCGG
Intercellular adhesion molecule-1 (*Icam*)	GGAGACAGCAGACCACTGTGCTT	CTCGCTCTGGGAACGAATACA	ACTGTGGCACCACGC
Claudin-5 (*Cldn5*)	CGGGCGTCCAGAGTTCAGT	TAGACGTAGTTCTTCTTGTCGTAATCG	CCAGTCAAGTACTCAGCACCAAGGCGA
Occludin (*Ocln*)	CCTAATGTGGAAGAGTGGGTTAAAAA	GTCGACTCTTTCCGCATAGTCA	CACACAAGACATGCCTCCACCCCC
Chemokine (C-X-C motif) ligand 9 (*Cxcl9*)	TTG CCC CAA GCC CTA ACT G	ACC CTT GCT GAA TCT GGG TCT AG	CAT CGC TAC ACT GAA GAA CGG AGA TCA
Chemokine (C-X-C motif) ligand 10 (*Cxcl10*)	CGT GCT GCT GAG TCT GAG T	GTC TCA GCG GCT GTT CAT	CTC AAG GGA TCC CTC TCG CAA GAA C
Chemokine (C-X-C motif) ligand 11 (*Cxcl11*)	GGT TCC AGG CTT CGT TAT GTT C	AAC TTC CTT GAT TGC TGC CAT T	CTG TCT TTG CAT CGA CCG CGG AGT

3.1.6 Kits

RevertAid First Strand cDNA Synthesis Kit	Thermo Fisher Scientific, USA

3.1.7 Equipment and consumables

3.1.7.1 Equipment

Animal Ventilator	Harvard Apparatus, USA
Cryobox	Nalgene, USA
Dounce homogenizer	Kimble Chase, USA
Drill	Foredom, USA
Gas Monitor (S5)	Ohmeda (GE Healthcare), USA
Metal cell strainer (40 µm)	UMG technical workshop, Germany
Multichannel pipette	StarLab, Germany
Pipettes (2.5; 10; 20; 100; 200; 1000 µl)	Eppendorf, Germany
Pipetus	Hirschmann, Germany
Syringe pump	B. Braun, Germany
Thermometer (West 6100)	West Control Solutions, USA
Stereotaxic manipulator (SR-5R-HT)	Narishige, Japan
Surgical instruments	Fine surgical tools (FST), Germany
Tuberculin glass syringes	Poulten & Graf, Germany

3.1.7.2 Consumables

Cell strainers (40 µm, 70 µm)	Greiner Bio-One, Austria / Germany
Cannulas (18G, 20G, 24G, 26G)	B. Braun, Germany
Reaction tubes (0.2, 1.5, 2 ml)	Sarstedt, Germany
Conical Falcon tubes (15, 50 ml)	Greiner Bio-One, Austria / Germany
Pipette tips (10, 100, 200, 1000 µl)	StarLab, Germany
Pipette filter tips (10, 100, 200, 1000 µl)	StarLab, Germany
Parafilm	Pichiney Plastic Packaging, USA
Cell culture plates (12-, 24-, 96-well)	Thermo Fisher Scientific, USA
qPCR plates	StarLab, Germany
Petri dishes (5, 10 ml)	Greiner Bio-One, Germany
Flasks (25 mm2 and 75 mm2)	Starstedt, Germany

Surgical sutures	B. Braun, Germany
Syringes (insulin syringes, 1, 5, 10 ml)	B. Braun, Germany
FACS tubes	BD Biosciences, USA

3.1.8 Instruments and machines

Axiovert 200M fluorescence microscope	Zeiss, Germany
Axiovert 40C binocular microscope	Zeiss, Germany
Centrifuge 5415 R	Eppendorf, Germany
CytoFLEX S	Beckman Coulter, USA
Dissection stereomicroscope	Leica, Germany
EV231 Power supply	Consort, Belgium
FACSAria II	BD Biosciences, USA
FACSCalibur	BD Biosciences, USA
Heracell 240 Incubator	Heraeus, Germany
Laminar flow hood	Heraeus, Germany
Mastercycler Nexus Gradient	Eppendorf, Germany
Multifuge 1 S-R	Heraeus, Germany
NanoDrop-ND1000	Thermo Fisher Scientific, US
Olympus FVMPE-RS Laser Scanning Microscope	Olympus, Japan
StepOnePlus Real-Time PCR System	Applied Biosciences, USA
Zeiss Laser Scanning Microscope 710	Zeiss, Germany

3.1.9 Software

CorelDraw (2017)	Corel Corporation, Canada
CytExpert (Version 2.40.28)	Beckman Coulter, USA
Endnote (Version 8.2)	Clarivate Analytics, USA/UK
FACSDiva Software (Version 8.0.1)	BD Biosciences, USA
FlowJo (Version 10)	FlowJo LCC, USA
GraphPad Prism (Version 9)	GraphPad, USA
Imaris x64 (Version 9.3.1 and 8.0.2)	Bitplane, USA
Microsoft Office (2016)	Microsoft, USA
RStudio (Version 1.1.463)	RStudio, USA

StepOnePlus Software (Version 2.0)	Applied Biosciences, USA
R (Version 3.6.0)	R Core Team
Zeiss ZEN (Version 8.1.11.484)	Zeiss, Germany

3.2 Methods

3.2.1 Animals

Wild-type (wt) rats, transgenic (tg)-bSYN animals (carrying in their immune repertoire more than 95% of T cells reactive against beta-synuclein)[20] both on a LEW/Crl background (*Rattus norvegicus*) were bred at the animal facility of the University Medical Centre Göttingen (UMG, Germany).

Breeding pairs of Prox-1-eGFP transgenic rats on a Sprague-Dawley background[149] were kindly provided by Young-Kwon Hong (University of Southern California, Los Angeles, California, USA). The animals were back-crossed to LEW/Crl background in the UMG facility for at least 5 generations before being used in experiments.

The animals were kept in GR9000 IVC cages under specific pathogen-free (SPF) conditions on a 12-hour light-dark cycle and *ad libitum* access to food and drink.

No differences in experimental outcome were noted between the sexes.

All experiments were performed in accordance with the local regulations of animal welfare of Lower Saxony, Germany.

3.2.2 Generation and culture of primary T cell lines

Rat $CD4^+$ T cells reactive against MBP, OVA or bSYN (T_{MBP}, T_{OVA} and T_{bSYN} cells, respectively) were generated and retrovirally engineered to express either fluorescent proteins (mTurquoise, eGFP or tdTomato) or a NFAT reporter (NFAT-YFP/Cherry-H2B) as previously described.[18,20,27] Briefly, 6-8 week old female wild type (for T_{MBP} or T_{OVA} cell lines) Lewis rats or tg-bSYN animals (for T_{bSYN} cells) were shortly anesthetized with diethyl ether and immunized subcutaneously with an emulsion of 1:1 complete Freund's adjuvant (CFA) containing *Mycobacterium tuberculosis* extract (BD Biosciences) at a concentration of 2 mg/ml and the selected antigen (bSYN, MBP or OVA; stock concentration: 1 mg/ml). The immunization paste was emulsified in tuberculin glass syringes (Poulten & Graf). A total of 150 µl was injected subcutaneously at the base of the tail (50 µl each side) and into the popliteal cavities (25 µl each side). After 7 (for T_{bSYN} cells) or 9 days (for T_{MBP} and T_{OVA} cells), animals were sacrificed by CO_2 asphyxiation and draining lymph nodes (popliteal, inguinal and para-aortal) were collected and passed through a 40 μm^2 metal cell strainer. The cell suspension was co-cultured with GP+E86 packaging cell lines producing replication-deficient retroviruses expressing a G-418 (for eGFP cells) or Puromycin (for tdTomato, mTurquoise or NFAT cells) resistance cassette. To this aim, the packaging cells had been previously expanded in 75 mm^2

flasks in T cell medium (TCM) containing 10 % FCS at 5 % CO2 and 37 °C. Subsequently, the GP+E86 cell were resuspended in restimulation medium (RM) and plated in U-bottom 96-well plates at a concentration of 1.5 x 10^6 per plate. Six hours later, the lymph node cell suspension was added to each well at a concentration of 20 x 10^6 (for T_{MBP} or T_{OVA} cell lines) or 7-10 x 10^6 (for T_{bSYN} cells) per plate. Depending on the antigen used for immunization, MBP, OVA or bSYN antigens were added at a concentration of 20 µg/ml (for T_{MBP} or T_{OVA} cell lines) or 10 µg/ml (for T_{bSYN} cell line). Cells were incubated at 10 % CO2 and 37 °C for 2 days, then, 50 µl of T-cell growth factor medium (TCGF) were added to each well. One or two days later, cells were transferred into flat bottom 96-well plates and T cell selection was started by adding TCGF supplemented with the appropriate antibiotic (G-418 at 0.4 mg / ml or Puromycin at 0.5 µg/ml). Six (D6, for T_{bSYN} cells) or seven (D7, for T_{MBP} or T_{OVA} cell lines) days after initial stimulation, T cells were re-stimulated. To this end, 100 µl of supernatant were carefully removed from each well and 100 µl RM, containing 1.4 x 10^6 irradiated thymocytes, the cognate antigen (10 µg/ml for T_{MBP} or T_{OVA} cell lines; or 5 µg/ml for T_{bSYN} cell line), and the selection antibiotic, were added to the culture. Two days later, 50 µl TCGF with the selection antibiotic were added to each well. Cell wells were then selected according to cell number and fluorescence brightness, indicative of transduction efficiency, and pooled into 10 cm^2 Petri dishes. On D6-7 post-stimulation, T cells were re-stimulated with irradiated thymocytes (70 x 10^6 cells per 3.5 x 10^6 T cells) and selection antibiotic. The above-described 6/7-day T cell restimulation cycle could be repeated, on average, up to 4 times. From the second re-stimulation, T cells could be frozen. To this end, 20 x 10^6 T cell blasts (D2 after stimulation) or resting T cells (D5-6 after stimulation) were centrifuged at 290xg and 4 °C for 6 min. The pellet was resuspended in 1.5 ml freezing medium (FM), transferred into freezing vials and cooled down to -80 °C in cryoboxes (Nalgene). Frozen cells could then be thawed to be adoptively transferred, in the case of T cell blasts, or further restimulated or amplified, in the case of resting T cells.

3.2.3 Experimental autoimmune encephalomyelitis (EAE)

3.2.3.1 Adoptive transfer EAE

EAE was induced in wild type Lewis rats by intravenous (i.v.) injection of fully activated T-cell blasts (two days after restimulation) resuspended in EH. Unless otherwise stated, the number of transferred T cells per animal was the following: T_{bSYN} cells: 2-3x10^6, T_{MBP} cells: 5x10^6; T_{OVA} cells (non-pathogenic): 5x10^6 cells.

Chronic EAE was induced as described.[20] Briefly, tg-bSYN animals were subject to repeated transfers of either $2x10^6$ T_{bSYN} cell blasts or $5x10^6$ T_{OVA} cells, which served as control. Upon each transfer, the animals transferred with T_{bSYN} cells developed a paralytic disease. The severity of the symptoms was comparable between bouts. On average, each bout of disease was induced 3- 4 weeks apart from the previous, when the animals had fully recovered.

3.2.3.2 Clinical scoring

Animals were monitored daily by measuring their weight and scoring disease progression. Classical signs of EAE were scored as follows: 0 = no disease; 1 = flaccid tail; 2 = gait disturbance; 3 = complete hind limb paralysis; 4 = tetraparesis; 5 = death. For atypical symptoms the following classification was used: 0 = no disease; 1 = occasional twitches and scratching with or without flaccid tail; 2 = frequent twitches and scratching, ataxia; 3 = severe tonic and myoclonic movements, severe gait impairment; 4 = tetraparesis; 5 = death.
Animals with a score greater than 3 were sacrificed.

3.2.4 Organ retrieval and processing

Animals were sacrificed by intramuscular injection of a lethal dose of ketamine/xylazine, i.e. 30 mg/kg xylazine (Ecuphar) combined with 150 mg/kg ketamine (Medistar). Blood samples were drawn by heart puncture in EDTA-moistened syringes. Cerebrospinal fluid (CSF) was collected from the cisterna magna using a stereotactic device. Animals were then perfused through a peristaltic pump for 6 minutes with ice-cold phosphate buffer solution (PBS) plus heparin. Their organs were then isolated and processed as follows:

3.2.4.1 CNS parenchyma and meninges

Brain parenchyma and leptomeninges were removed by surgical dissection. Then the brain dura of the hemispheres, sagittal and transversal sinuses and basicranium was detached from the skull, after removing any visible remnants of optical nerves, epiphysis and hypophysis. When required, the dura of the cranial vault was separated into hemispheric dura and sinuses under a dissection microscope (Leica) (**Figure 11**). Sagittal and transverse sinuses were pooled and processed together. Leptomeninges were separated from the brain parenchyma under a dissection microscope. Spinal cord dura and leptomeninges were separated from the spinal cord parenchyma under a dissection microscope. The spinal nerve roots were removed from the

spinal cord dura with a pair of fine tweezers. To avoid contamination of the dura by the lumbosacral roots, the sacral part of the spinal cord was discarded.

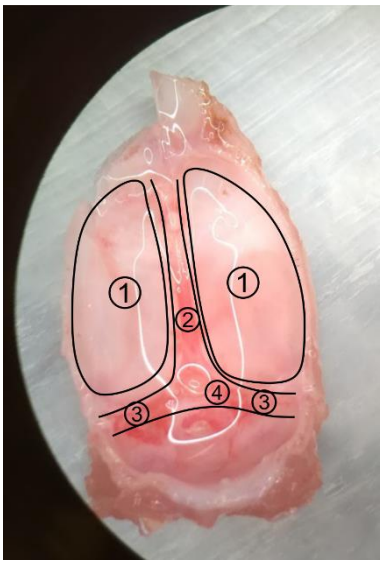

Figure 11: Overview of the different areas of the dura. Representative sample of the hemispheric and sinus dura still attached to the skull cap. Under a dissection microscope, the following regions of the dura were identified and dissected: hemispheric parietal dura (1), dura sagittal sinus (2) and transverse sinuses (3). The epiphysis (4) was removed prior to dissection.

Brain and spinal cord parenchyma were passed through a cell strainer (40-µm^2) and myelin debris were removed by a Percoll-density gradient (30 min at 700xg and 4 °C with minimal break). The pellet was washed once in PBS and resuspended in a definite volume of EH medium.

Dura and leptomeninges were first minced into small pieces, collected in 5 ml EH and centrifuged at 290xg for 5 min. The supernatant was removed and tissue fragments were suspended in either 500 microliters of 0,15% collagenase II from *C histolyticum* (Sigma) plus 60 U ml^{-1} of DNase1 (Roche) in EH or, for endothelial cell isolation and antigen presentation assay, in 0.41 U ml^{-1} of Liberase TM (Roche) and 60 U ml^{-1} of DNase1 in EH. The suspension was kept at 37° for 30-40 min and resuspended every 5 minutes. Afterwards, the cell suspensions were diluted in EH + EDTA 2mM and filtered through a 40-µm^2 cell strainer. Myelin debris were removed by a Percoll-density gradient (30 min at 700xg and 4 °C), the pellet was washed once in PBS and resuspended in a definite volume of EH medium.

3.2.4.2 Lymph nodes

Inguinal (ingLNs) and deep cervical lymph nodes (dcLNs) were isolated by following anatomical reference points: inguinal lymph nodes became immediately visible upon a superficial midline incision along the ventral surface of the abdomen and retraction of the skin flaps. Deep cervical, CSF-draining, lymph nodes were at first identified by intrathecal (i.t.) injection of Evans Blue (**Figure 12**). After a superficial incision of the neck, retraction of the submandibular glands and sternomastoid muscle, dcLNs were located laterally to the

sternohyoid muscle. Lymph nodes were then mashed through a metal cell strainer (40-µm^2) and centrifuged at 290xg for 6 min at 4 °C. The cell pellet was then dissolved in EH medium.

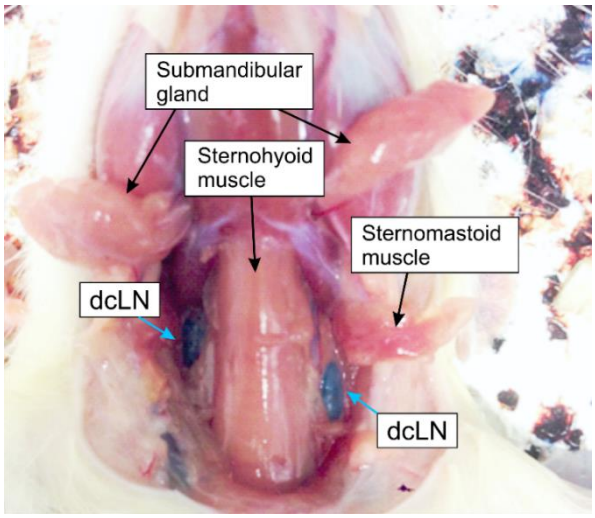

Figure 12: Identification of dcLNs and anatomical reference points employed during dissection. The CSF-draining dcLNs were identified by injecting Evans blue i.t. 5 minutes prior. The dcLNs appeared as Evans-blue positive oblong structures, typically one on each side of the sternhyoid muscle, right underneath the sternomastoid muscle.

3.2.4.3 Spleen

The spleen was removed by cutting open the peritoneal cavity and resecting the splenic hilum. The organ was mashed through a metal cell strainer (40-µm^2) and centrifuged at 290xg for 6 min at 4 °C. Erythrocytes were lysed by incubation for 5 min in 5 ml of ACK buffer on ice. The sample was then filled up with ice-cold PBS (45 ml), spun down and collected in 5 ml EH medium.

3.2.4.4 Blood

To isolate circulating leukocytes, first, blood samples were diluted 1:1 with PBS, then Lymphocyte Separation Medium 1077 (PromoCell) was laid underneath the sample with a 70 mm long 20 G needle (Sterican) at a 4:1 concentration. Blood was then centrifuged for 30 min at 840xg at 20°. The obtained interphase was collected and washed once with ice-cold PBS. The cell pellet was incubated for 2 min in 1 ml of ACK buffer on ice in order to lyse erythrocytes. Lysis was stopped with ice-cold PBS, then the sample was pelleted by centrifugation and resuspended in EH medium.

3.2.5 Flow cytometry

3.2.5.1 Cell staining

Single cell suspensions, prepared as previously described, were transferred to a V-bottom 96-well plate (Thermo Fischer Scientific). Cells were pelleted by centrifugation for 3 min at 4 °C and 300xg. The pellet was washed with PBS, spun down and resuspended in FACS buffer + 3% rat serum and incubated on ice for 20 minutes. The cells were then spun down, resuspended in primary antibody mixes diluted in FACS buffer and incubated on ice protected from light for 30 minutes. Cells were then washed once in FACS buffer and taken up in 100 µl FACS

buffer. If the staining required a secondary antibody, cells were washed twice in FACS buffer, incubated for 20 minutes with the secondary antibody, washed twice with FACS buffer and then taken up in 100 µl FACS buffer. The following antibody clones were employed: RT1B-FITC (clone OX-6, BD Biosciences), CD11b/c-PE and CD11b-AF647 (clone OX-42, BioLegend), αβTCR-AF647 (clone R73, BioLegend), CD45-AF647 and CD45-PerCP (clone OX-1; BioLegend), CD45RA-PE (clone OX-33; BioLegend), CD8α-FITC (OX-8; BioLegend), CD31 (clone TLD-3A12, Bio-Rad), CD4-PE/Cy5 (W3/25; BD Biosciences). Mouse IgG1κ (MOPC 31C, Sigma-Aldrich) served as isotype control; CD25 (clone OX39, non-conjugated, BioRad), CD134 (clone OX40, non-conjugated, BioRad). For non-conjugated anti-CD25 and anti-CD134 antibodies, APC-labeled anti-mouse IgG antibody (Jackson) was used as secondary antibody. Antibody dilutions are indicated in **Table 1**.

3.2.5.2 Flow cytometry cell quantification

Cytofluorometric quantification of fluorescent T cells or antibody-stained immune cell populations was performed by relating the number of cells to a predefined absolute amount of Calibrite APC fluorescent beads (BD Biosciences). The samples were acquired using a FACSCalibur (BD Biosciences) or CytoFLEX S (Beckman Coulter). Data analysis was performed using FlowJo (BD Biosciences). Gating strategies are indicated in **Figure 13**.

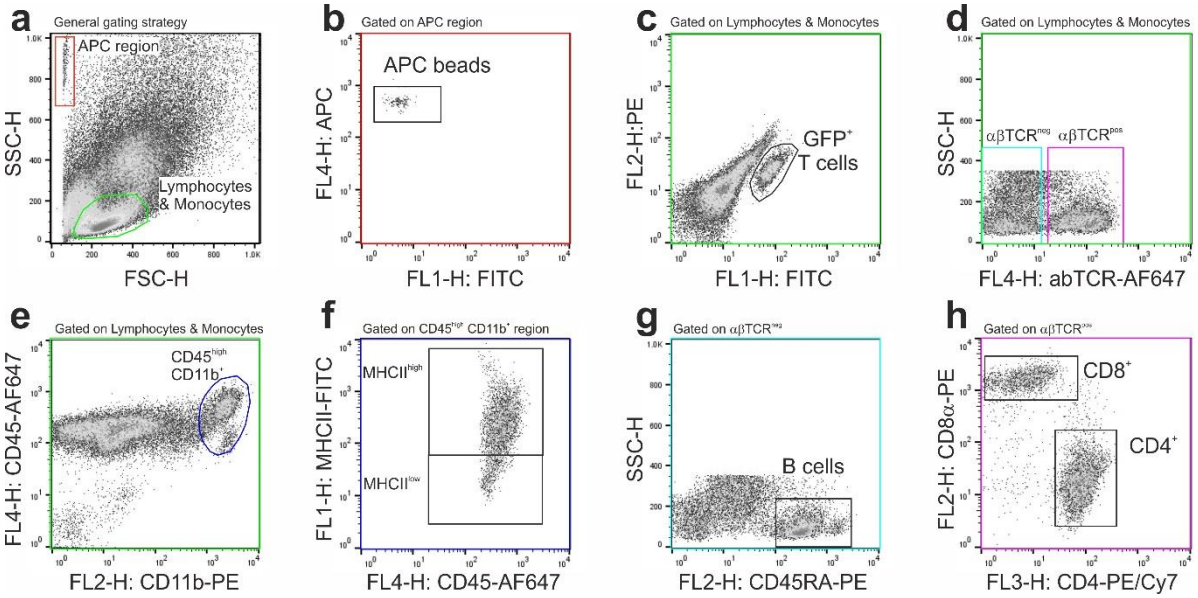

Figure 13: Gating strategy for FACS quantification of different immune cell populations. (a-h) Representative gating strategies for the quantification of different immune cell types. (a) Physical parameter gating strategy to distinguish lymphocytes and monocytes from APC beads. (b) Gating for APC beads. (c) Gating for fluorescently labeled (here GFP) T_{bSYN}, T_{MBP} or T_{OVA} cells. (d-h) Gating strategies for the identification of (d) αβTCR$^+$ T cells, (e,f) CD45^{high} CD11b$^+$ myeloid cells and their MHCII^{high} and MHCII^{low} subgroups, (g) αβTCR^{neg} CD45RA$^+$ B cells, (h) αβTCR$^+$ CD8$^+$ and αβTCR$^+$ CD4$^+$ T cells. The gating strategy is color-coded: identical colors of gate and frame indicate parent population and subpopulation, respectively. The antibodies used for cell surface stainings are indicated in **Table 1**.

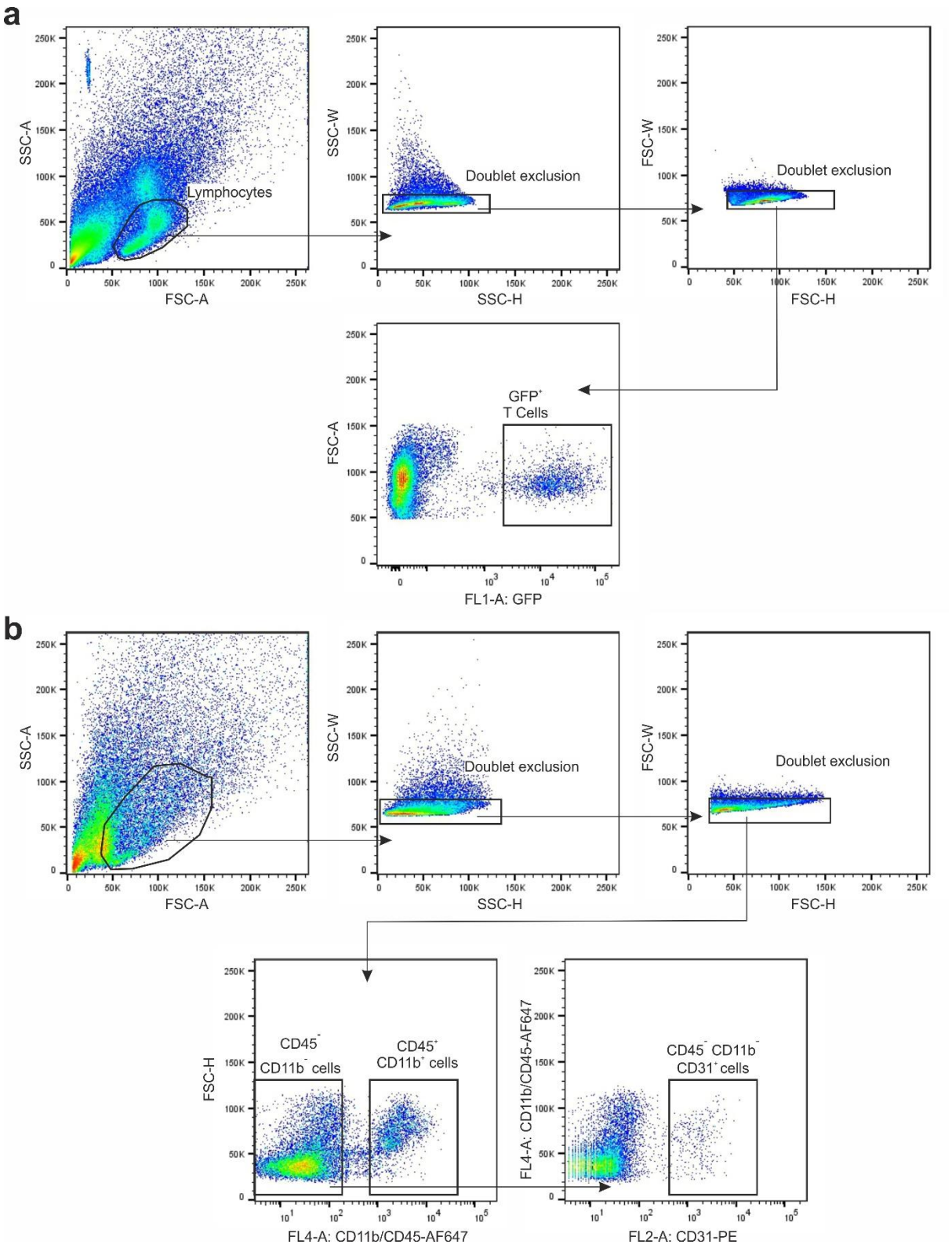

Figure 14: Gating strategy for FACS sorting of fluorescently labeled T cells and endothelial cells. (a, b) Representative gating strategies employed for FACS sorting of (a) fluorescently labeled (here in the example GFP) T_{bSYN} cells and (b) endothelial cells. The antibodies used for cell surface stainings are indicated in **Table 1**.

3.2.5.3 Flow cytometry cell sorting

Endogenously fluorescent T cells and antibody-labelled $CD11b^-$ $CD45^-$ $CD31^+$ endothelial cells were sorted using a FACSAria 4L SORP cell sorter (BD Biosciences). Prior to sorting, each sample was filtered through a 40-μm^2 filter and kept on ice. Samples were sorted at a low flow rate in a collecting tube containing ice-cold EH. The amount of cells sorted varied according to the tissue of origin and disease phase. Whenever possible, we sorted equal amounts of cells from each compartment.

On average, 300 – 5000 T cells or 300 – 3000 endothelial cells were sorted for further qPCR experiments. In case T cells or endothelial cells were sorted for next-generation sequencing (NGS), single cell suspensions of 4-6 animals were pooled. The sorted cells were rapidly spun down 1000xg at 4 °C for 4 min and the pellet was resuspended in 200 µl TRI reagent (Merck) and 1 µl glycogen (Roche). The samples were stored at -80 °C until further processing.

Gating strategies for the sorting procedure are indicated in **Figure 14**.

3.2.6 RNA isolation, cDNA synthesis and quantitative real-time PCR

RNA from sorted cells or total tissue, preserved in TRI reagent, was extracted by phase separation with chlorophorm and subsequent isopropanol precipitation. The RNA pellet was solubilized in 12 µl of nuclease-free water (Thermo Fischer Scientific) and stored at -80°. When required, reverse transcription of the sample into cDNA was performed with the RevertAid First Strand cDNA synthesis kit (Thermo Fischer Scientific) according to manufacturer's instruction. To perform quantitative PCR (qPCR), cDNA from sorted cells samples was diluted 1:10 (if the cells sorted were less than 5000) or 1:20 (if the cells sorted were more than 5000), while cDNA from total tissue was diluted always 1:30. qPCR was performed on a Real-Time PCR system (StepOnePlus, Applied Biosystems) with target-specific TaqMan probes quenched with TAMRA and labeled with FAM. Beta-actin served as house-keeping gene. All measurements were performed in duplicates and the difference in the CT values between the individual measurements did not exceed 0.5 amplification cycles. The combinations of primers and probes used have previously been described[25,28] and are listed in **Table 2**.

3.2.7 Next-Generation Sequencing of sorted T cells and endothelial cells

As previously indicated, total RNA was purified using the TRIzol protocol from two set of samples:

1) $CD11b^{-}$ $CD45^{-}$ $CD31^{+}$ endothelial cells isolated *ex vivo* (10000–20000 cells/replicate) from brain dura and brain leptomeninges of naïve animals.

2) T_{bSYN} cells isolated from brain (dura, leptomeninges and parenchyma), blood, CSF, ingLNs and dcLNs on day 3 p.t. . Between 10000–100000 T_{bSYN} cells were sorted from each sample.

All the samples were sorted with more than 98 % purity. Three to 4 different biological replicates were prepared for each sample and 3- 5 animals were pooled for each sample.

RNA extraction, cDNA library preparation, and RNA sequencing was undertaken as described.[28] Library preparation for RNA-seq was performed using the TruSeq RNA Sample Preparation Kit (Illumina, Cat. N°RS–122–2002) starting from 100-500ng of total RNA. Single read (45 bp) sequencing was conducted using a HiSeq 2000 (Illumina). Fluorescence images were transformed to BCL files with the Illumina BaseCaller software. Samples were demultiplexed to FASTQ files with CASAVA. Sequencing quality was checked and approved via the FastQC software. Sequences were aligned to the genome reference sequence of Rattus norvegicus using the STAR alignment software[150] allowing for 2 mismatches within 45 bases. Subsequently, conversion of resulting SAM files to sorted BAM files, filtering of unique hits and counting was conducted with SAMtools[151] and HTSeq[152]. Data was preprocessed and analyzed in the R/Bioconductor environment using the DESeq2 package[153]. Gene annotation was performed using *Rattus norvegicus* entries from Ensembl v78 via the biomaRt package[154]. The Transcriptome and Genome Analysis Laboratory (TAL) of the University Medical Center Göttingen (UMG), under supervision of Dr. Gabriela Salinas, performed all the above-mentioned procedures**.**

Additional statistical analysis and graphical depiction was performed by Michael Haberl using Microsoft Excel and GraphPad Prism. Principal component analysis (PCA), gene counts and cluster analysis were performed by Michael Haberl using R.

3.2.8 Intravital two-photon laser scanning microscopy (TPLSM)

3.2.8.1 Surgical procedure

Animals were anaesthetized with 10 mg/kg xylazine combined with 50 mg/kg ketamine. Animal preparation was performed according to a protocol established in the laboratory.[25,155] Briefly, animals were intubated via a small incision of the trachea with an 18G cannula (B. Braun) and immediately attached to a ventilator (Harvard Apparatus) with 1.5–2% isoflurane and 50-60% O_2. Both inspired and expired air was monitored via a gas monitor (Ohmeda). Animals were stabilized in a custom-made microscope stage; their body temperature was

measured through a rectal thermometer (West Control Solutions) and maintained at 37-37.5°C via a heated pad connected to a thermo-controller. An i.v. catheter (B. Braun) was placed in the rat tail-vein to allow injection of tracers during imaging and continuous hydration through a Perfusor device (B. Braun) at a 0.6 ml/h rate with 0.9% NaCl saline solution.

Imaging of the dura was performed through a thinned-skull cranial window.[156] To this end, the parietal, interparietal and frontal bones of the skull were accessed by a midline incision along the scalp. The skull was then fixed with dental paste to a custom-made head-holder. Drilling was performed with a 2-mm drill head (Foredom) onto the parietal bone, roughly following the coordinates of x= +1.5 mm and y= -1.5 mm from bregma. To minimize friction-induced heating of the skull and underlying structures, the imaging window was continuously irrigated with ice-cold 0.9% NaCl solution. Drilling was performed until the bone vessel layer was reached, then, the final polishing were performed manually with a sharp arc blade until dural vessels became visible through the thinned skull. At this point, an agarose ring was created around the imaging field to allow continuous hydration of the thinned skull and objective immersion. To minimize potential imaging artefacts caused by drilling-induced transient vasodilation of the dural vessels, imaging was performed after a rest period of a minimum of 60 min, as recommended.[157]

The underlying leptomeningeal vessels could be visualized either through the same thin skull window or through an open skull window as previously described.[20] Briefly, drilling was performed to create an ellipsoid area of thinned bone between the coronal, transverse and sagittal suture. The thinned ellipsoid was removed by carefully drilling with a 0.5 mm drill burr head, until a superficial break in the bone was visible. The bone flap was then carefully removed and the periosteal layer of the dura was then peeled away with a pair of fine tweezers. Tissue was constantly irrigated with saline solution to prevent dehydration. The open skull window did not affect T cell motility parameters compared to the thinned skull window.

For intravascular studies, venules were identified according to size and direction of blood flow. Vessels of comparable diameter were analyzed.

Imaging of the dura lymphatics was performed in Prox-1-eGFP transgenic rats through a thinned-skull window at the sinus confluence and transverse sinuses. To access the lymphatic vessels, drilling was performed along the lambdoid and sagittal sutures until the dural sinuses became visible through the tinned bone. When the density of the bone around the sutures did not allow visualization of the underlying vessels, the bone was further cleared and polished by applying locally a 12% EDTA solution for 5 minutes. Prox-1-eGFP-positive lymphatic vessels

were located under the fluorescence microscope based on their expected anatomical location (along the dural sinuses) and subsequently imaged.
Whenever traumatic hemorrhages in the dural vessels occurred, the imaging window was discarded.

3.2.8.2 Technical equipment and labelling procedures

TPLSM imaging was performed with the following equipment: (1) Zeiss Laser Scanning Microscope 710 with a Coherent 10 W Ti:Sapphire chameleon laser (Coherent), controlled by Zeiss ZEN 2012 software; and (2) Olympus FVMPE-RS TPLSM combined with a Spectra-Physics Mai Tai Ti:Sapphire oscillator and a Mai Tai DeepSee Ti:Sapphire oscillator. The excitation wavelength was tuned to 880 nm, 1010 nm or 1100 nm and routed through a 20× water 1.0 numerical aperture (NA) immersion objective W Plan Apochromat (Carl Zeiss) for the Zeiss system or a 25× water 1.05 NA immersion objective Olympus Scaleview for the Olympus system. Excitation at 1100 nm was generated by either a Ti:Sapphire laser pumped optical parametric oscillator (OPO) in the Zeiss TPLSM or a Mai Tai DeepSee Ti:Sapphire oscillator in the Olympus TPLSM. Laser intensity was kept at a minimum to avoid phototoxicity (typically around 10-15% of laser power). Emitted fluorescence was detected using non-descanned detectors equipped with 442/46 nm, 483/32 nm and 624/40 nm band-pass filters. On average, scanning areas were 424.27 μm × 424.27 μm (Zeiss) or 508.93 μm × 508.93 μm (512 × 512 pixels, Olympus). Stack height ranged between 50 μm (for imaging of either the dura or the meninges) and 150 μm (for imaging the dura and the leptomeninges together in the same video). For overviews, several tile scans were acquired sequentially and stitched together. To allow reproducible motility analyses, the interval time for stack acquisition was kept at 32 s, with a total acquisition time of 30 min per video. Blood vessels were labeled by i.v. injection of 70 KDa or 2000 KDa dextran just before the imaging session. For evaluation of the BBB permeability, 3 KDa dextran was injected i.v. through a tail vein catheter directly during the imaging session. Collagen was detected by TPLSM-generated second-harmonic signals. When required, dural phagocytes were labelled by 3KDa dextran injected i.v. 12 hours prior the imaging session. To differentiate dural from leptomeningeal macrophages, the latter were visualized by i.t. injection of a SeTau647-labelled anti-CD11b antibody 12 hours before the imaging session. Procedural details for i.t. injections can be found at section 3.2.10.

3.2.8.3 In vivo blockade of integrin signaling

In order to block integrin signaling on intravascular T cells in vivo, a neutralizing mouse anti-rat monoclonal antibody directed against VLA-4 (anti-CD49d, clone TA-2)[158] was injected i.v. during the imaging session at a single dose of 100 µg. The antibody was kindly provided by Prof. Thomas Issekutz (Grace Health Center, Dalhousie University, Halifax, Canada).

3.2.8.4 In vivo blockade of CXCL9-11 signaling

In order to block chemokine CXCL9-11 signaling on intravascular T cells in vivo, a neutralizing Hamster anti-rat CXCR3 antibody (clone XR3.2, courtesy of Prof. Thomas Issekutz, Grace Health Center, Dalhousie University, Halifax, Canada) was administered i.v. at a dose of 4 mg/kg. The effective dosage was previously established in the laboratory by Dr. Christian Schläger and Michael Haberl.

3.2.8.5 Genetic deletion of CXCR3 signaling on T cells

To further characterize the effect of CXCR3 signaling on the motility of T cells in the dura and leptomeningeal vessels, T_{OVA} cells with a genetic deletion of the CXCR3 gene via CRISPR-Cas9 were employed. T_{OVA} cells established with a guide-RNA targeting an irrelevant sequence in the Rosa26 locus were co-injected as controls. The cells were generated and functionally tested in the laboratory by Michael Haberl.

3.2.8.6 Evaluation in vivo of dura vessel responsiveness to inflammatory stimuli and of dura antigen presentation capacity

To test the responsiveness of the dura vessels to inflammatory stimuli in steady state conditions, CNS-ignorant effector T cell blasts (T_{OVA} cells) were injected i.v. in wild-type rats. On day 2.5-3 post transfer (p.t.), TPLSM was performed. The dura window was prepared as described and TPLSM was performed as described in two selected imaging areas. Afterwards, 200 µg recombinant rat IFNγ (Peprotech, MW: 15.6 KDa) and 200 µg recombinant rat TNFα (Peprotech, MW: 17.3 KDa) were dissolved in 500 µl PBS and applied directly on the thinned skull of the imaging window. Imaging was carried out for the next 210 minutes in the two selected spots to analyze changes in T cell motility.

To evaluate the capacity of the dura APCs to activate antigen-specific T cells, T_{OVA} cells reactive against the $OVA_{323-339}$ peptide were enriched by restimulating polyclonal T_{OVA} cells with the $OVA_{323-339}$ peptide for three rounds of restimulation. T_{OVA} blasts were then injected

i.v. in wild type Lewis Rats and animals were imaged on day 4 p.t., when some T_{OVA} cells could be observed outside of the vessels, in the meningeal milieu. TPLSM of the dura were performed as described in two distinct imaging areas. Afterwards, 200 µg $OVA_{323-339}$ peptide (1.8 KDa) were dissolved in 500 µl PBS and applied on the thinned bone. Imaging was carried out as described for the next 210 minutes in the two selected spots to analyze changes in extravascular T cell motility.

For both treatments, the transcranial route of administration was preferred to epidural administration because it avoided craniotomy and therefore minimized potential damage of the dura. Importantly, both the cytokines and the peptide have a MW below 40KDa and therefore are able to pass through the thinned skull.[55] Imaging was initiated immediately after application of the solutions and the solutions were kept in place throughout the imaging session by an agar ring. Animals that underwent the same surgical and imaging procedure, but did not receive cytokines or antigen in the imaging window, were employed as controls.

3.2.8.7 Analysis of time-lapse videos

Imaris software (Bitplane) was used for 3D reconstructions and 4D analysis of acquired raw TPLSM data. Crawling cells were tracked using the automated Imaris Track module followed by manual revision. Intravascular fast rolling, rolling and crawling T cells in the different meningeal compartments were counted manually within a 30-min acquisition period in the imaging field. Fast rolling T cells appeared as round or oblong fluorescent dots present in only one imaging frame; rolling T cells were defined as previously described[25,28] i.e. as cells appearing as a single or several round-shaped dots on more than one imaging frame, moving exclusively in the same direction of the blood flow with an instantaneous velocity >50 µm/min instantaneous velocity and/or a track duration inferior to 2 minutes. Crawling cells displayed an amoeboid movement on the endothelium wall that was independent from the direction of the blood flow, could be tracked for more than 2 minutes and had an instantaneous velocity <50 µm/min. Statistical evaluations were performed with Excel and GraphPad software. For graphical visualization of the mean square displacement, the MotilityLab software (http://www.motilitylab.net) was employed. The graphical visualization of individual cell tracks normalized by the coordinate of origin was generated in R by Michael Haberl.

For representation of T cell tracks over time, 30min-time projections were created by a maximum intensity projection of each time-point of the video stacked onto each other.

3.2.9 Intrathecal reactivation of T_{OVA} cells

Five million T_{OVA} cell blasts were injected in wild type Lewis rats. On day 3.5 p.t., animals were anesthetized with a combination of 10 mg/kg xylazine and 50 mg/kg ketamine and fixed on a stereotactic device (Narishige). The parietal bones were exposed by a midline scalp incision and a small area of the bone was thinned with a 2 mm drill head circa 1.5 mm lateral and 0.5 mm caudal from bregma. The solution was loaded into a syringe with a 30G needle and the injection was performed by piercing directly the thinned skull. The needle was then lowered -4.0 mm from skull surface and the solution was injected at a rate of 10 µl in 10 minutes. For antigen delivery, 25 µg OVA in 25 µl of PBS, 10 µg OVA in 10 µl of PBS or equivalent volumes of PBS were stereotactically injected. At the end of the injection, the needle was left in place for 5 minutes. Afterwards, the needle was retracted with a speed of 1 mm every 5 minutes to avoid reflow through the injection route. The skin was then sutured and rats treated locally with analgesics. Circa 8 hours post OVA injection, animals were sacrificed and brain dura, leptomeninges, parenchyma, blood, deep cervical lymph nodes and inguinal lymph nodes were isolated and processed as described above. T_{OVA} cells were then retrieved by FACS sorting as described above and their activation status was assessed by qPCR.

3.2.10 Intrathecal migratory kinetic of T_{OVA} cells

To investigate the distribution kinetic of intrathecal T cells in the meningeal compartments of the non-inflamed brain, $1x10^6$ resting T_{OVA} cells (day 5 after antigen encounter) dissolved in in 25 µl PBS were injected in the cisterna magna. To this aim, wild-type Lewis rats were anesthetized and fixed on a stereotactic device as described above. The injection needle was placed into a stereotactic holder at 90° to the skin surface. The injection site was identified as the space between the occipital bone and the atlas. The injection was performed at a depth of 3.5 mm from the skin surface using a 30G needle. The correct positioning of the needle was ensured by applying minimal negative pressure to allow inflow of CSF into the syringe. The T cell solution was injected at a rate of 10 µl in 10 minutes (around 25 minutes per animal). At the end of the injection, the needle was left in place for 10 minutes before carefully retracting it.

3.2.11 In vitro T cell stimulation by ex vivo-isolated cells

In order to evaluate the antigen presentation capacity of APCs isolated from different CNS and peripheral compartments, single cell suspensions were obtained from brain parenchyma,

leptomeninges, dura and lymph nodes as described above, under sterile conditions, from naïve animals and from animals at the peak of T_{bSYN} EAE (day 3 after T_{bSYN} cell injection). For each compartment and condition, $30x10^3$cells from the total cell suspension were cultured with $10x10^3$ resting antigen specific T cells (T_{bSYN}, T_{MBP} or T_{OVA} cells) in 96-U well plates in presence of their cognate antigen, an irrelevant antigen or PBS. Irradiated thymocytes (professional antigen presenting cells) were used as positive control. The following measurements were used as read-out of T cell activation: (1) pro-inflammatory cytokine expression at mRNA level by qPCR 24 hours after antigen encounter; (2) pro-inflammatory cytokine expression at protein level by ELISA 48 hours after antigen encounter; (3) expression of the surface activation markers CD25 and CD134 was evaluated 48 hours after antigen encounter by flow-cytometry.

ELISA for IFNγ was carried out at a 1:50 dilution according to the manufacturer's instructions in duplicate technical replicates.

3.2.12 T_{bSYN} cell anergy assay

To evaluate the anergy status of T_{bSYN} cells in the dura, single cell suspensions were obtained from brain leptomeninges and dura a as described above, under sterile conditions, from animals at the peak of T_{bSYN} EAE (day 3 p.t.). Given the low yield of cells from the dura compartment, T_{bSYN} cells could not be purified from the total cell suspension. Therefore, the total cell suspension was plated at a concentration of $30x10^3$ cells for each compartment in 96-U well plates in presence of their cognate antigen, an irrelevant antigen or PBS. Read-outs for T cell activation were the same as above.

3.2.13 AAV-mediated ablation of dural lymphatic vessels

Lymphatic depletion was ensured by i.t. injection of an AAV encoding a VEGF-C trap (ratVEGFR3-hFc/ AAV9), which deprives the dural lymphatic vessels of their necessary survival factor. The AAVs were provided by collaborators at the University of Helsinki (Prof. Kari Alitalo, Dr. Dmitri Chilov). In particular, the AAVs were produced by the AAV Gene Transfer and Cell Therapy Core Facility, HiLIFE, University of Helsinki. For AAV transduction, a single dose ($4x10^{11}$ viral particles in 40 µl) of ratVEGFR3-hFc/ AAV9 was i.t. injected as above. Control rats received either the same number of particles of AAV without payload (AAV9/S2) or PBS. T_{bSYN} cell EAE was induced as described above 14 weeks post AAV injection. This time point was determined by preliminary experiments that showed no

detectable changes in immune cell composition in the brain dural, leptomeningeal or parenchymal compartments but at the same time sustained effective depletion of the lymphatic vessels as confirmed by histological analysis.

3.2.14 Confocal microscopy

Confocal microscopy was performed using a Zeiss Laser Scanning Microscope 710 (Carl Zeiss) with a 40x oil NA1.3 immersion Plan Apochromat objective and controlled by Zeiss ZEN 2012 software. Fluorophores were excited using a 405 nm UV-diode, 488 nm Argon laser, a 561 nm DPSS laser and a 633 nm HeNe laser. Images were acquired using a pinhole size of 50-60 µm and a z-step size of 0.5-1 µm. For overviews, several tile scans were acquired sequentially and stitched together.

3.2.15 Histology and immunohistochemistry

Animals were intracardially perfused with saline (10 min), then leptomeninges and dura were removed as described in section 3.2.4.1 and fixed in 4% PFA overnight.

Immunohistochemical stainings were performed on whole meningeal mounts. The samples were incubated free-floating with the following antibodies: mouse anti-rat-CD68 (clone ED1, BioRad), mouse anti-rat-CD43 (clone W3/13, BioRad), rabbit anti-Lyve1 (Origene). Goat anti-mouse or goat anti-rabbit IgG Abs labelled with Alexa Fluor 488, Alexa Fluor 555 or Alexa Fluor 647 were used as secondary antibodies.

Images were acquired using a VS120 Virtual Slide Microscope (Olympus) equipped with a 10x objective or with a Zeiss LSM700 confocal microscope equipped with a 40x Zeiss objective.

3.2.16 Statistical analysis

Statistical analysis was performed using GraphPad Prism and Microsoft Excel. Unless indicated otherwise, data are represented as mean + SEM (standard error of the mean). The statistical tests underlying data analysis are stated in the corresponding figure legends. Briefly, for comparing two-data sets statistical significance was determined via unpaired two-tailed t-test. For comparing more than two data sets, statistical significance determined via one-way ANOVA with Tukey's multiple comparisons test. If datasets did not satisfy the normality test, non-parametric tests were employed. Significance levels were set as *$p < 0.05$; **$p < 0.01$; ***$p < 0.001$, ****$p < 0.0001$.

4 RESULTS

4.1 Infiltration kinetics of T effector cells in the different meningeal compartments

To dissect the kinetic of meningeal infiltration by T cells, we employed two distinct models of CNS inflammation and one model for basal T cell trafficking.

- **T_{bSYN} cell lines,** which are reactive against the neuronal protein beta-synuclein (bSYN), infiltrate the gray matter of the brain and spinal cord and induce atypical EAE symptoms characterized by hemiparesis, head tilting and ataxia.[20]
- **T_{MBP} cell lines**, which are reactive against the myelin basic protein (MBP), infiltrate predominantly the white matter of the spinal cord and cause a classical EAE with an ascending symmetrical paralysis of the hindlimbs.[25,28]
- **T_{OVA} cell lines,** which are reactive against an indifferent antigen (ovalbumin, OVA) and therefore do not cause EAE or infiltrate the CNS parenchyma.[19] These cells mimic basal immune surveillance by effector T cells.

To facilitate *ex vivo* and *in vivo* tracking, the T cell lines were retrovirally transduced with fluorescent proteins. The distribution of the cells in the different meningeal layers of the brain was assessed by flow cytometry at different days after intravenous (i.v.) transfer of the T cells (**Figure 15a**). Predictably, T_{bSYN} cells invaded massively the leptomeninges and, at the onset of disease (**Figure 15a**, the clinical phase is indicated by a gray background), day 3.5 post T cell transfer (p.t.), cells accumulated in large numbers also in the parenchyma. T_{MBP} cells, which mostly infiltrate the spinal cord, accumulated in lower numbers in the brain compared to T_{bSYN} cells but showed a similar distribution kinetic, rapidly reaching the leptomeninges and, at the onset of symptoms, invading the parenchyma.

Regardless of antigen specificity, both T_{bSYN} and T_{MBP} cells were consistently lower in the dura than in the leptomeninges.

Importantly, also CNS-ignorant T_{OVA} cells distributed preferably in the leptomeninges when compared to the dura, suggesting that the differential distribution of T cells in the meningeal layers was independent from T cell antigen specificity.

Imaging by two-photon laser scanning microscopy (TPLSM) of the hemispheric dura and underlying leptomeninges, performed at the peak of T cell infiltration, confirmed the cytofluorimetric analysis (**Figure 15b**).

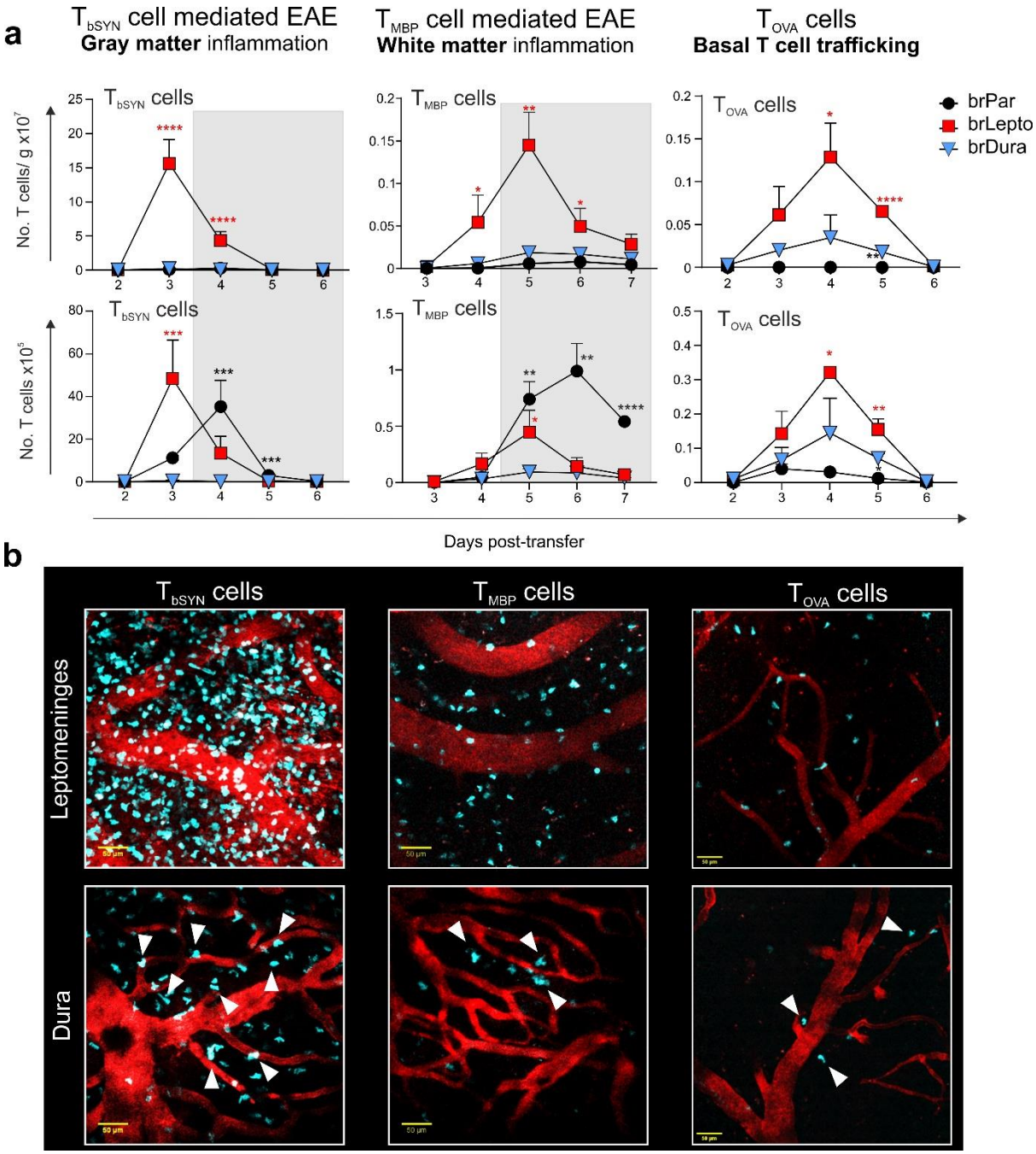

Figure 15: T cells infiltrate the leptomeninges in larger numbers than the dura mater. (a) The graphs show T_{bSYN}, T_{MBP} and T_{OVA} cells in the brain parenchyma (BrPar, black), brain leptomeninges (brLepto, red) and brain dura (brDura, blue) quantified by flow cytometry at the indicated time points after T-cell transfer. The upper panels report the total number of T cells normalized per tissue weight (No. T cells/g). The lower panels indicate the absolute numbers of T cells in the tissue (No. T cells). Gray background: Clinical EAE phase. Data are mean + SD and are representative of 4 independent experiments, each including at least 3 animals/group/time point. Statistics: one-way ANOVA with post-hoc correction for multiple comparisons. Red asterisks indicate comparisons between dura and leptomeninges; Black asterisks indicate comparisons between dura and parenchyma. *p<0.05, **p<0.01, ***p<0.001, ****p<0.0001. (b) Representative TPLSM snapshots at the peak of T_{bSYN}, T_{MBP} and T_{OVA} cell invasion in the brain leptomeninges and dura. Fluorescently transduced T cells are in turquoise, vessels, in red, were labelled by i.v. injection of 70KDa dextran. Representative dura T_{bSYN}, T_{MBP} and T_{OVA} cells are highlighted by filled white arrowheads.

4.2 Intravascular T cell motility in the leptomeningeal and dural vessels

As detailed in the introduction, T cells reach peripheral tissues via the blood circulation following a multi-step process of adhesion to the vessel wall, which results in the arrest of T cells on the vessel endothelium, scanning of the endothelial surface ("crawling") and eventually extravasation. As shown in **Figure 15b**, both the dura and leptomeninges vessels display a rich vascular bed. Therefore, we hypothesized that different properties in the leptomeningeal and dural vasculature could explain the divergent accumulation of T cells between the brain dura and leptomeninges. To test this hypothesis we analyzed the intravascular motility behavior of T cells in the dura and leptomeningeal vessels.

First, we established a system to reliably visualize the dura vasculature (**Figure 16** and Methods). We observed that the vessels of the dura are embedded within a tight matrix of collagen and are located right above the parietal skull (**Figure 16a**). Leptomeningeal vessels could be detected right below the layer of dura collagen. No evident communicating vessels were visible between the two vascular beds (**Figure 16b**).

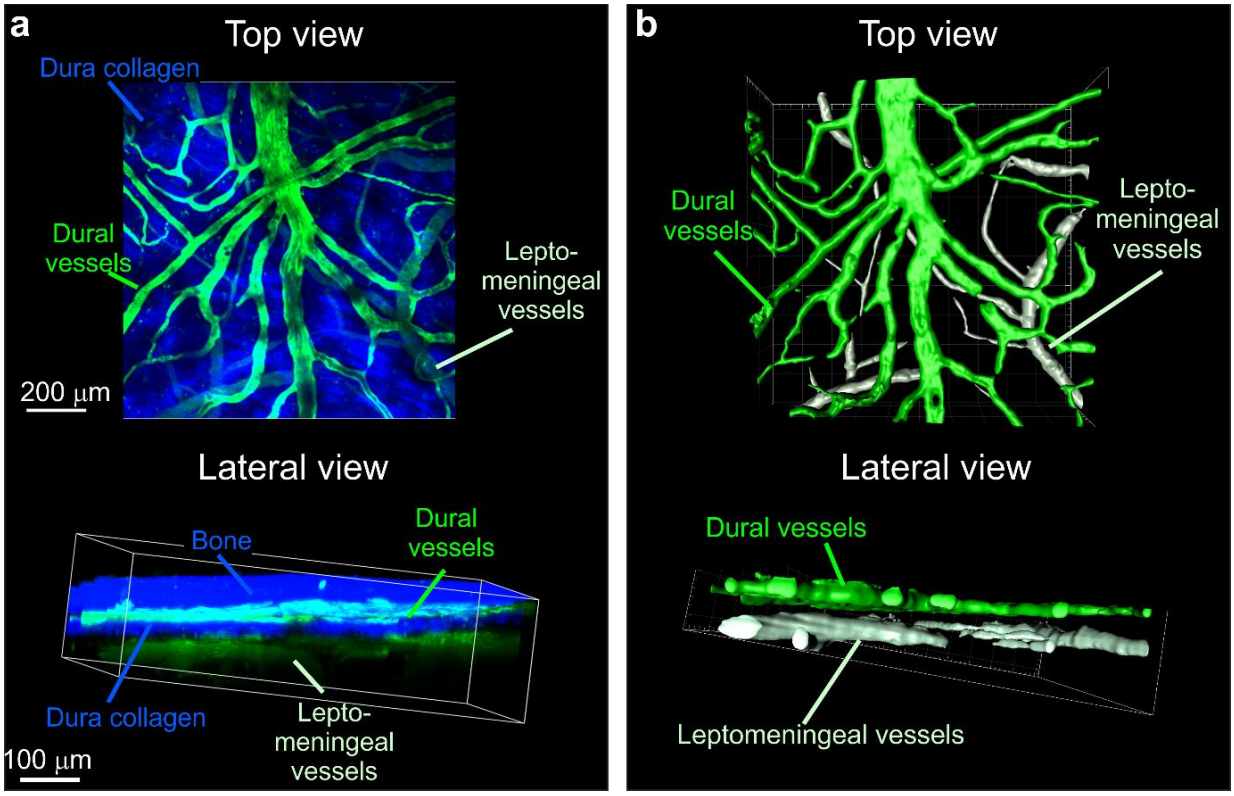

Figure 16: Simultaneous visualization of dural and leptomeningeal vasculature. (a) TPLSM snapshot of dura vessels visualized through the thinned bone and embedded in the dural collagen. Leptomeningeal vessel are visible underneath the dura collagen. The lateral view shows the dura vessels located between the skull bone and the dura collagen. Vessels (in green) were visualized by injection of 70KDa dextran, collagen and bone (in blue) were visualized by second-harmonic generated signal. (b) 3D reconstruction of the picture in (a), collagen signal omitted, to better visualize the dural vessels (in bright green) and underlying leptomeningeal vessels (in light green). The 3D reconstruction lateral view shows the lack of communicating vessels between dural and leptomeningeal vasculature.

Injection of a small molecular weight tracer (3 KDa) revealed the different permeability properties of the vessels. The tracer rapidly leaked out from the dural vessels and was taken up by dural macrophages. In contrast, the leptomeningeal vessels were impermeable to the passage of the tracer, which only transiently appeared in the circulation and was not taken up by leptomeningeal macrophages (**Figure 17**). This observation was consistent with the presence of a blood meningeal barrier in the leptomeningeal vessels; on the other hand, fenestrated endothelia have been described in the vessels of the dura, thus making them permissive to the extravasation of solutes up to 40KDa.[72]

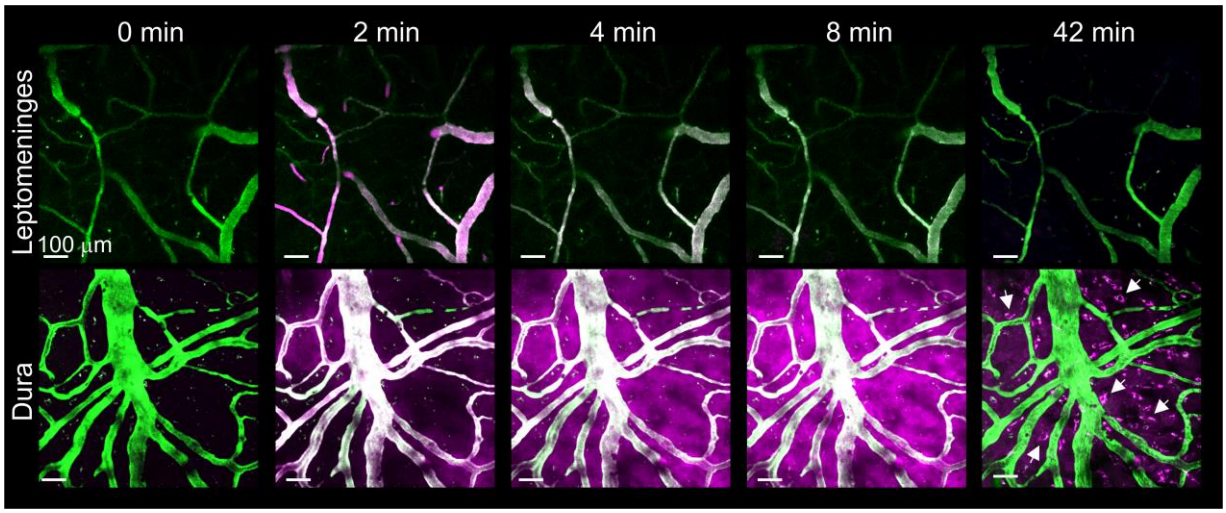

Figure 17: Permeability of leptomeningeal and dural vasculature. Representative TPSLM images of brain leptomeningeal (upper panel) or dural vessels (lower panel) at the indicated time points after i.v. injection of 3KDa dextran (magenta). Vessels were visualized by prior i.v. injection of 70KDa dextran (green). Note that the 3KDa dye promptly leaked out from the dural vessels into the surrounding tissue and was taken-up by resident phagocytes (arrows). No dye leakage was detected in the leptomeninges.

We then analyzed if the dura vasculature was equally permissive to the trafficking of T cells. To this aim, we transferred i.v. T cells with the different antigen specificities (T_{bSYN}, T_{MBP} and T_{OVA} cells) and analyzed their motility during the intravascular phase (day 2-3 p.t.) in leptomeningeal and dural venules of comparable caliber.

TPLSM imaging revealed a different behavior of the transferred cells in the pial and dural vessels (**Figure 18** and **Figure 19**). In the leptomeninges, as previously described, a substantial number of T_{bSYN} and T_{MBP} cells interacted firmly with the endothelium (**Figure 19a, b**), scanning the luminal surface of the vessel with a slow amoeboid movement, termed "crawling", (**Figure 18**). In the dural vessels, only very few cells showed this migration pattern. Instead, we identified a great proportion of either rolling or fast rolling T cells.

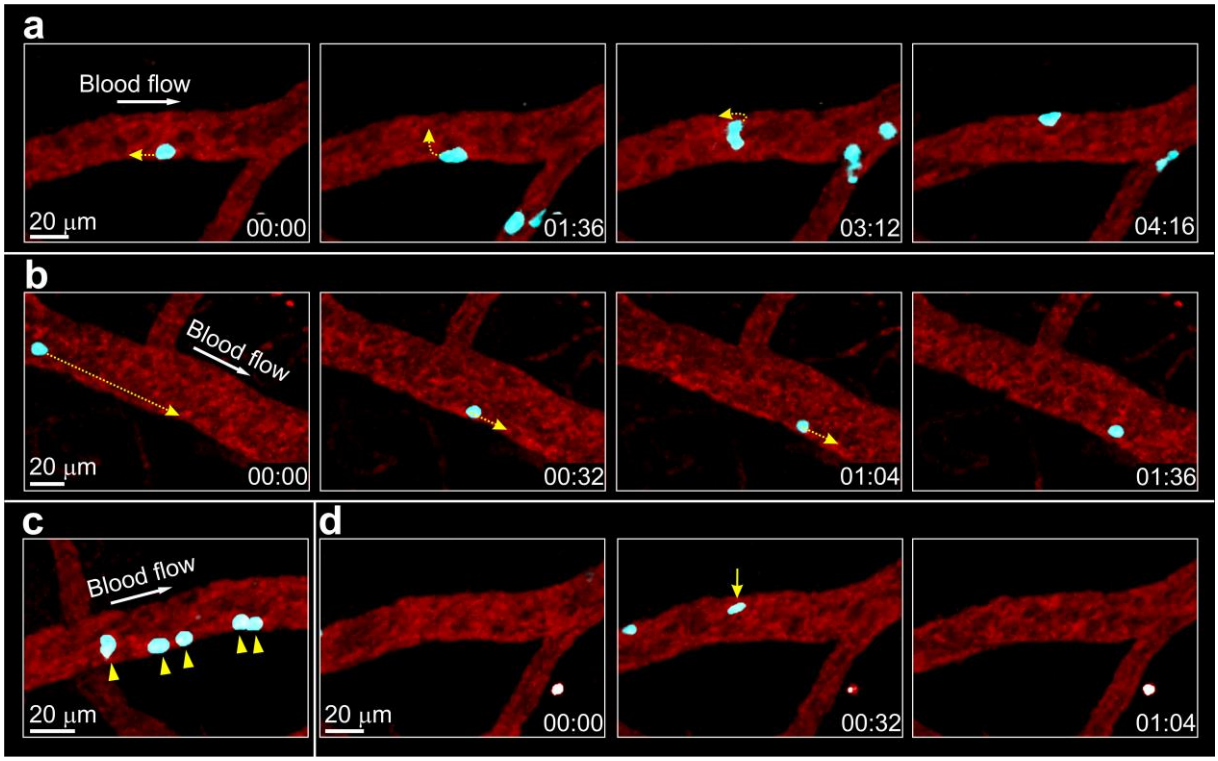

Figure 18: Examples of T cell intravascular motility pattern in the leptomeninges. (a) Representative motility pattern of a crawling T cell in a leptomeningeal venule. Note the amoeboid shape and slow movement (yellow dotted line) independent of the blood flow. (b) Representative motility pattern (yellow dotted line) of a rolling T cell. The T cell moves in the direction of the blood flow and at a relatively high speed. (c) A single rolling T cell can also appear as a string of round-shaped cells, here highlighted by the yellow filled arrowheads. (d) Representative fast rolling cell, here highlighted by the yellow arrow, appearing as a single dot in a single frame. Fluorescently transduced T cells are in turquoise, vessels, in red, were labelled by i.v. injection of 70KDa dextran. Time is indicated relative to the first frame as minutes:seconds.

Also non-encephalitogenic T_{OVA} cells displayed this clear different intravascular migration behavior (**Figure 19c**), thus excluding the possibility that the autoinflammatory response of the leptomeningeal tissues might have caused an increased adhesiveness of the leptomeningeal vasculature.

In conclusion, although the fenestrated dura vessels were very permissive to the passage of solutes, they did not seem to be permissive to T cell crawling.

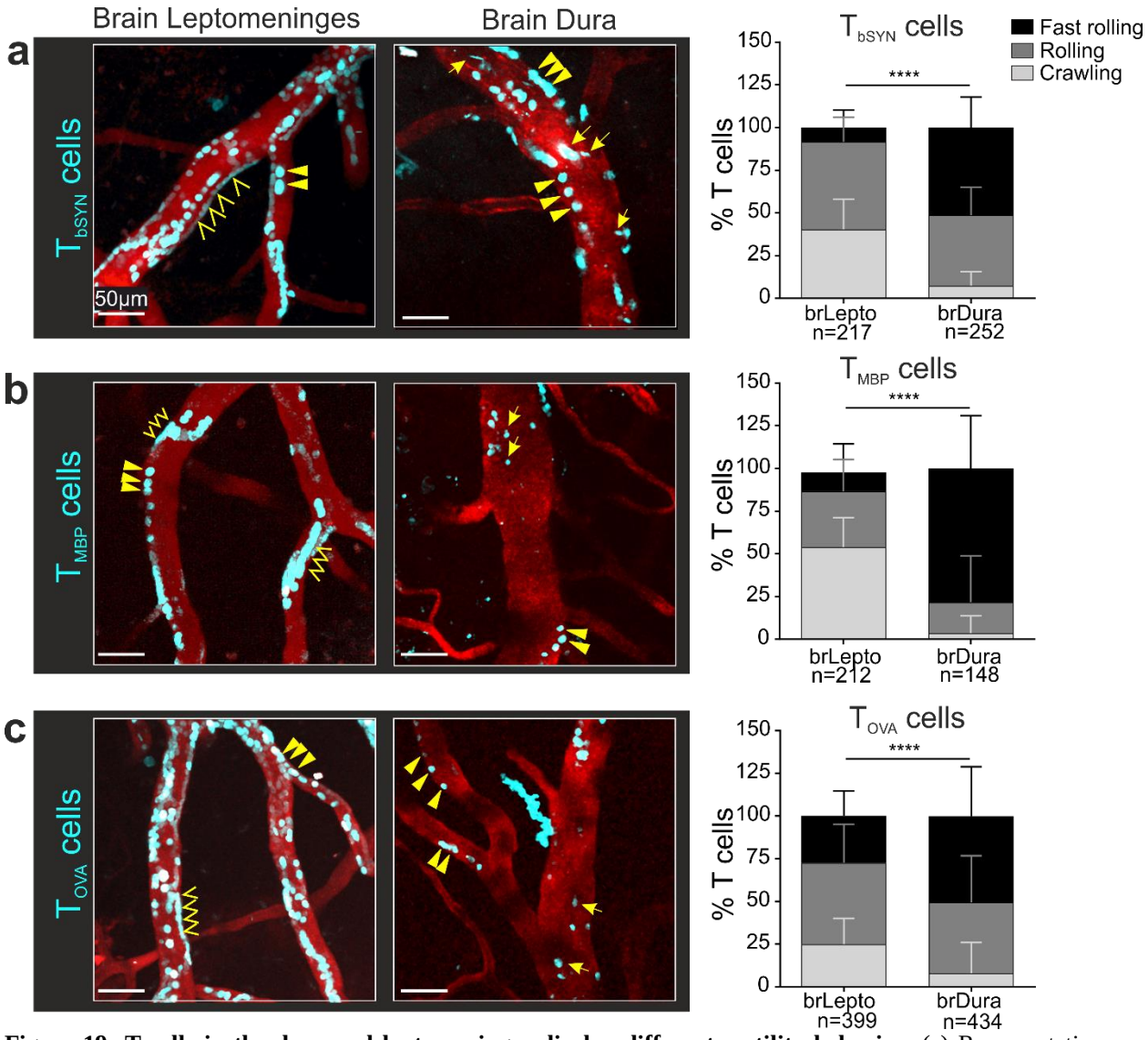

Figure 19: T cells in the dura and leptomeninges display different motility behavior. (a) Representative 30min TPLSM time projections of T_{bSYN}, T_{MBP} and T_{OVA} cells (2.5-3 days p.t.) in the indicated meningeal compartments. Fluorescently labelled antigen-specific T cells are in turquoise; 70KDa dextran labelled vessels are in red. Representative rolling cells are indicated by filled yellow arrowheads, fast rolling cells by yellow arrows and crawling cells by empty arrowheads. The graphs show the corresponding percentages of crawling, rolling or fast rolling T cells within a 30min recording period. Y-axis is extended over 100% to accommodate the stacked standard deviations. Numbers of analyzed T cells are indicated below each graph. Data are mean + SD and are cumulative of at least 8 movies/T cell specificity/compartment. Statistics: chi square. ****p<0.0001.

4.3 Molecular mediators of T cell motility in the leptomeningeal and dura vessels

To investigate the molecular underpinnings of these paradoxical findings, we performed next generation sequencing (NGS) of the endothelial cells of the leptomeninges and of the dura. Principal component analysis sharply separated leptomeningeal and dural vessels (**Figure 20a**). As expected, genes encoding BBB-associated molecules, such as occludin (*Ocln*) and claudin-5 (*Cln5*) were highly expressed in the leptomeninges (**Figure 20b**). However, the profile of adhesion molecules diverged between the dura and leptomeninges. While the dura expressed at high level selectins (*Sele*, *Selp*), which mediate rolling, the leptomeningeal endothelium expressed several chemokines, in particular the chemokine (C-X-C motif) ligand 9,10 and 11 (*Cxcl9-11*), which bind to the CXC receptor 3 (CXCR3), and a variety of integrin ligands, including vascular cell adhesion molecule 1 (*Vcam1*) and fibronectin (*Fn1*), which are crucial for T cell arrest and crawling (**Figure 20b, c**).

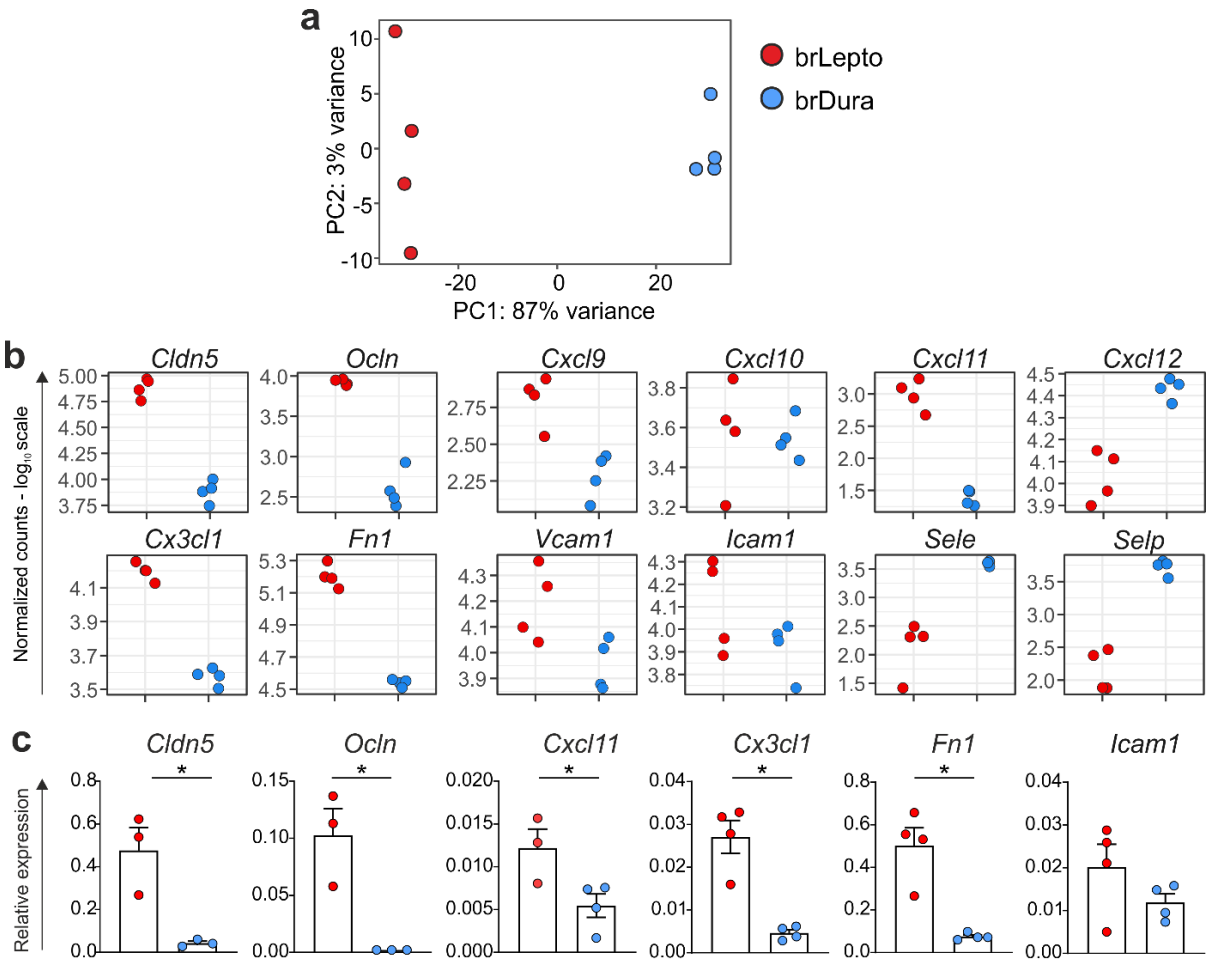

Figure 20: Dura and leptomeningeal vessels are transcriptionally distinct. (a) PCA plot of endothelial cells isolated from the brain leptomeninges (brLepto, red) and brain dura (brDura, blue) compartments from naïve animals. (b) Normalized counts displayed on a $\log_{10}$ scale, extracted from NGS data for the indicated tight junction proteins, chemokine ligands, integrin ligands and selectins in the meningeal endothelia. (c) Validation of selected targets from NGS by qPCR on naïve endothelial cells. Expression levels of the selected targets are relative to the housekeeping gene: β-actin. Data are mean + SEM. Each dot represents a pool of 4-6 animals. Statistics: unpaired two-tailed t-test. *p<0.05

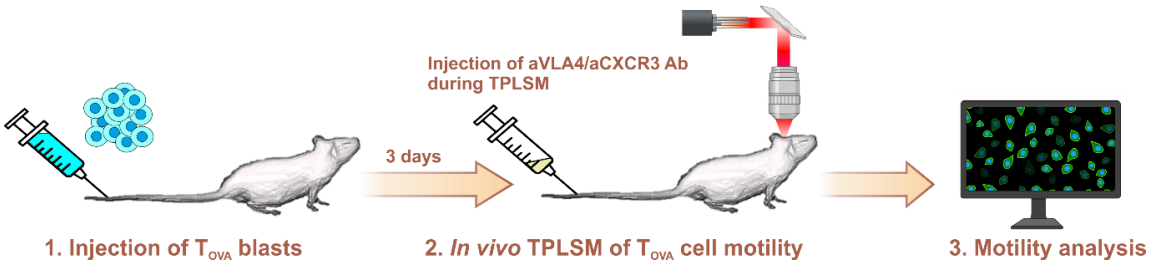

Figure 21: Experimental setup for *in vivo* interference with integrin and chemokine signaling in T cells. T_{OVA} cell blasts are injected i.v. into naïve animals. After 3 days, when most of the injected cells are circulating in the vasculature, TPLSM is performed in the leptomeninges or dura to analyze T cell motility. After acquiring scans of T cell motility in basal conditions, anti-VLA4 or anti-CXCR3 antibodies are injected and scans are performed at different time-points after injection. T cell motility before and after antibody injection is analyzed.

Integrin ligands and chemokines are crucial mediators for T cell adhesion to the vessel wall. The differential expression of these factors may thus explain the motility pattern of T cells in the leptomeninges and in the dura.

Therefore, we then tested how inhibition of integrin or chemokine signal affects T cell motility in the two meningeal compartments in the steady state (**Figure 21**).

To functionally interfere with integrin signaling, we administered an antibody directed against VLA-4, the essential integrin for T cell adhesion and arrest, and evaluated T_{OVA} cell motility by TPLSM.

In the leptomeninges, upon anti-VLA-4 (aVLA4) administration, the number of T_{OVA} cells in the vasculature readily dropped within the first 30-40 minutes and the remaining circulating T_{OVA} cells were almost all fast rolling (**Figure 22**). This data indicated that, in the leptomeninges, T_{OVA} cell adhesion and motility was strongly dependent on integrin signaling.

In the dura, where cells are mostly rolling or fast-rolling, the effect was less pronounced: fewer T_{OVA} cells disappeared from the circulation and the ones remaining retained their motility profile. This suggested that, unlike in the leptomeninges, integrin signaling mediates only in part T cell adhesion in the dura vessels and has no effect on their motility behavior.

To investigate the role of chemokines in T cell motility and adhesion in the dura, we employed an analogue strategy by injecting an anti-CXCR3 (aCXCR3) antibody, which blocks the CXCL9-11 chemokines, crucial mediators of integrin activation and thus initial T cell adhesion and arrest.

In the leptomeninges, aCXCR3 had an effect on T cell adhesion, although not as marked and as pronounced as aVLA4. Upon aCXCR3 treatment, around 50-60% of the cells detached (**Figure 23b**), while aVLA4 caused an almost complete depletion (>90%) of the T cells from

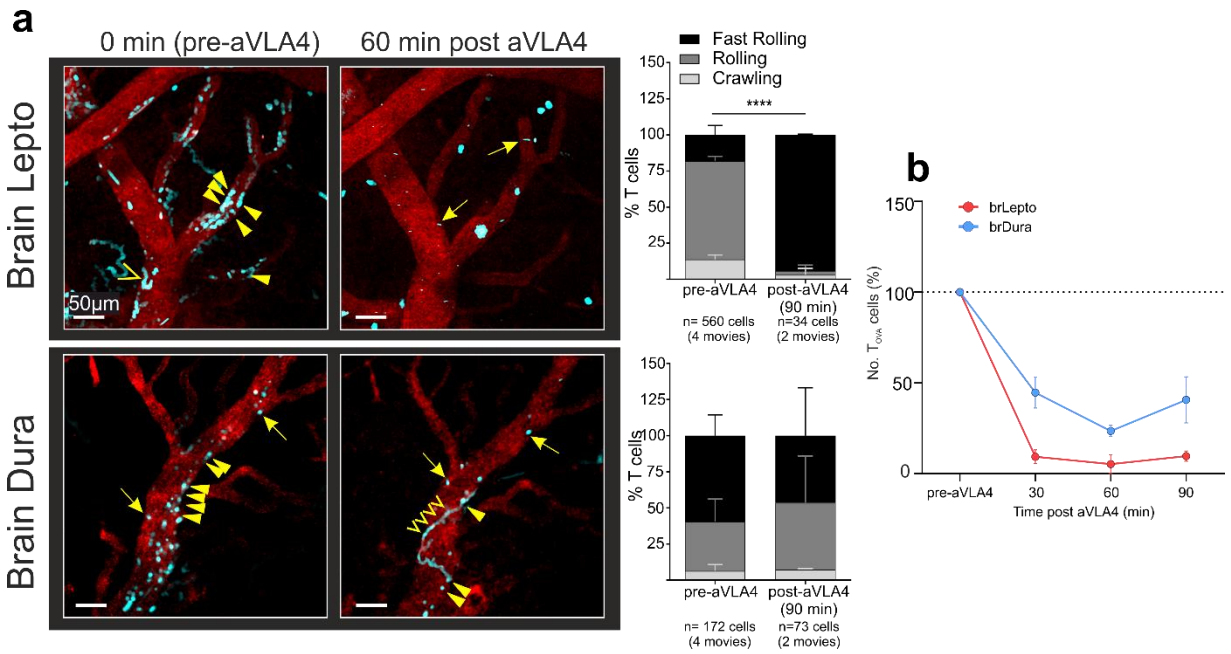

Figure 22: Inhibition of alpha 4-integrin signaling is less efficient in blocking T cell adhesion in dural than in leptomeningeal vessels. (a) Representative 30min TPLSM time projections of T_{OVA} cells (3 days p.t.) in the indicated meningeal compartments recorded before and 60min after i.v. injection of blocking aVLA4 antibody. Fluorescently labelled T_{OVA} cells are in turquoise, 70KDa dextran labelled vessels are in red. Representative rolling cells are indicated by filled yellow arrowheads, fast rolling cells by yellow arrows and crawling cells by empty arrowheads. The graphs show the corresponding percentages of crawling, rolling or fast rolling T cells within a 30min recording period before and after aVLA4 antibody. Y-axis is extended over 100% to accommodate the stacked standard deviations. Numbers of analyzed T cells and movies are indicated below each graph. Data are mean + SD. Statistic: chi square. **** $p<0.0001$ (b) Percentage reduction of intravascular T_{OVA} cells in dural (brDura, blue) or leptomeningeal (brLepto, red) vessels after anti-VLA4 antibody treatment. T_{OVA} cell numbers were calculated as the average number of cells per time frame in a 30min TPLSM videos. Data are mean ± SEM and are cumulative of 2 independent experiments.

the leptomeningeal vessels. Similarly, aCXCR3 influenced motility behavior, with a reduced number of crawling T cells and an increase in rolling cells (**Figure 23a**). However, unlike aVLA4, the number of fast rolling T cells remained largely unaffected.

In the dura, albeit a statistically significant reduction of fast rolling cells was noted, the profile of T cell motility remained overall unaltered, with a low percentage of crawling cells and a predominance of rolling/fast rolling events. Furthermore, aCXCR3 had no effect on T cell adhesion to the dura vessels, as the number of T cell in the vessels oscillated around the starting value (**Figure 23b**).

Based on these findings, the CXCL9/10/11-CXCR3 axis could mediate, in concert with integrins, the differential motility behavior of T cells in the dura; moreover, it could represent a potentially novel determinant of T cell motility in the brain leptomeningeal vessels.

Therefore, to further characterize the role of CXCR3 on T cells, we took advantage of T_{OVA} cells in which the CXCR3 locus was deleted via CRISPR-Cas9 (T_{OVA} -X3KO cells).

We co-injected T_{OVA} -X3KO cells with control cells, in which the Cas9 deletion was directed to the Rosa26 locus (T_{OVA}-R26 cells), and analyzed their motility behavior in the leptomeningeal vessels (**Figure 24**).

When we compared the motility behavior of the two cell populations, T_{OVA}-X3KO were indistinguishable from the controls (**Figure 24b**). Similarly, the total number of cells in the vessels did not vary between the two cell types (**Figure 24c**). These findings were in contrast with what we had observed with the aCXCR3. To exclude potential off-targets effects of the aCXCR3 antibody, we injected aCXCR3 in animals co-injected with T_{OVA} -X3KO cells and T_{OVA}-R26 control cells (**Figure 24a**, experimental setup). During the recordings, T_{OVA}-R26 cells progressively detached from the vessels while T_{OVA} -X3KO cells were unaffected (**Figure 24d**), thus partially excluding off-target effects of the antibody. Taken together, these data suggested that, while acute inhibition of CXCR3 signaling via aCXCR3 antibody had a demonstrable effect on T cell adhesion and motility behavior, T cells chronically lacking CXCR3 may upregulate other adhesion molecules that could surrogate CXCR3 function.

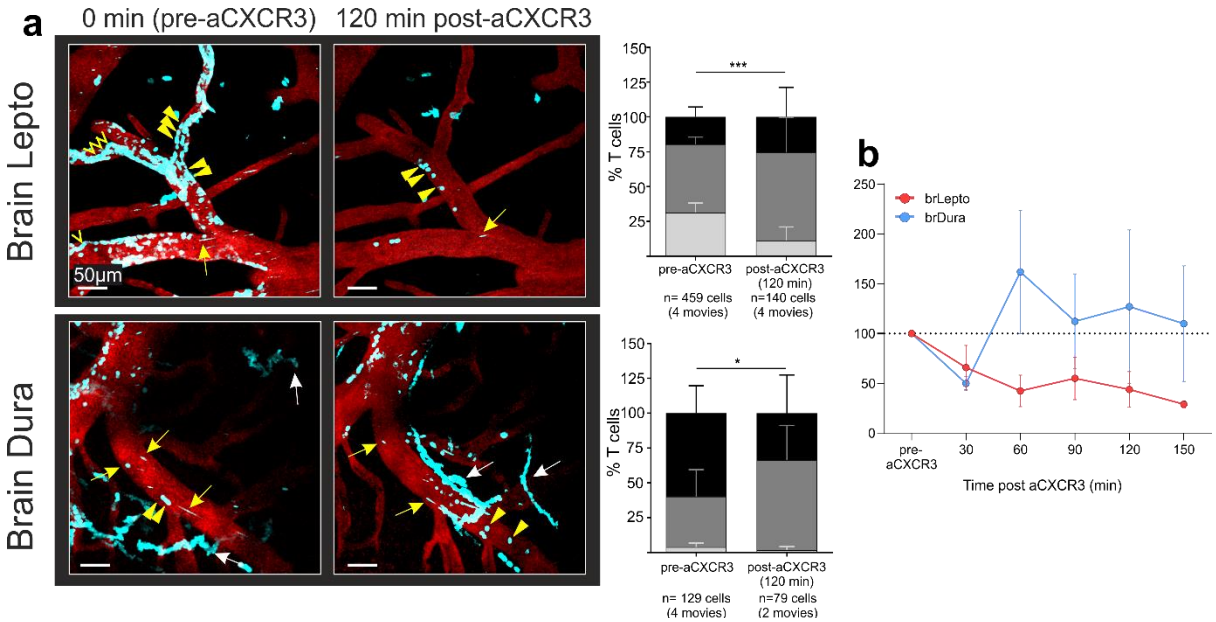

Figure 23: Inhibition of CXCR3 signaling has no effect on T cell motility in the dura. (a) Representative 30min TPLSM time projections of T_{OVA} cells (3 days p.t.) in the indicated meningeal compartments recorded before and 120min after i.v. injection of blocking aCXCR3 antibody. Fluorescently labelled T_{OVA} cells are in turquoise, 70KDa dextran labelled vessels are in red. Representative rolling cells are indicated by filled yellow arrowheads, fast rolling cells by yellow arrows and crawling cells by empty arrowheads. Representative extravascular rolling cells are indicated by white arrows. The graphs show the corresponding percentages of crawling, rolling or fast rolling T cells within a 30min recording period before and after aCXCR3 treatment. Legend is the same as in Figure 22. Numbers of analyzed T cells and movies are indicated below each graph. Data are mean + SD. Statistics: chi square. *** $p<0.001$; *$p<0.05$ (b) Percentage reduction of intravascular T_{OVA} cells in dural (brDura, blue) or leptomeningeal (brLepto, red) after aCXCR3 antibody treatment. T_{OVA} cell numbers were calculated as the average number of cells per time frame in a 30min TPLSM videos. Data are mean ± SEM and are cumulative of 2 independent experiments.

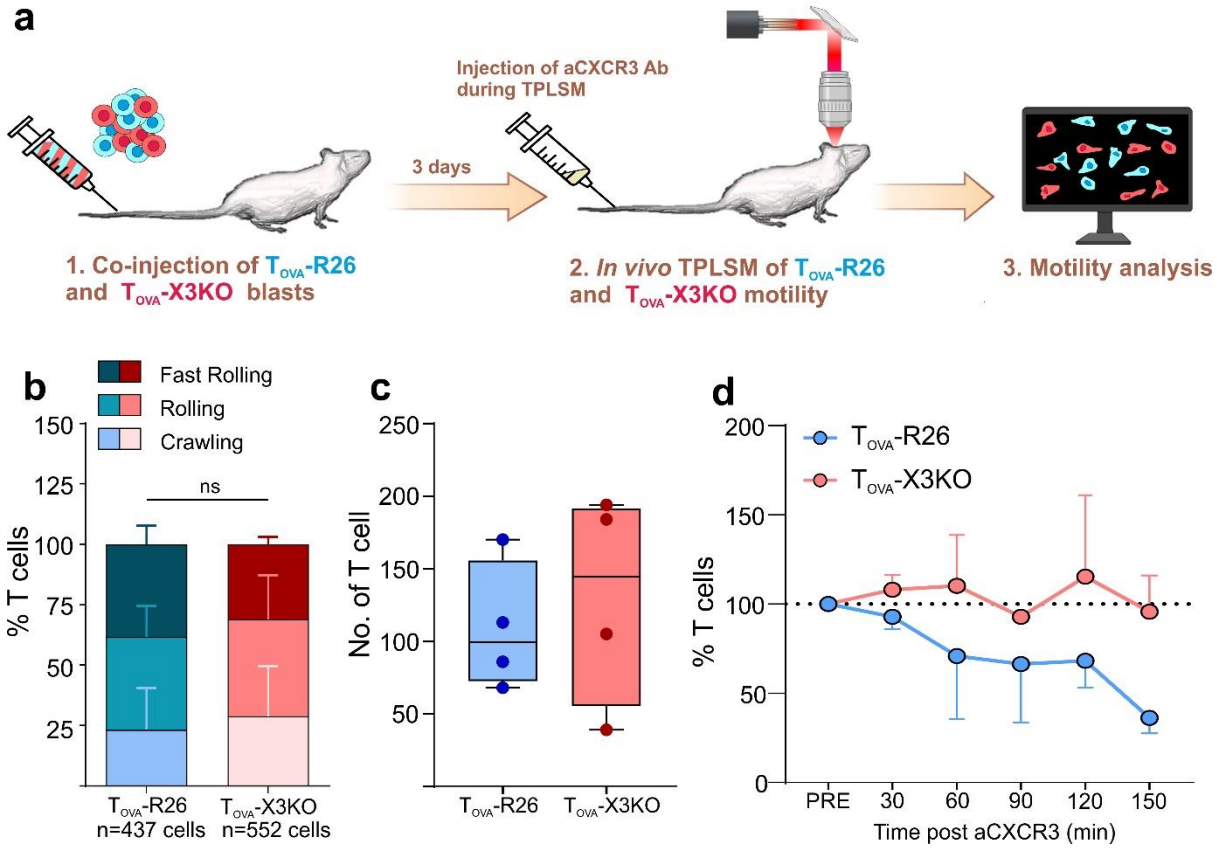

Figure 24: T cells KO for CXCR3 exhibit a similar motility pattern to control T cells in leptomeningeal vessels. (a) Experimental setup. T_{OVA}–R26 and T_{OVA}-X3KO cells are co-injected i.v. in the same naive animal. Cells can be distinguished due to the expression of different fluorescent proteins. T_{OVA}–R26 and T_{OVA}-X3KO cell motility is recorded on day 3 after transfer in leptomeningeal vessels via TPLSM. After basal recording, aCXCR3 antibody is administered and movies are acquired at defined time points. Intravascular T_{OVA} –R26 and T_{OVA} -X3KO cell motility behavior in the steady state and after aCXCR3 is analyzed. (b) T cell motility parameters for T_{OVA} –R26 and T_{OVA} -X3KO cells showing percentages of crawling, rolling or fast rolling T cells within a 30min recording period. Y-axis is extended over 100% to accommodate the stacked standard deviations. Numbers of analyzed T cells are indicated below the graphs. Data are mean + SEM and are cumulative of 4 movies from 2 independent experiments. Statistics: chi square, ns= not significant. (c) Average T_{OVA} –R26 and T_{OVA} -X3KO cell number was calculated over the 30min recording video. Data are represented as box and whiskers with line at the median and boxes extending to the 25th and 75th percentile. Whiskers extend to the minimum and maximum value. Each dot represents a different recording from 2 independent experiments. (d) Percentage reduction of intravascular T_{OVA}–R26 and T_{OVA}-X3KO cells in the leptomeningeal vessels at different time points after aCXCR3 antibody treatment. T cell numbers were calculated as the average number of cells per time frame in a 30min TPLSM video. Data are mean ± SEM and are cumulative of 5 different movies from 3 independent experiments.

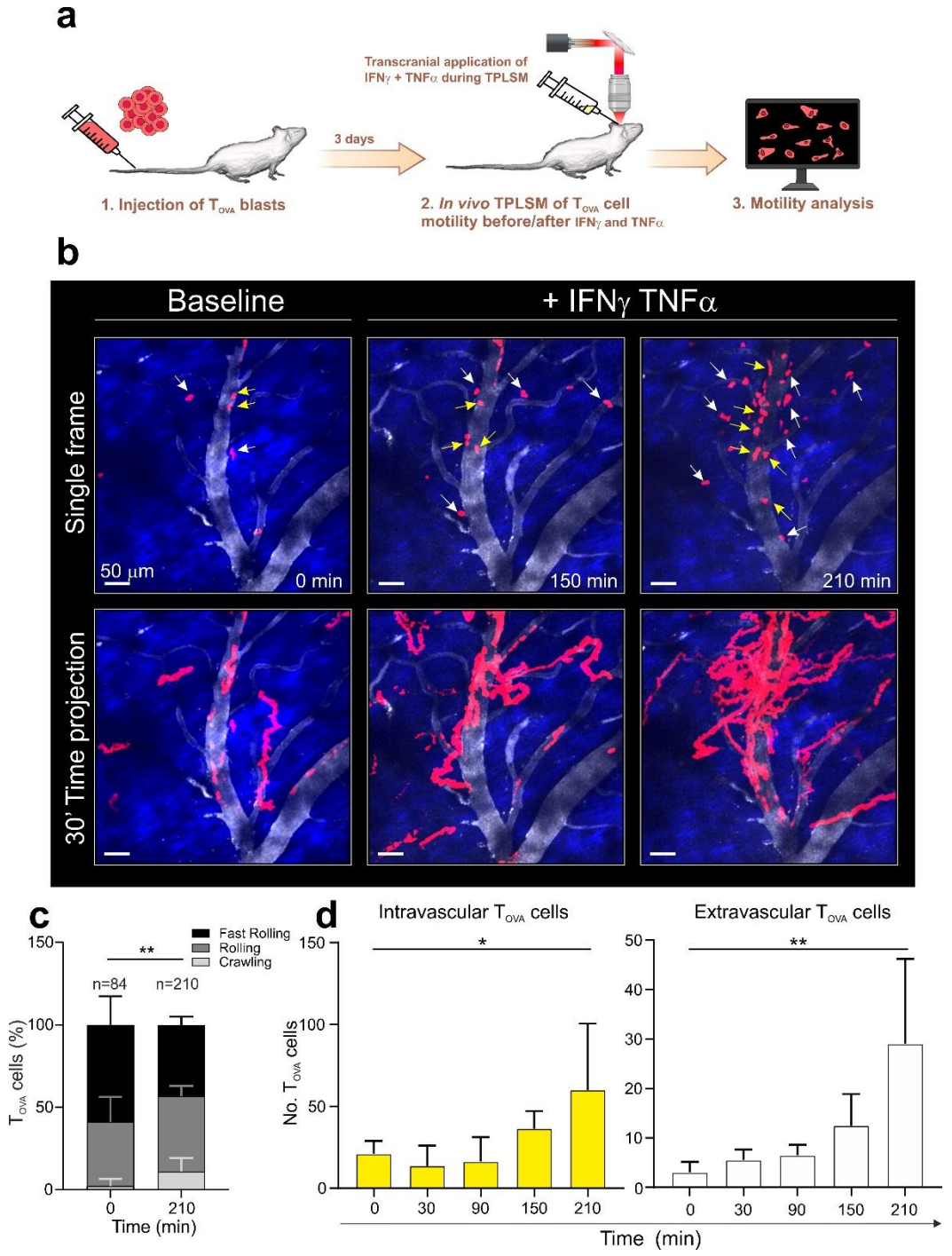

Figure 25: T cells adhere to dura vessels under inflammatory conditions. (a) Experimental setup. T_{OVA} cell blasts are injected i.v. . During the intravascular phase (day 3 p.t.), TPLSM is performed. After recording in basal conditions, IFNγ and TNFα are administered transcranially through the thinned skull of the imaging window. (b) Representative single frame from a 30min TPLSM recording and respective 30min time projections from the same recording showing T_{OVA} cell motility at baseline and at different time-points after IFNγ and TNFα application. Fluorescently labeled T_{OVA} cells are in red, 70Kda dextran-labeled blood vessels are in gray. Dura collagen (2^{nd}-harmonic signal) is in blue. Yellow arrows indicate intravascular T cells. White arrows indicate extravascular T cells. Note the progressive increase in both intravascular and extravascular T cells. (c) Quantification of T_{OVA} cell locomotion behavior in the dural vessels before and 210 minutes after cytokine administration. Y-axis is extended over 100% to accommodate the stacked standard deviations. Data are mean + SD and are cumulative data of 2 independent experiments. Statistics: chi square. (d) Quantification of the average number of intravascular (in yellow) and extravascular (in white) T_{OVA} cells at the indicated time-points after IFNγ and TNFα. T_{OVA} cell numbers were calculated as the average number of T_{OVA} cells per frame in a 30min TPLSM videos. Data are mean + SD and are cumulative data of 2 experiments. Statistics: two-tailed t-test. (c, d) *p<0.05, **p<0.01.

4.4 The dura vessels are permissive to T cell adhesion and extravasation during dura inflammation

We had observed that both encephalitogenic T_{bSYN} and T_{MBP} cells as well as CNS-ignorant T_{OVA} cells accumulated less in the dura than in the leptomeninges. This was linked to a reduced competence of the dura vessels to T cell trafficking in the steady state, due to lower expression of chemokines and integrin ligands. We therefore hypothesized that the inertness of the dura vasculature to effector T cell adhesion may also justify its inability to recruit T cells during inflammatory conditions, as we observed during T_{bSYN} and T_{MBP} cell-induced EAE (**Figure 15**). To test this hypothesis, we devised a system (**Figure 25a**, **Methods**) to induce inflammation directly on the dura by transcranial application of cytokines. Activation of the dura endothelium by interferon-γ (IFNγ) and tumor necrosis factor-α (TNFα) resulted in adhesion and crawling of the T cells on the dura vessels and, eventually, massive extravasation into the dura milieu (**Figure 25b**). The dura vessels were therefore fully competent in recruiting T cells under these inflammatory conditions.

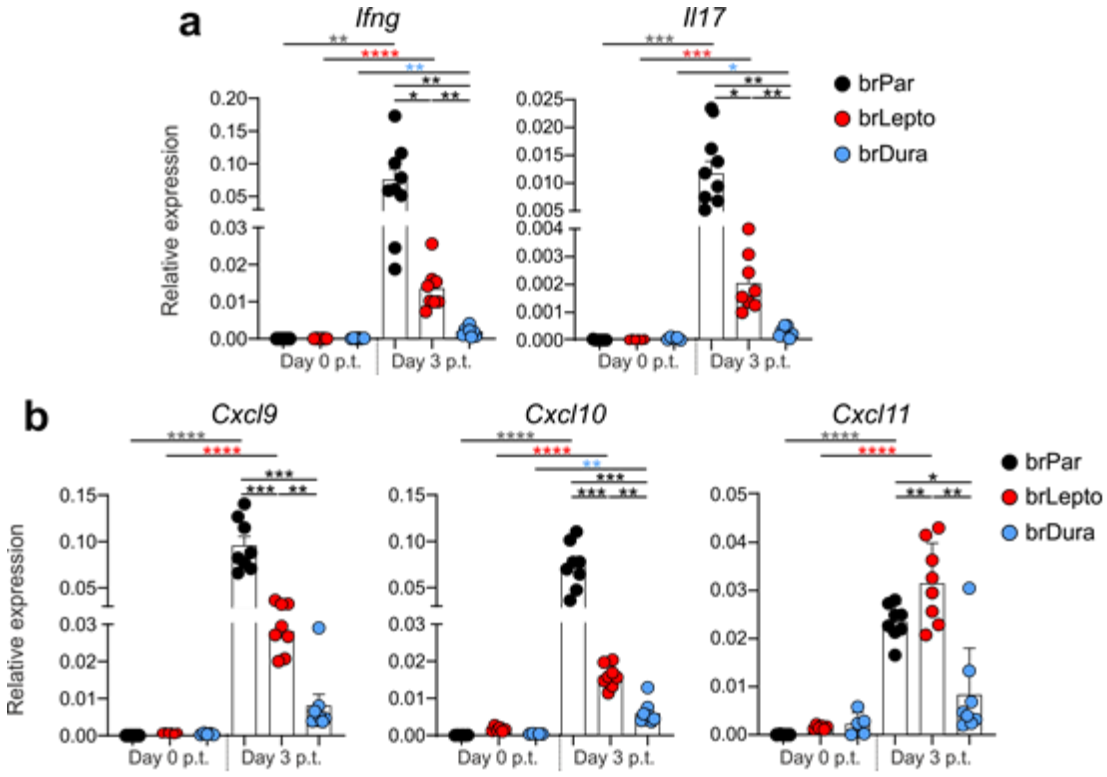

Figure 26: The dura tissue is less inflamed than the CNS parenchyma and leptomeninges during EAE. (a,b) qPCR for cytokines (a) and chemokines (b) expression in the brain parenchyma (brPar, black), brain leptomeninges (brLepto, red) and brain dura (brDura, blue) in naïve animals and on day 3 p.t. of T_{bSYN} cells. Gene expression was calculated relative to the house-keeping gene, β-actin. Data are mean + SEM and are cumulative of 3 independent experiments. Statistic between different compartments within the same time point (black asterisks): one-way ANOVA with post-hoc comparison. Statistic between different time points within the same compartment (gray, red and blue asterisks): two-tailed t test. *p<0,05; **p<0,01; ***p<0,001; ****p<0,0001

4.5 The dura mater is spared by the inflammatory response during T_{bSYN} EAE

Although the dura mater could efficiently recruit T cells upon induction of epidural inflammation with IFNγ and TNFα, this was not the case during T_{bSYN} and T_{MBP} cell-EAE: T_{bSYN} and T_{MBP} cells did not accumulate selectively in the dura at any point of T cell infiltration, nor adhered to the dura vessel walls (**Figure 15a, b; Figure 19**). This led us to conclude that the dura may be largely spared by the inflammatory process during EAE.

To investigate this aspect, we took advantage of the T_{bSYN} cell-EAE animal model. We therefore injected naïve rats with fully activated T_{bSYN} cells and, at the peak of T cell infiltration (day 3 p.t.), isolated the various CNS compartments (brain dura, leptomeninges and parenchyma) and compared their expression profile and immune cell composition.

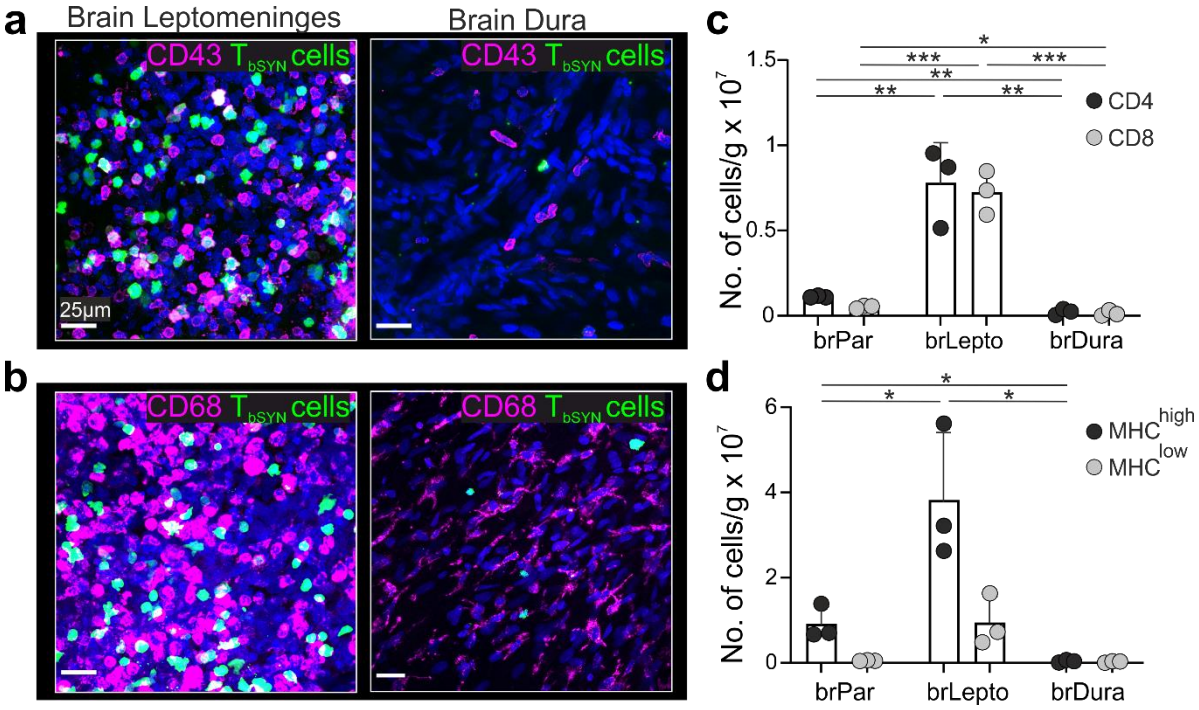

Figure 27: Inflammatory cells preferentially infiltrate the brain leptomeninges over the dura in beta synuclein-directed EAE. (a, b) Representative confocal pictures illustrating the infiltration pattern of $CD43^+$ lymphocytes (a) and $CD68^+$ monocytes/macrophages (b) in the brain leptomeninges and dura at the peak of EAE. Recruited cells are in magenta, T_{bSYN} cells are in green. (c, d) Cytometry quantification of infiltrating T lymphocytes (c) and monocytes (d) at the peak of disease severity (day 4 p.t.). Data are mean +SD and are representative of 4 independent experiments each including at least 3 animals/group. Statistics: two-tailed t test. *p<0,05; **p<0,01; ***p<0,001

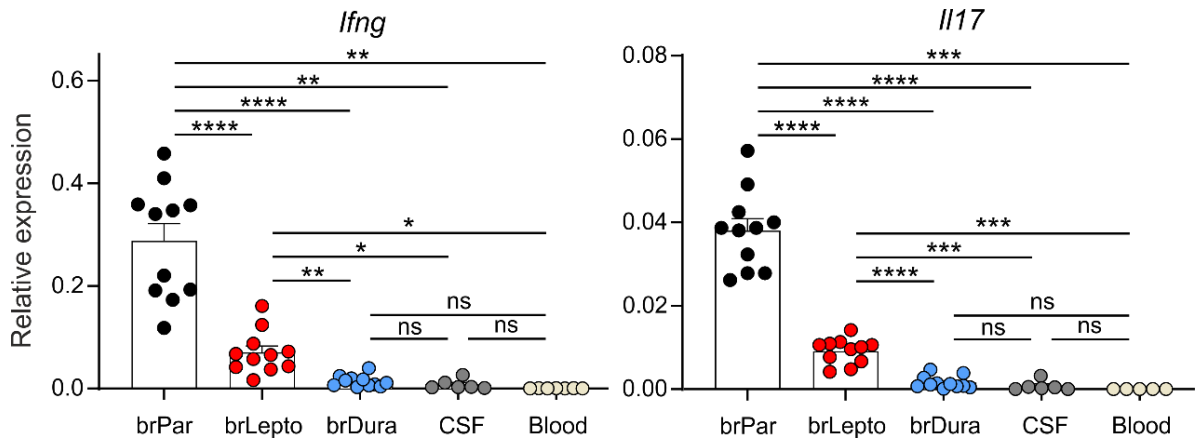

Figure 28: T_{bSYN} cells are less activated in the dura compared to T_{bSYN} cells in leptomeninges and parenchyma. qPCR for the activation markers *Ifng* and *Il17* of T_{bSYN} cells sorted at the peak of T cell infiltration (day 3 p.t.) from the indicated brain compartments and blood. Gene expression was calculated relative to the house-keeping gene, β-actin. Data are mean + SEM and are cumulative of 3 different experiments. Statistics: one-way ANOVA with post-hoc correction. *p<0,05; **p<0,01; ***p<0,001; ****p<0,0001; ns, not significant

qPCR data on the total tissues showed that the dura mater expressed significantly lower levels of the inflammatory cytokines IFNγ and interleukin-17 (IL17) and chemokines CXCL9-11, when compared to the leptomeninges and parenchyma (**Figure 26**). Consistently, secondary recruitment of T cells and monocytes was significantly lower in the dura than in the leptomeninges and parenchyma, as visualized by histology and confirmed by flow cytometry (**Figure 27**).

As indicated in the introduction, EAE is initiated when the CNS-reactive T cells encounter in the CNS the cognate antigen presented by local APCs. This contact activates the CNS-reactive T cells to produce locally proinflammatory cytokines, which stimulate endothelial cell activation and chemokine production by resident cells. Other immune cells are thus attracted to the CNS (secondary recruitment) and mediate tissue destruction and clinical symptoms.

When we sorted T_{bSYN} cells at the peak of infiltration, we observed that they were significantly less activated in the dura than in the leptomeninges and parenchyma, as they expressed lower levels of IFNγ and IL17 (**Figure 28**).

The low activation of T_{bSYN} cells in the dura would explain the low level of pro-inflammatory cytokines and chemokines observed in the dura tissue and therefore the practically absent secondary immune cell recruitment.

4.6 T_{bSYN} cells reaching the dura are phenotypically and functionally similar to leptomeningeal T_{bSYN} cells.

We then set out to understand what determined the different level of activation of the encephalitogenic T_{bSYN} cells in the dura and in the leptomeninges. One possibility was that T_{bSYN} cells reaching the dura are a distinct, anergic subgroup than the ones that reached the leptomeninges. Transcriptome of T_{bSYN} cells isolated at the peak of T cell infiltration disproved this hypothesis: T_{bSYN} cells both in the dura and in the leptomeninges displayed a very similar $T_H1/17$ phenotype, with no increased expression of regulatory or anergy genes (**Figure 29**).
In line with this finding, T_{bSYN} cells isolated from the dura at the peak of EAE could be re-stimulated *in vitro* by administration of the cognate antigen, confirming that the T_{bSYN} cells reaching the dura are fully functional (**Figure 30**).

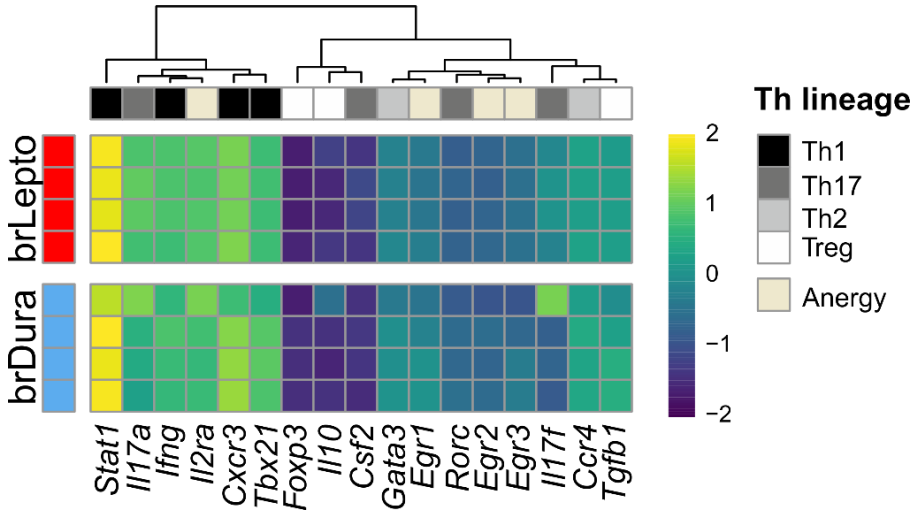

Figure 29: T_{bSYN} cells in the dura and leptomeninges have a comparable differentiation profile. Transcriptional profile of T_{bSYN} cells isolated from the indicated compartments 3 days p.t. Heat map shows hierarchically clustered expression values (log10-transformed RPKM) of genes related to T_H lineage and anergy. Each line represents a biological replicate obtained by pooling 4-5 animals.

4.7 T cells move freely in the dura extravascular space and can be re-activated by local antigen-presenting cells *in vivo*

T cells in the leptomeninges move in a tridimensional mesh of loose collagen by sensing chemokine cues and come into contact with leptomeningeal APCs that present CNS antigens. As previously mentioned, this encounter is essential for triggering the disease. The dura possesses a very tight collagen organization, which may impair the locomotion freedom of extravascular T cells within the tissue and their interaction with local APCs, thus limiting T cell reactivation.

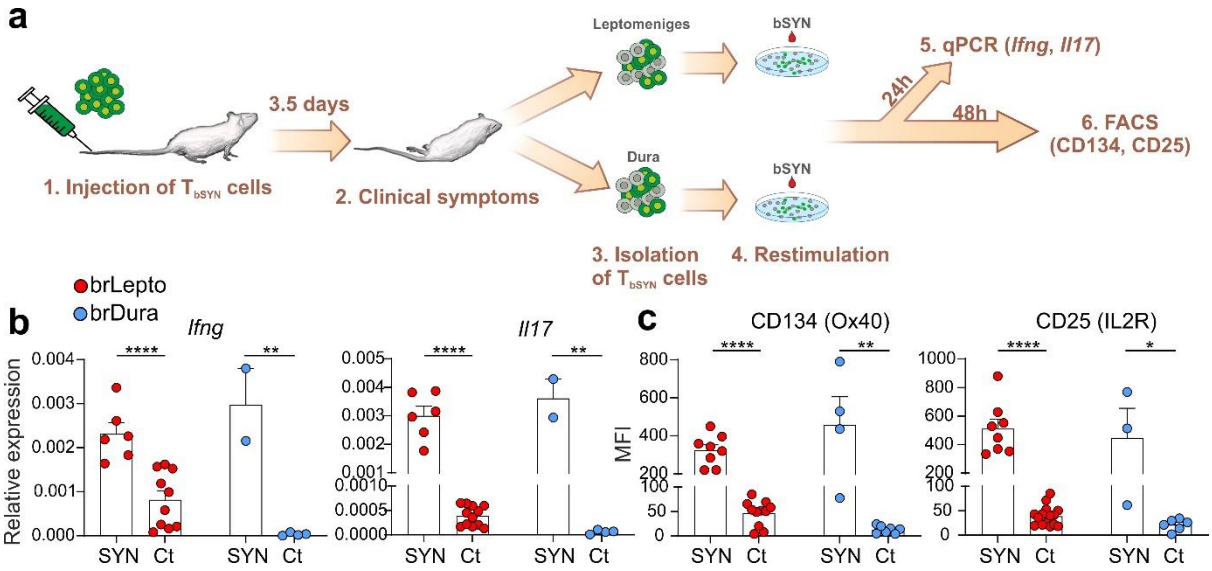

Figure 30: T_{bSYN} cells in the dura are not anergic. (a) Experimental set-up. Upon injection of T_{bSYN} cells, animals developed EAE. At the peak of disease severity, dura and leptomeningeal cell suspensions containing T_{bSYN} cells were isolated from the sick animals and stimulated *in vitro* in the presence of the cognate antigen (bSYN). T_{bSYN} cultured in the absence of the bSYN antigen were used as controls (Ct). T cell activation was assessed by qPCR (b) and FACS (c). (b) qPCR for the activation markers *Ifng* and *Il17* in T_{bSYN} cells that had been isolated from the brain leptomeninges (brLepto, red) and brain dura (brDura, blue) and then stimulated *in vitro*. Gene expression was calculated relative to the house-keeping gene, β-actin. Data are mean + SEM and are cumulative of 2 independent experiments. Statistics: two-tailed t test. (c) Median fluorescence intensity (MFI) of the expression of CD134 and CD25 on the surface of T_{bSYN} cells. Groups are same as in (b). Data are mean + SEM and are cumulative of 3 independent experiments. Statistics: two-tailed t test. (b,c) *p<0.05; **p<0,01; ***p>0,01; ****p<0,0001

To evaluate the motility behavior of extravascular T cells and their interaction with macrophage APCs contemporarily in the dura and leptomeninges, we exploited the different permeability properties of the dura vessels and dura-arachnoid barrier. By i.v. injecting low-molecular weight dextran, which passes through the fenestrated endothelia of the dura vessels but does not cross the BBB (**Figure 17**), dural macrophages were predominantly labeled. Labelling of leptomeningeal macrophages was achieved by injecting intrathecally (i.t.) a fluorescently labelled anti-CD11b antibody (**Figure 31a**). In order to investigate T cell movement in the steady state, we employed CNS-ignorant T_{OVA} cells. Surprisingly, T cells moved unrestricted in the dura tissue, covering the same area as in the leptomeninges (**Figure 31b**) with a mean velocity and displacement that was even higher than in the leptomeninges (**Figure 31c, d**). T cells in the dura also interacted regularly with local macrophages (**Figure 31e**).

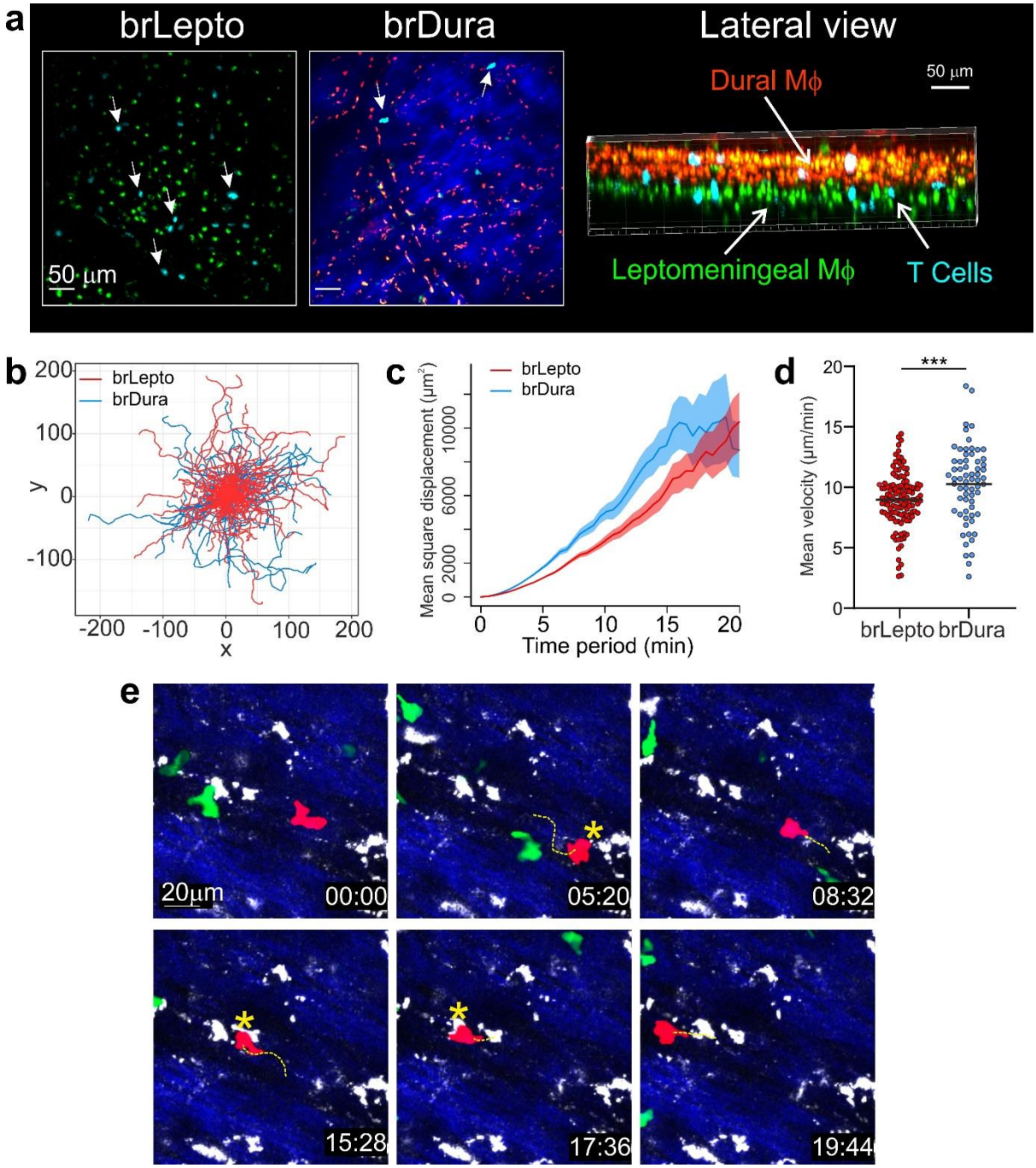

Figure 31: T cells in the dura move unrestricted. (a) Visualization of macrophages in the brain leptomeninges (brLepto) and overlaying dura (brDura) by i.t. injection of CD11b antibody (in green) and i.v. injection of 3KDa dextran (in red). T_{OVA} cells are in turquoise and are highlighted by white arrows. The dura layer was also distinguishable by the presence of dense collagen (2^{nd} harmonic signal, in blue). (b-d) Cell tracks (b, normalized by the coordinates of origin), mean square displacement (c) and mean velocity (d) of extravascular T_{OVA} cells in the leptomeninges (129 tracks) and dura (68 tracks). Statistics: Mann-Whitney test. ***p<0,001 (e) Representative TPLSM snapshots of a T_{OVA} cell (pseudocolored in red) making repeated contacts (yellow asterisks) with dural macrophages (in white) at the indicated time-points (minutes:seconds). The migratory path of the T_{OVA} cell of interest in between the depicted timepoints is indicated by a yellow dashed line. Other T_{OVA} cells are in green. Dura collagen is in blue.

To determine if T cells in the dura could be effectively re-activated *in vivo* by dural macrophages, we designed a system to activate T cells in the dura in a controllable and selective manner (**Figure 32a**). To this aim, we injected animals with CNS-ignorant T_{OVA} cells, which cannot be activated unless their cognate antigen (OVA) is exogenously provided. To activate the T_{OVA} cells selectively in the dura, we transcranially administered an OVA peptide through the imaging window (**Figure 32a**). After a few minutes, T_{OVA} cells in the dura had progressively slowed their locomotion velocity and some became stationary, both indirect parameters of T cell activation (**Figure 32b**). Consequently, more T_{OVA} cells were being recruited to the dura (**Figure 32c, d**). As a further confirmation of successful T cell activation in the dura, qPCR performed on dura tissue isolated from the activated dura meninges showed increased expression of IFNγ and IL17 when compared to controls or the underlying leptomeninges (**Figure 32e**). Accordingly, we detected translocation of the transcription factor nuclear factor of activated T cells (NFAT) from the cytosol to the nucleus, an early and necessary event in T cell activation, in T_{OVA} cells expressing the NFAT-YFP reporter (**Figure 32f**).

Taken together, these data demonstrated that, dura APCs were fully capable of activating T cells *in vivo* when the antigen was exogenously provided.

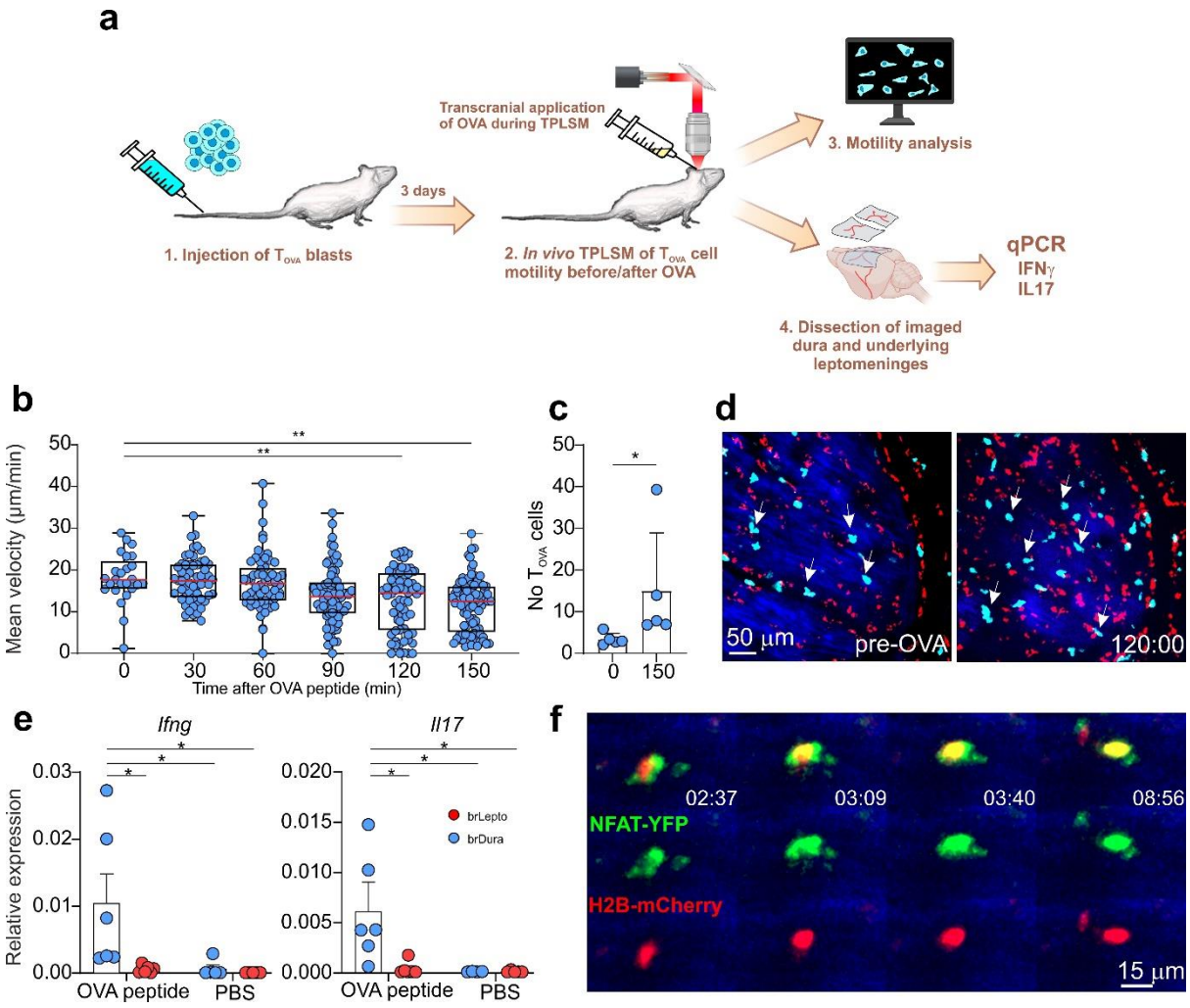

Figure 32: T cells in the dura can be activated by local APCs when the antigen is exogenously provided. (a) Experimental set-up. To activate T_{OVA} cells *in vivo*, OVA peptide was administered transcranially on top of the thinned skull window during the imaging session. Animals which underwent the same imaging session but did not receive OVA peptide were used as control (PBS). Motility and number of T_{OVA} cells was analyzed before and after antigen application. Immediately after imaging, the hemispheric dura and underlying leptomeninges were isolated and snap-frozen. Tissue activation was then measured by qPCR. (b) Mean velocity of T_{OVA} cells in the dura at different time-points after OVA peptide transcranial administration. Data are represented as box and whiskers with line at the median and boxes extending to the 25th and 75th percentile. Whiskers extend to the minimum and maximum value. Each dot represents a different T cell track. Data are pooled from 5 independent experiments. Statistics: Kruskall Wallis test with post-hoc correction. (c) Average number of T_{OVA} cells per time frame before OVA peptide administration (time 0) and 150min afterwards (time 150). Each dot represents one recording. Data are mean +SD. Statistics: two tailed t test. (d) Representative TPLSM snapshots of the hemispheric dura showing T cell numbers before and 120min after OVA peptide transcranial application. T_{OVA} cells are in turquoise, examples of T_{OVA} cells are indicated by white arrows, macrophages are labelled with 3KDa dextran and are in red. Dura collagen is visible by second harmonic and is in blue. (e) qPCR for IFNγ and IL17 performed on the dura (in blue) and leptomeningeal (in red) tissues isolated 150min after transcranial OVA or PBS application. Gene expression was calculated relative to the house-keeping gene, β-actin. Data are mean + SEM and cumulative of three independent experiments. Statistics: one-way ANOVA with post-hoc correction for multiple comparisons**.** (f) TPLSM snapshots depicting NFAT translocation from cytosol to nucleus (indicative of T cell activation) in a $T_{OVA\text{-}NFAT\text{-}YFP\ H2B\text{-}mCherry}$ cell. Images were acquired 120min after transcranial OVA peptide application. Timing of the translocation (minutes:seconds) is indicated. (b, c, e): *p<0,05; **p<0,01.

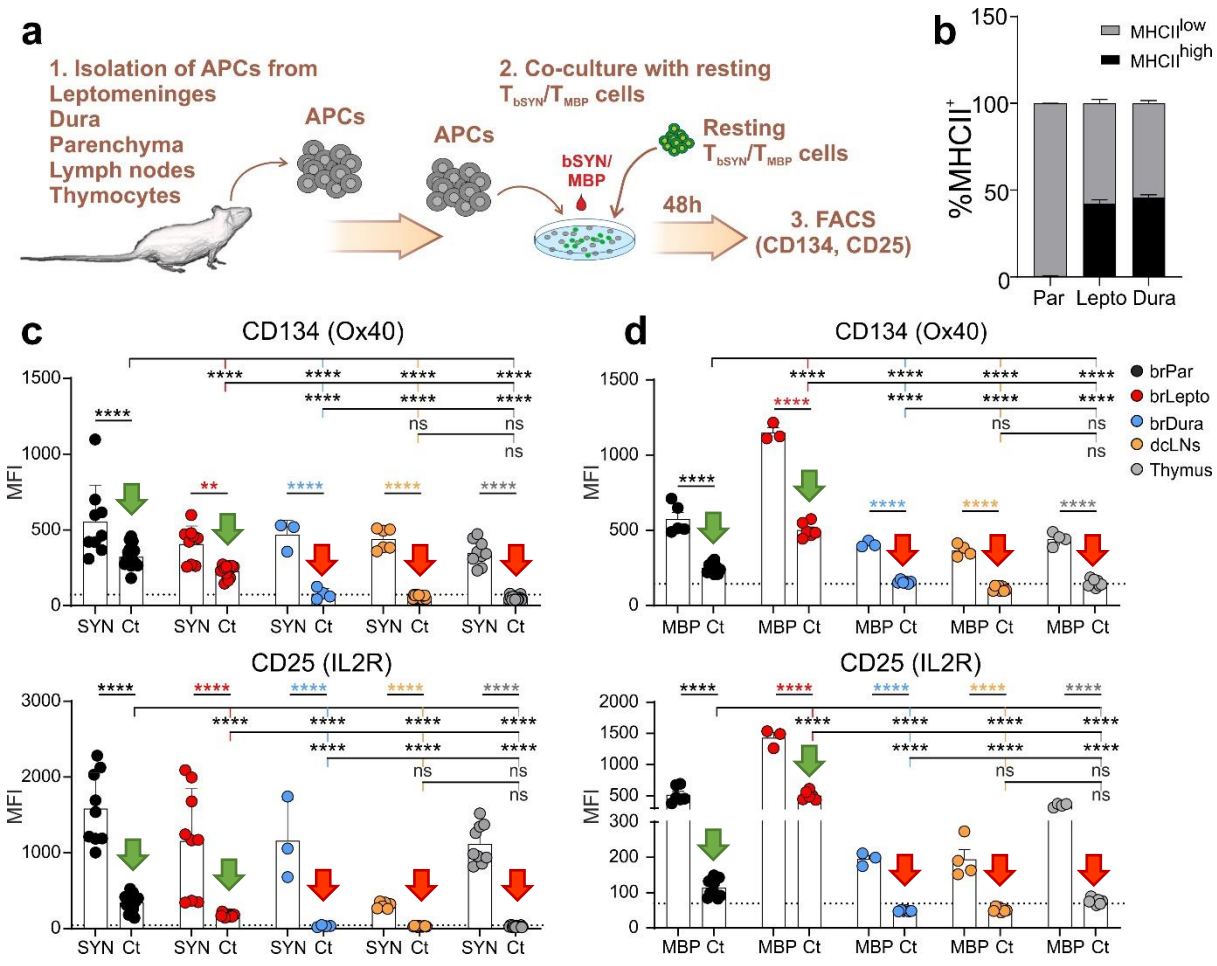

Figure 33: Dura cells cannot spontaneously present CNS antigens. (a) Experimental setup. Cells were isolated from naïve rats from brain parenchyma (brPar), brain leptomeninges (brLepto), brain dura (brDura), deep cervical lymph nodes (dcLNs) and thymus and co-cultured with resting T_{bSYN} of T_{MBP} cells in the presence or absence of the cognate antigens. Two days later, T cells were assessed for the expression of the activation markers. (b) Percentage of $MHCII^{high}$ $CD11b^{+}$ $CD45^{high}$ myeloid cells in brain parenchyma, leptomeninges and dura quantified by flow cytometry. Data are mean + SEM and are representative of 3 experiments (each 3 animals per group). (c, d) Median fluorescence intensity (MFI) of CD134 (OX40) and CD25 (IL2R) quantified by flow cytometry in T_{bSYN} cells (c) and T_{MBP} cells (d). APCs were isolated from the indicated compartments of naïve animals and cultured with T_{bSYN} (c) or T_{MBP} cells (d) in the presence of the cognate antigen (SYN/MBP). As control (Ct), an irrelevant antigen (OVA) or PBS were added to the culture (values pooled together). Note that, in Ct conditions, T_{bSYN} or T_{MBP} cells upregulated the activation markers only when co-cultured with parenchyma or leptomeninges (green arrows).This was not the case when co-cultured with dura, dcLNs or thymocytes (red arrows). The dotted line marks the mean MFI value of the negative control (T cells co-cultured with thymocytes in the absence of the cognate antigen). Data are mean + SEM and are cumulative of 4 (c) or 2 (d) experiments. Statistics between compartments (black asterisks): one way ANOVA with post-hoc correction for multiple comparisons. Statistic within the same compartment (colored asterisks): two-tailed t test. (c,d) **p<0,01; ****p<0,0001; ns: not significant.

4.8 APCs in the dura do not spontaneously reactivate CNS-reactive T cells.

The data so far indicated that, in the dura, neither defects in the T cells nor intrinsic limitations in the antigen presenting capacity of the resident macrophages could justify the lack of activation of autoreactive T_{bSYN} cells we observed during EAE.

Therefore, we investigated if a reduced availability of CNS antigens may be the crucial factor limiting T cell activation in the dura during EAE. To test this hypothesis, we evaluated the ability of the dura to spontaneously, i.e., without exogenous antigen administration, reactivate CNS-autoaggressive T cells. To this end, we co-cultured *in vitro* single-cell suspensions of the dura tissue with CNS-reactive T_{bSYN} and T_{MBP} cells and tested the expression of activation markers on the T cells 48h later (**Figure 33a**, Methods). Of note, the isolated dural cells expressed MHCII to a comparable proportion to cells isolated from the leptomeninges, suggesting a potentially equal ability of these two compartments to present antigens (**Figure 33b**).

In line with our *in vivo* findings (**Figure 32**), when we exogenously provided the antigen (bSYN or MBP) to the cell culture, dura cells activated T_{bSYN} and T_{MBP} cells to levels comparable to the leptomeninges and professional APCs (thymocytes) (**Figure 33c, d)**.

However, when the antigen was not provided, the dura cells failed to spontaneously activate T_{bSYN} and T_{MBP} cells, whereas leptomeninges and parenchyma were able to do so (**Figure 33c, d** red and green arrows).

Taken together, data *in vivo* and *in vitro* indicated that APCs in the dura were potentially fully competent to activate CNS-reactive T cells but failed to do so because the corresponding CNS antigen was not available.

4.9 Drainage of CNS antigens to the deep cervical lymph nodes in steady-state and neuroinflammation

Recent literature has proposed that local lymphatic vessels drain CNS antigens via the dura to the deep cervical lymph nodes (dcLNs) (**Figure 10**).[122,159]

Indeed, TPLSM in our system confirmed the presence of a passage for solutes injected in the CSF to the dcLNs. After i.t. injection of a 70KDa dextran in the cisterna magna, transient labelling of the dural lymphatic vessels and a subsequent accumulation of the dye within the dura could be observed (**Figure 34**).

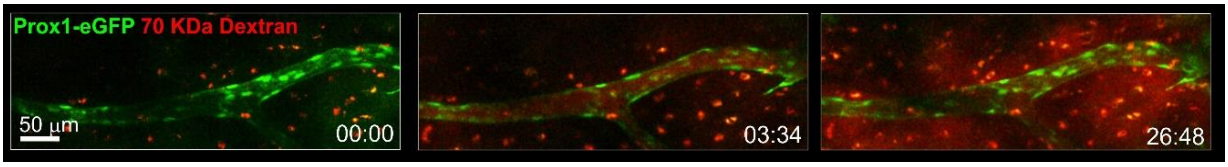

Figure 34: Solutes injected intrathecally are rapidly drained to the dura lymphatics. TPLSM recording of a lymphatic vessel in the region of the transverse sinus of a Prox-1-eGFP rat at different time-points after i.t. injection. Note the transient intraluminal passage of the solute (in red) along the lymphatic vessel (in green) and rapid diffusion in the surrounding tissue.

To see if such route was present also for antigens, we injected OVA intracerebroventricularly (i.c.v.) and, after 8 hours, collected single cell suspensions from the parenchyma, leptomeninges, dura, dcLNs and, as control, inguinal lymph nodes (**Figure 35a**). The cells collected from the leptomeninges, dura and dcLNs were able to stimulate T_{OVA} cells *ex vivo* without addition of the antigen in culture, indicating that the antigen had been successfully taken up by these structures through this draining route (**Figure 35b**). As confirmation, peripheral lymph nodes, which do not drain the CSF, were not capable of reactivating T cells unless the antigen was exogenously provided (+Ag in the figure). We also noted, however, that the intensity of the T cell response was significantly lower in the dura and dcLNs than in the leptomeninges, or parenchyma, which was suggestive of a higher antigen uptake by the leptomeningeal/parenchymal APCs.

To confirm this data *in vivo*, we injected animals with T_{OVA} cells and then attempted to activate them by administering OVA antigen i.c.v. (**Figure 36a**): T cells were recruited almost

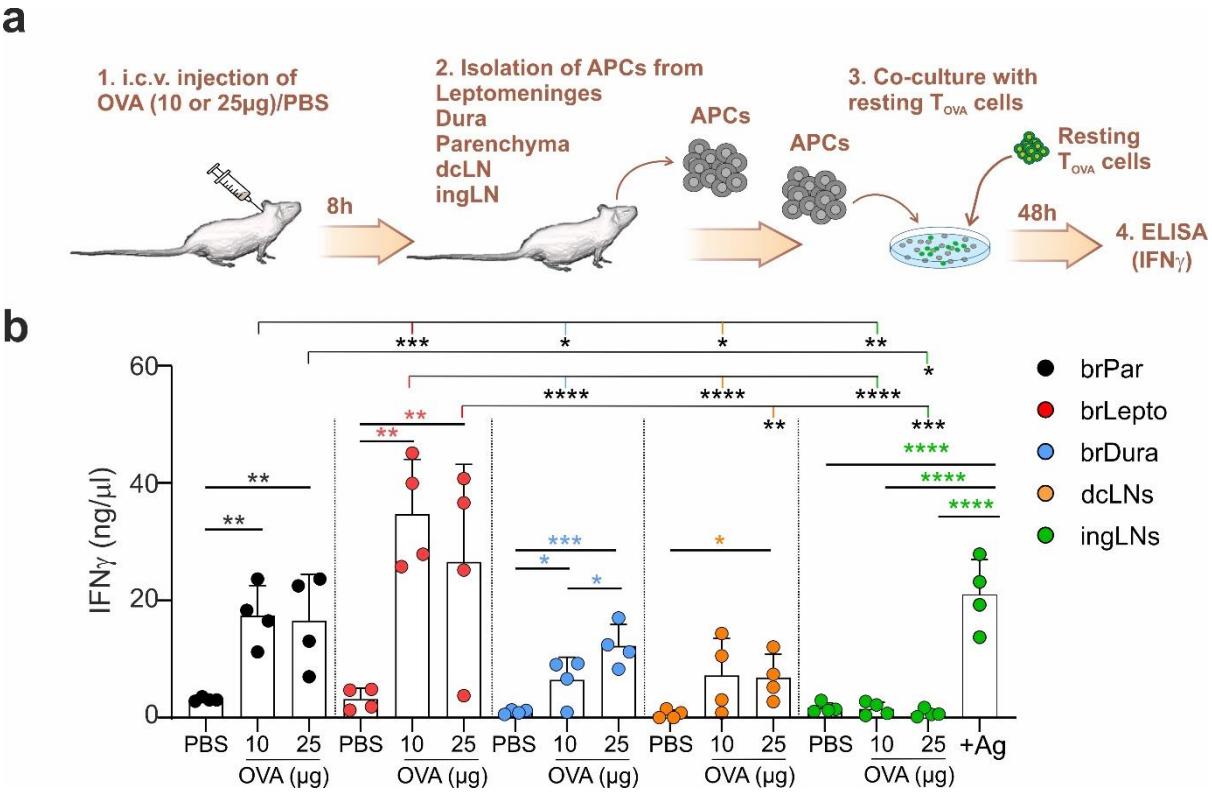

Figure 35: i.c.v.-injected antigens reach the dura and dcLNs. (a) Experimental setup. OVA antigen at different concentrations is injected i.c.v. in the lateral ventricle. Eight hours later, cells are harvested from the indicated compartments and co-cultured with resting T_{OVA} cells. T cell activation is then assessed 48 hours later by measuring IFNγ levels in the culture supernatant. (b) IFNγ production by T_{OVA} cells co-cultured with cells isolated from the indicated compartments. +Ag indicates T_{OVA} cells co-cultured with APCs from the ingLNs in the presence OVA. Data are mean + SEM and are cumulative of 2 independent experiments. Statistic for comparison within the same compartment (colored asterisks): two-tailed t-test. Statistic for comparison within different compartments (black asterisks): one-way ANOVA. *p<0.05, **p<0.01; ****p<0,001, ****p<0.0001.

exclusively to the leptomeninges and, to a lower extent, to the parenchyma (**Figure 36b**). We did not detect a significant accumulation of T_{OVA} cells in the dura or dcLNs.

Therefore, we concluded that, although drainage of i.c.v.-administered antigens to the dura and to the dcLNs was present; its potential role to activate autoreactive T cells in physiological conditions was overpowered by the significantly higher ability of the leptomeninges to take up and present CSF- and CNS-derived antigens. In line with this observation, also cells isolated from the dcLNs were not capable to spontaneously re-activate T_{bSYN} or T_{MBP} cells *in vitro* (**Figure 33c, d**).

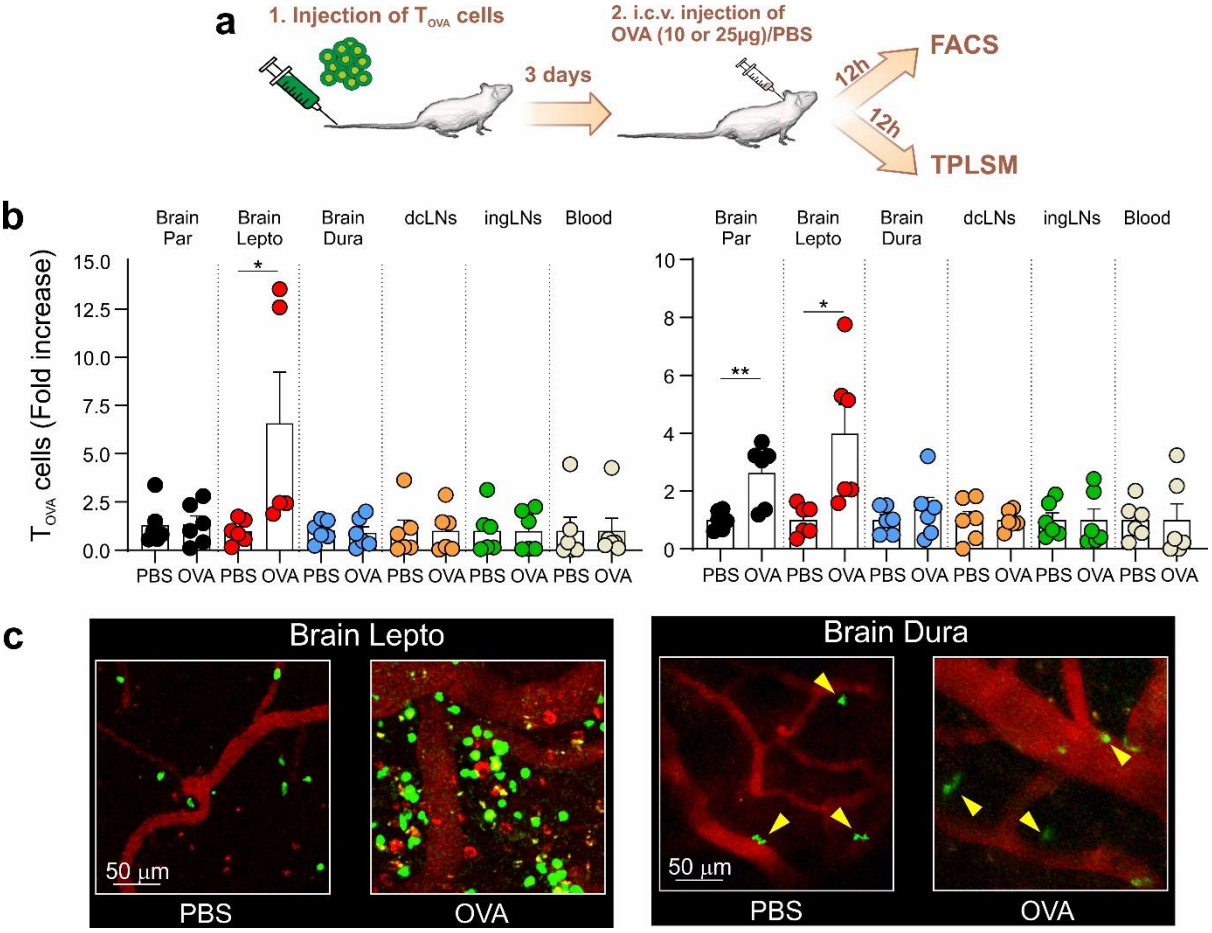

Figure 36: T_{OVA} cells accumulate in the leptomeninges but not in the dura or dcLNs after i.c.v. re-activation. (a) Experimental set-up. Three days after i.v. injection of T_{OVA} cells, 10 or 25 µg OVA or PBS (control) were injected i.c.v. Twelve hours later T cell distribution was assessed by FACS and TPLSM. (b) Flow cytometry quantification of the number of T_{OVA} cells after injection of 10 (left plot) or 25 µg (right plot) of OVA antigen. Data are normalized on the average number of T_{OVA} cells in the control group for each compartment (PBS). Data are mean + SEM and are cumulative of 2 (for 10 µg OVA) and 3 (for 25 µg OVA) experiments. Statistics: two-tailed t-test. *p<0,05; **p<0,001 (c) Representative TPLSM images of T_{OVA} cells (green) in leptomeninges and dura 12 hours after i.c.v. injection of 25 µg OVA in animals transferred 3 days before with T_{OVA} cells. PBS-injected animals were used as control. T_{OVA} cells located in the dura are highlighted by yellow arrowheads. Blood vessels were labelled with 2000KDa dextran and are in red.

We next checked if CNS antigen could be drained outside the CNS in acute or chronic neuroinflammatory conditions. During EAE, tissue destruction perpetrated by the infiltrating inflammatory cells causes the release of CNS antigens into the CSF.[160,161] We hypothesized that in this condition the dura and dcLNs may be exposed to higher quantities of antigen, sufficient to activate pathogenic T cells.

To this end, we tested the antigen presentation capacity of the dura in two distinct conditions of T_{bSYN} cell-mediated CNS damage: 1) in animals at the peak of T_{bSYN} cell EAE severity (**Figure 37**); 2) in animals which had undergone repeated bouts of EAE (**Figure 38**). As previously described, these animals have experienced multiple cycles of inflammatory destruction of the CNS parenchyma and display markers of persistent neurodegeneration, such as cortical atrophy and loss of neurofilaments.[20]

In both these experimental set-ups, we collected single cell suspensions from the CNS compartments and dcLNs and used them to stimulate resting T_{bSYN} cells *in vitro*, similarly to **Figure 33**. Also in these conditions, in contrast with the parenchyma and leptomeninges, we could not detect any spontaneous antigen presentation in the dura or dcLNs. However, as previously shown, when autoantigen was provided, cells from all sites were competent to stimulate the pathogenic effector T cells.

These data indicated that autoantigen was not spontaneously presented within the dura or dcLNs not only in acute but also in chronic autoimmune CNS lesions.

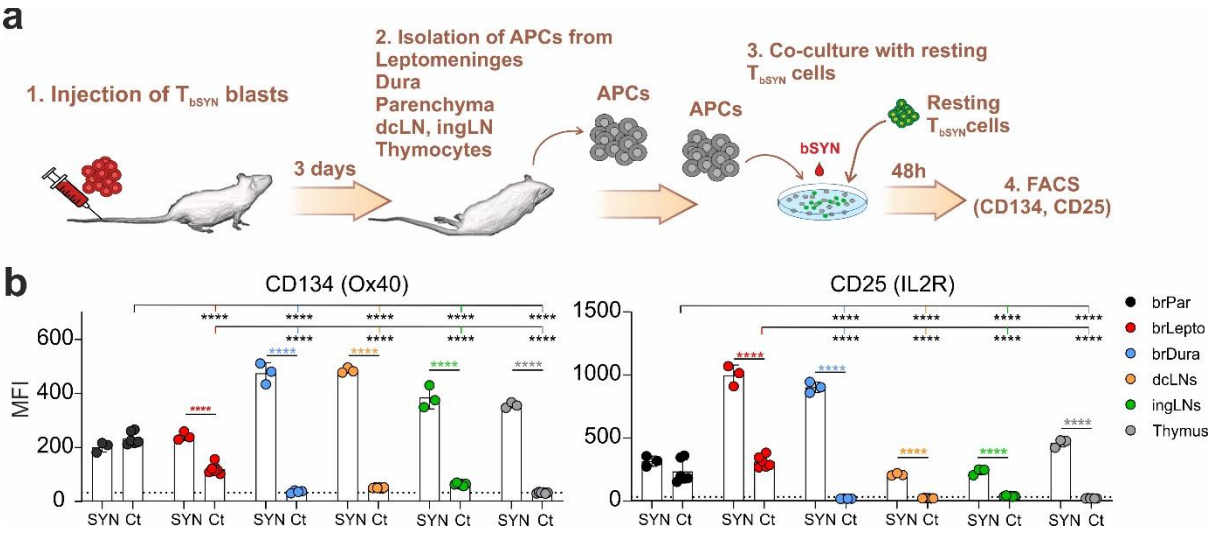

Figure 37: Dura-derived or dcLN-derived APCs isolated from EAE animals at the peak of disease severity do not spontaneously activate T_{bSYN} cells. (a) Experimental setup. T_{bSYN} cell-mediated EAE was induced by i.v. injection of T_{bSYN} blasts. At the peak of disease severity, cells were isolated from the indicated compartments and co-cultured with resting T_{bSYN} cells. After 48 hours T_{bSYN} cells were evaluated for markers of activation by FACS. (b) Median fluorescence intensity for the activation markers CD134 (Ox40) and CD25 (IL2R) of T_{bSYN} cells co-cultured for 48 hours with APCs from the indicated compartments. One experiment with three independent biological replicates. Data are mean + SEM. Statistic as in Figure 33.

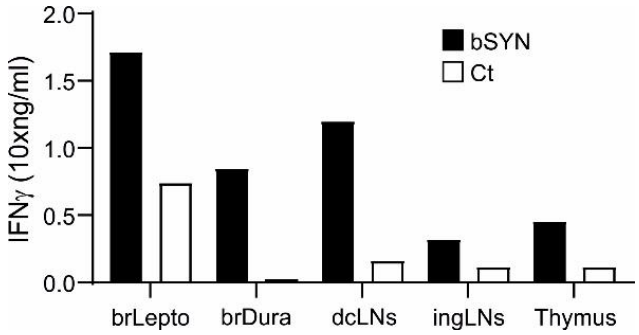

Figure 38: No spontaneous antigen presentation in the dura in chronic autoimmunity. IFNγ production measured by ELISA in the supernatant of T_{bSYN} cells cultured for 48h with APCs isolated from the indicated compartments of animals that had experienced four bouts of inflammatory attacks 3 months prior. T_{bSYN} cells were cultured in the presence of the cognate antigen (bSYN) or in presence of an irrelevant antigen or no antigen (control values pooled together). Due to the low number of cells, cells were pooled from 3 animals. Representative data of 2 independent experiments.

4.10 The dura lymphatic system does not play a role in the trafficking of T cells during EAE

Previous studies have suggested that the dura and the dura lymphatics may act as a pathway also for T cells, which may exit the CNS via the dura lymphatics to the dcLNs.

When we injected migratory T_{OVA} cells directly in the CSF, the cells distributed mostly in the leptomeninges (**Figure 39a**). Only a few of them could be detected in the dura and in the dcLNs (**Figure 39b**). This suggested that the trafficking of T cells from the CNS to the dura and dcLNs was low.

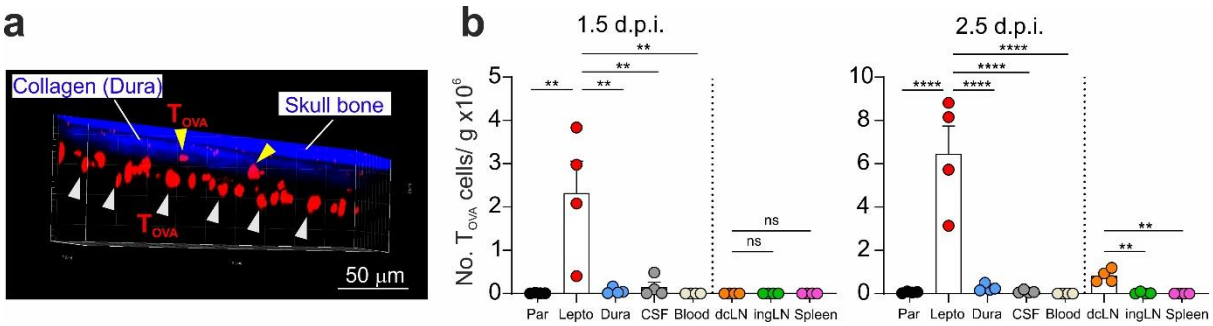

Figure 39: T_{OVA} cells injected i.t. accumulate predominantly in the leptomeninges and reach the dura and dcLNs only in low numbers. (a) Representative 3D reconstruction of a TPLSM recording depicting the localization of T_{OVA} cells (red) in the dura and leptomeninges 1.5 days after i.t. T cell injection. White and yellow filled arrowheads indicate T_{OVA} cells in the leptomeninges or in the dura, respectively. (b) Flow cytometry quantification of T_{OVA} cells in the indicated brain and peripheral compartments measured 1.5 days and 2.5 days post i.t. T cell injection. Data are mean + SEM and are cumulative of 2 independent experiments. Statistics: one way-ANOVA with post-hoc correction for multiple comparisons. **p<0.01, ****p<0.001, ns: not significant.

To evaluate the extent of the trafficking of the pathogenic T cells *in vivo* in the lymphatic vessels of the dura, we imaged T_{bSYN} cells in the dura lymphatics of animals that expressed eGFP under the Prox-1 promoter, a transcription factor highly expressed in the lymphatic

vasculature but not in blood vessels. We detected very rare T_{bSYN} cells with a round morphology within the lumen of the lymphatics (**Figure 40**).

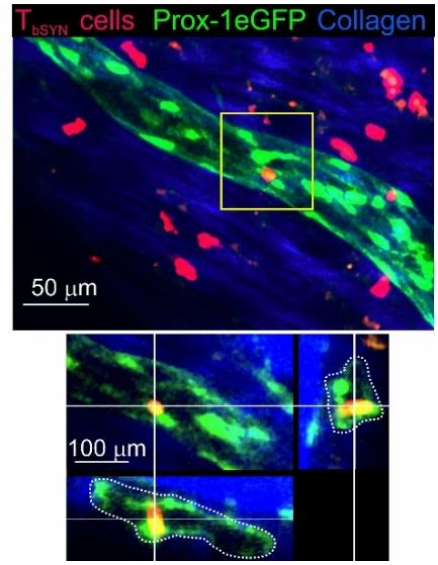

Figure 40: *In vivo* visualization of T_{bSYN} cells trafficking in the dural lymphatics vessels. Representative TPLSM picture of a T_{bSYN} cell (red) in a dural lymphatic vessel (green) of a Prox-1-eGFP transgenic rat on day 3.5 p.t. . The orthogonal views (bottom) show the intraluminal localization of the T cell depicted in the yellow square. Note that most of the T_{bSYN} cells in the dura are outside the lymphatic vessel.

Consistently, also the number of T_{bSYN} cells accumulating in the dcLNs was low (**Figure 41a**), although still significantly higher than in the non CNS-draining ingLNs. This relative accumulation was only observed for T_{bSYN} cells and not in T_{MBP} or T_{OVA} cells. Despite this minimal accumulation, the T_{bSYN} cells in the dcLNs were transcriptionally indistinguishable from T_{bSYN} cells found in the ingLNs (**Figure 41b, c**). In particular, the markers of T cell activation IFNγ and IL-17 were expressed at the same level as in the blood, suggesting that the cells found in the dcLNs might rather be of peripheral origin than coming from the CNS (**Figure 41d**).

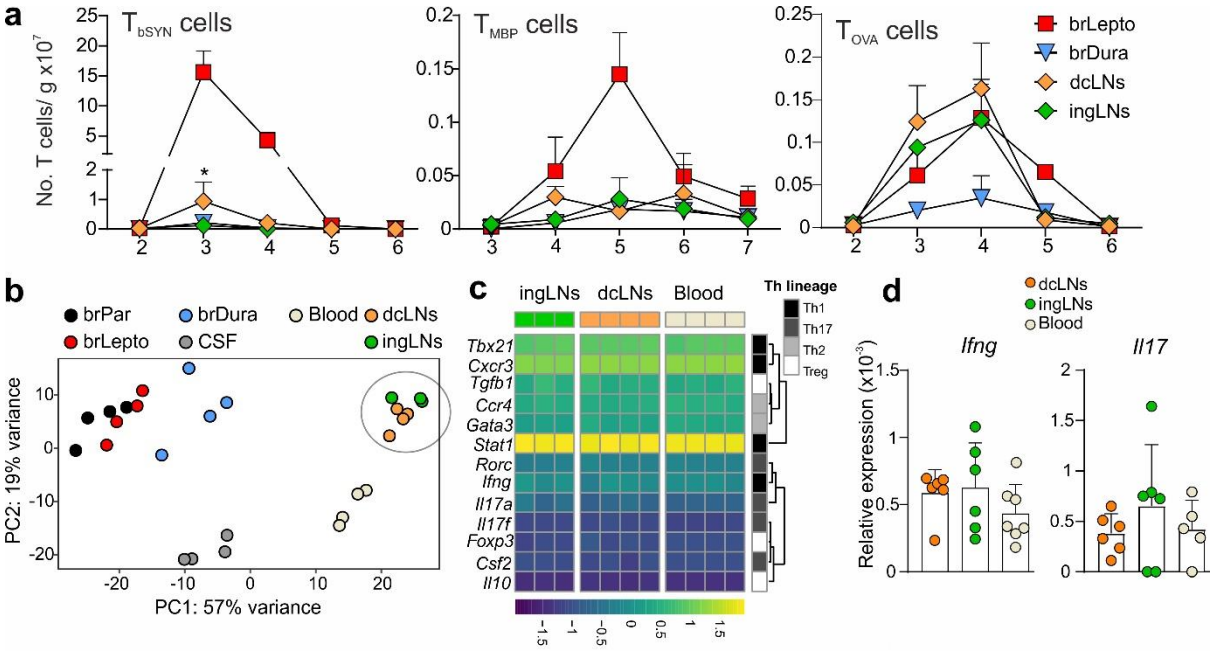

Figure 41: Role of dcLNs in EAE. (a) Flow cytometry quantification of T_{bSYN}, T_{MBP} and T_{OVA} cells (relative to organ weight) isolated from the specified compartments at the indicated time points p.t. Data are Mean + SD and are representative of 3 (T_{bSYN} cells) and 4 (T_{MBP} and T_{OVA} cells) independent experiments. Statistics: two-tailed t test comparing dcLNs vs ingLNs. Statistical analysis was performed to highlight the relative T_{bSYN} cell accumulation in the dcLNs. (b) PCA plot of NGS data on T_{bSYN} cells isolated from the indicated compartments on day 3 p.t. Note that T_{bSYN} cell derived from dcLNs and ingLNs cluster together. (c) Heat map of hierarchically clustered values of the same NGS data as in (b), showing genes related to Th lineage. (d) qPCR performed on T_{bSYN} cells sorted from the indicated compartments on day 3 p.t. Gene expression was calculated relative to the house-keeping gene, β-actin. Data are mean + SEM and are cumulative of three independent experiments. (a) *p<0.05

4.11 Dura lymphatic vessel ablation does not influence EAE course

The data suggested that the dura lymphatic drainage pathway was not a major trafficking route for antigens or encephalitogenic T cells and, thus, its role in EAE may be limited.

To clarify the role of the dura lymphatic system in EAE, we ablated dura lymphatic vessels by depriving them of their essential survival factor, VEGF-C/D,[109] prior to EAE induction. We injected i.t. an AAV vector encoding a VEGF-C/D trap. After 14 weeks, we induced EAE. At this time point lymphatic vessels were still absent (**Figure 42a**).

We observed that the disease course of animals with ablated dura lymphatics (AAV-rVEGFR3) was comparable to controls injected i.t. with either a sham AAV vector (AAV-Sham) or PBS (**Figure 42b**).

Consistently, lymphatic ablation did not influence the number of pathogenic T cells, nor the secondary recruitment of inflammatory cells in the dura, leptomeninges and CNS parenchyma at the peak of EAE disease severity (**Figure 43**).

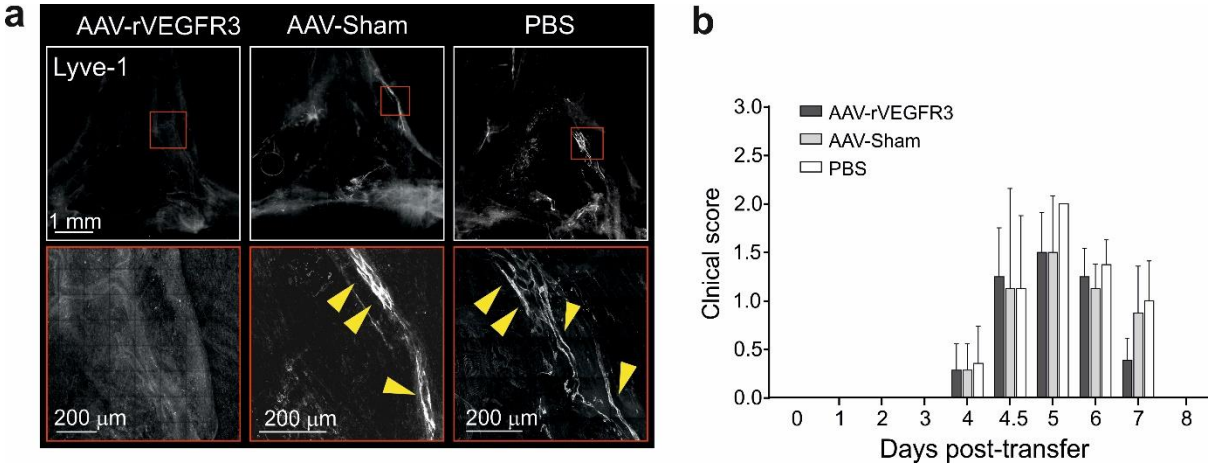

Figure 42: Dural lymphatic ablation does not alter the clinical course of EAE. Lymphatic vessels were ablated by i.t. injection of AAV encoding for VEGF-C trap (AAV-rVEGFR3). Control rats were treated with either an empty AAV (AAV-Sham) or PBS. Fourteen weeks later, EAE was induced by transfer of T_{bSYN} cells. (a) Representative confocal pictures of sinus confluence stained for Lyve-1 (grayscale), and relative magnifications of the indicated areas (red squares), showing the absence of Lyve-1-positive lymphatic vessels in animals treated with AAV-rVEGFR3. Lyve-1 fluorescence was still visible in AAV-Sham and PBS controls (yellow arrowheads). (b) Clinical course of animals treated with AAV-rVEGFR3, AAV-Sham or PBS. Data are mean + SD and are representative of 2 independent experiments, each with n=9 per group.

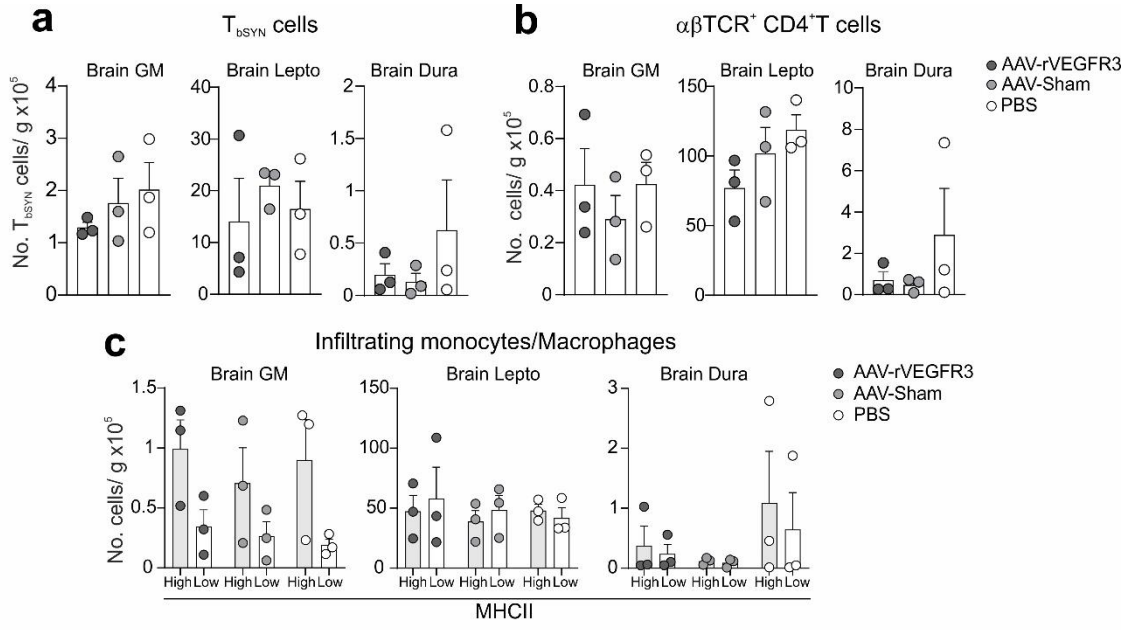

Figure 43: Ablation of the dural lymphatic vessels does not affect CNS inflammation in T_{bSYN} cell-mediated EAE. Experimental set-up as in Figure 42. (a-c) Flow cytometry quantification at the peak of disease severity of the numbers (per tissue weight) of (a) T_{bSYN} cells, (b) recruited $\alpha\beta TCR^+$ $CD4^+$ T cells and (c) $CD11b^+$ $CD45^{high}$ myeloid cells. Data are mean + SEM and are representative of two independent experiments each with n=3.

4.12 Preliminary investigations in the role of the dural sinuses in EAE

Recent publications describe accumulation of immune cells, including T cells, around the venous sinuses of the dura, both in the steady state and inflammatory conditions.[32] To determine if the sinuses of the dura may be a site of T cell trafficking during EAE, we assessed T_{bSYN} cell distribution by histology at the peak of disease infiltration in the different areas of the dura. Indeed, we found an accumulation of T_{bSYN} cells around the sinus confluence (**Figure 44a**), when compared to the hemispheric dura. However, T_{bSYN} cells distributed also largely and diffusely on the leptomeninges. FACS quantification confirmed the relative increase in T_{bSYN} cell numbers around the dural sinuses, relative to the hemispheric dura, which however remained significantly lower than the number of T cells in the leptomeninges (**Figure 44b**). More importantly, T_{bSYN} cells isolated from the dural sinuses did not display an activated phenotype (**Figure 44c**). Consistently, APCs isolated from the peri-sinus areas were unable to spontaneously activate T_{bSYN} cells (**Figure 44d**).

The dura sinuses have also been speculated as areas of T cell arrest and extravasation. Preliminary data on T_{OVA} cell motility in the dura sinuses do not support this hypothesis: T_{OVA} cells in the dura sinuses loosely rolled along the vessel wall or were quickly washed away (**Figure 44e**), with a motility pattern that closely resembled the one observed in vessels of the hemispheric dura (**Figure 19c**).

Figure 44 (following page): T_{bSYN} cell recruitment and functional characteristics in peri-sinus areas. (a) Confocal pictures of the indicated anatomical regions showing the increased number of T_{bSYN} cells (in red) around the sinus confluence (COS), near the superior sagittal sinus (SSS) and transverse sinuses (TS), compared to the hemispheric dura. Leptomeninges show diffuse and dense recruitment of T_{bSYN} cells. (b) Flow cytometry quantification, relative to organ weight (left) and absolute (right) of T_{bSYN} cells collected 3 days p.t. from the indicated compartments. Note the change of scale to highlight the relative accumulation of T_{bSYN} cells in the dura sinus (Sinus, light blue), compared to the dura hemispheres (Hem, dark green). Data are mean + SEM and are representative of 2 independent experiments. Statistics: one way-ANOVA. (c) qPCR from T_{bSYN} cells isolated from the indicated compartments 3 days after i.v. injection. Data are mean + SEM. One experiment with n=4. Statistic: one way-ANOVA with post-hoc correction for multiple comparisons. (d) Flow cytometry quantification of the median fluorescence intensity (MFI) of CD134 (Ox40) and CD25 (IL2R) in T_{bSYN} cells cultured for 48 h with APCs isolated from the indicated compartments of naive animals in presence of the cognate antigen (SYN). As control (Ct), an irrelevant antigen (OVA) or no antigen were added to the culture (values pooled together). Experimental setup as in Figure 31. Data are mean + SEM and are representative of 2 experiments. Statistics as in Figure 33. (e) Two photon analysis of T_{OVA} cell motility in the dura sinuses. On the left, TPLSM time-projection of intravascular T_{OVA} cells (in turquoise) in the SSS (labelled by 70KDa dextran, in red) performed on day 3 after T-cell transfer. The attenuation of laser intensity by erythrocytes limits the detection of T cells in the central part of the sinus. Exemplary rolling cells are filled arrowheads, fast-rolling cells are arrows. On the right, quantification of the percentage of T cells crawling, rolling or fast rolling within a 30min recording time. Numbers of analyzed T cells are indicated. Data are mean + SD and are cumulative of 6 movies. (b,c,d): *$p<0.05$, **$p<0.01$, ***$p<0.01$,****$p<0.0001$.

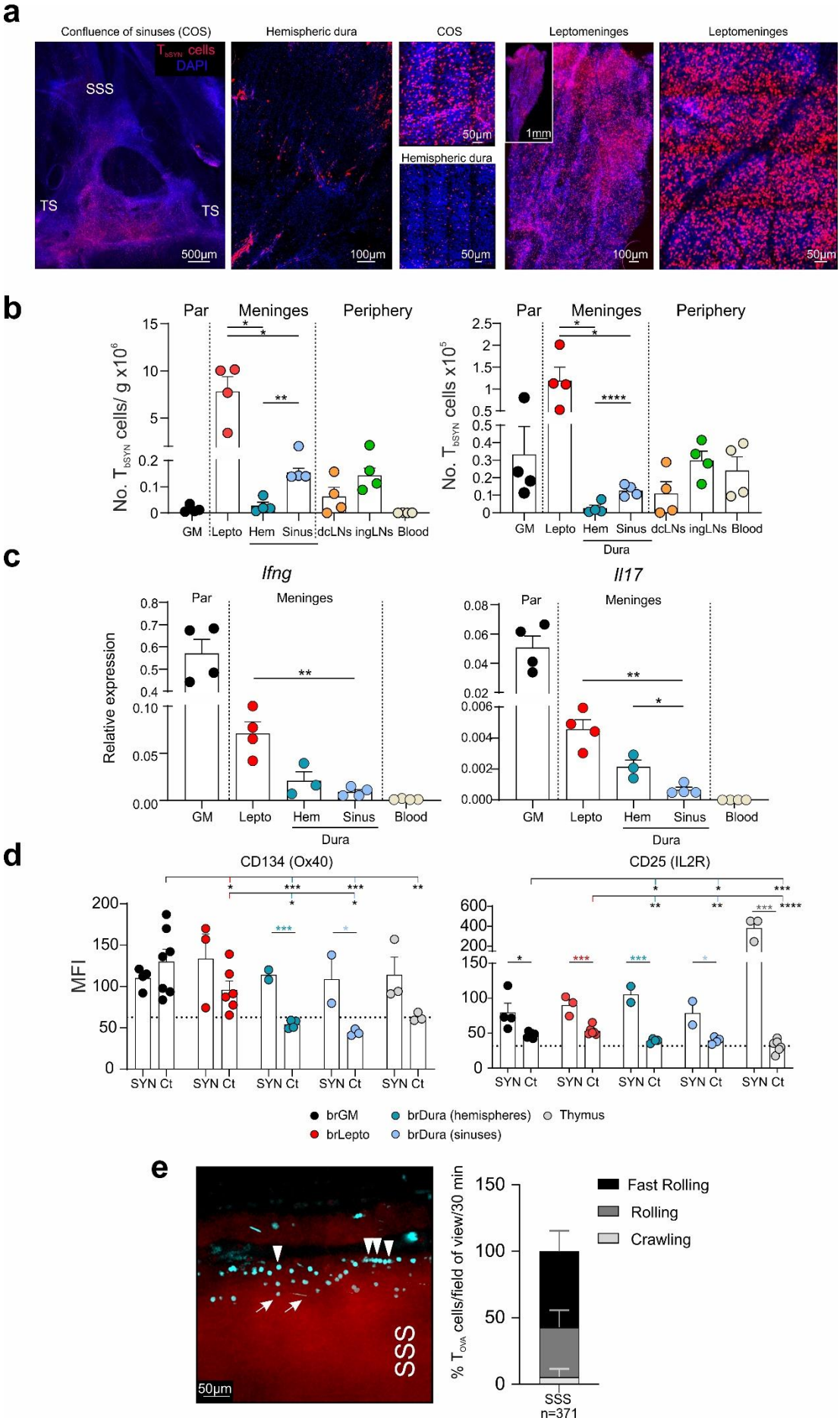
a
Confluence of sinuses (COS)
Hemispheric dura
COS
Leptomeninges
Leptomeninges
SSS
TS
TS
500µm
100µm
50µm
50µm
1mm
100µm
50µm
b
Par
Meninges
Periphery
No. T bSYN cells/ g x10^6
No. T bSYN cells x10^5
GM
Lepto
Hem
Sinus
dcLNs
ingLNs
Blood
Dura
c
Ifng
Il17
Relative expression
d
CD134 (Ox40)
CD25 (IL2R)
MFI
SYN Ct
brGM
brLepto
brDura (hemispheres)
brDura (sinuses)
Thymus
e
SSS
50µm
% T OVA cells/field of view/30 min
Fast Rolling
Rolling
Crawling
SSS
n=371

5 DISCUSSION

In this study, we dissected the role of the different meningeal layers in a model of multiple sclerosis, the transfer EAE of the Lewis rat. In this model, fully activated CNS-reactive (encephalitogenic) T cells are injected i.v. to induce EAE. CNS-reactive T cells access the CNS through the leptomeninges, where they are re-activated by local APCs and initiate the recruitment of other immune cells, which ultimately results in tissue damage.[20,25,27,28] The leptomeninges are therefore a crucial checkpoint for disease initiation. It is unknown if also the other vascularized meningeal layer, the dura, participates in disease development.

We discovered that, despite their topographical proximity, the dura and the leptomeninges participate to markedly different extents to the inflammation process: CNS-reactive T cells migrated in significantly lower numbers in the dura than in the leptomeninges; further, CNS-reactive T cells in the dura showed a significantly lower activation level than in the leptomeninges. This resulted in lower levels of inflammatory cytokines and chemokines in the dura milieu and eventually reduced secondary recruitment of other T cells and inflammatory monocytes.

We investigated several anatomical and functional properties of the dura that may explain its minimal contribution to EAE.

5.1 Dural vessels are less permissive to T cell trafficking in the steady state

TPLSM recordings of the intravascular motility of T cells showed that both CNS-reactive and CNS-ignorant T cells had very minimal interaction with the vessels of the dura, with most of the cells rolling or passing by, a motility pattern that has been observed for effector T cells in peripheral tissues.[25] NGS of the endothelial cells sorted from the leptomeninges and from the dura vessels showed that the two vascular beds are transcriptionally distinct. We observed that leptomeninges had a higher expression of chemokines and integrin ligands. As mentioned in the introduction, chemokines and integrin ligands are required for the firm adhesion of T cells to the endothelium and for their crawling on the luminal surface of the vessel, the pre-requisite step for T cell extravasation. Interfering with integrin signaling on T cells with an anti-VLA4 antibody, resulted in the detachment of almost all the T cells from the leptomeningeal vessels and a nearly complete abolition of crawling and rolling cells. In contrast, this effect was not as pronounced in the dura vessels, where T cells retained their motility profile. The dura vessels, similarly to the vasculature of other peripheral organs, express in fact high levels of selectins, which are weak mediators of effector T cell adhesion to the endothelium.[162] It is therefore

possible that, in the dura vessels, most of T cell motility is mediated by these weak interactions. Of note, upon anti-VLA4 treatment, T cell numbers also were reduced in the dura vessels, albeit to a lesser extent than in the leptomeninges, suggesting that integrins retain an important function for T cell adhesion and arrest also in this compartment.

Interestingly, expression levels of the major $\alpha_4\beta_1$ ligand VCAM1, were not significantly different between the leptomeninges and the dura, although there was a trend of increased expression in the leptomeninges. However, the leptomeninges expressed several other integrin ligands, among which fibronectin, which can bind to VLA-4 with a strength that is at least comparable to VCAM1.[163]

Further, alternative splicing of both VCAM1 and fibronectin can modulate their affinity for $\alpha_4\beta_1$.[164-167]

It would therefore be of interest to precisely dissect how these different integrin ligands mediate T cell motility in the leptomeninges. On the other hand, blocking of selectin signaling may clarify their role as mediators of T cell motility in the dura vessels.

The data concerning the effect of the inflammatory chemokines CXCL9-11 on T cell motility in the meningeal vessels were less conclusive. While acute blockade of the receptor CXCR3 with a blocking antibody had a measurable effect on T cell adhesion and motility in the leptomeninges, this result was not replicated by genetic deletion of CXCR3 by CRISPR-Cas9 on T cells (T-X3KO cells).

Although at present we cannot completely rule out off-target effects of the anti-CXCR3 antibody, a possible explanation is that T-X3KO cells upregulate other adhesion molecules that compensate for the lack of CXCR3 signaling. Further experiments, investigating the expression profile of other adhesion molecules on T-X3KO cells and their migratory ability in inflamed conditions, will help clarify the role of CXCR3 on T cell migration.

It is worth mentioning that other factors besides the endothelial transcriptional profile may influence T cell motility in the dura and leptomeningeal vessels. Among those, shear stress, that is the tangential force imposed by the blood flow to the endothelium, affects both T cell and endothelial cell adhesiveness.[168-170] In particular, effector T cells enter non-lymphoid organs via post-capillary venules thanks to their ability to form slings and tethers in conditions of high shear stress.[169] Although we imaged venules of comparable diameter in both dura and leptomeninges, differences in shear stress in these two vascular beds may also contribute to the observed T cell motility behavior.

5.2 The dura tissue is largely spared by the immune response during EAE

We could demonstrate that the indifference of the dura vessels to T cell trafficking was not absolute: activation of the dura vessel endothelium by the cytokines IFNγ and TNFα induced a rapid and profound change in T cell motility: T cells started to adhere to the dura endothelium and changed their motility pattern, with more cells adhering and crawling along the vessel wall and progressively more cells extravasating in the dura milieu.

This finding was in stark contrast with what we observed during T_{bSYN} and T_{MBP} cell-mediated EAE: despite both cell lines cause overt inflammation in the CNS, T_{bSYN} and T_{MBP} cells did not accumulate selectively in the dura at any point of T cell infiltration, nor adhered to the dura vessel walls.

This suggested that, during EAE, the dura tissue was mostly indifferent or only marginally affected by the inflammatory process. In fact, during T_{bSYN} cell-mediated EAE, we observed significantly lower expression of inflammatory mediators. Consequently, also the recruitment of immune cells was significantly lower in the dura than in the leptomeninges. This was associated with a significantly lower activation level of T_{bSYN} cells in the dura, compared to the leptomeninges.

We investigated multiple immunological parameters that may justify the reduced T cell activation in the dura.

First, we excluded that T_{bSYN} cells reaching the dura represented a regulatory (T_{reg}) or non-reactive subgroup. Next generation sequencing showed that T_{bSYN} cells in the dura had a T_H1/T_H17 phenotype, similar to T cells in the leptomeninges, and they did not upregulate genes associated with T cell anergy, exhaustion or T_{reg} differentiation. Indeed, T_{bSYN} cells extracted from the dura could be readily re-activated *in vitro* by supplementation with the cognate antigen. Second, we turned to investigate if antigen presentation was intact in the dura tissue. The dura hosts a diverse immune cell population with several potential antigen-presenting cells.[81] Accordingly, we found that the dura harbored $MHCII^+$ myeloid cells in comparable proportions to what we had observed in the leptomeninges.

T cells in the dura moved freely in the extravascular space, making frequent contacts with the resident macrophages. Upon exogenous antigen administration, the T cells could be effectively reactivated, as demonstrated by NFAT translocation, reduction in T cell velocity and arrest, upregulation of inflammatory cytokines and recruitment of other T cells to the dura.

Given the full competence of T cells in the dura to be activated and of dural APCs to present antigens, we concluded that the crucial limiting factor must be the availability of the antigen

itself. Limited supply of CNS antigens to the dura could therefore explain why T_{bSYN} cells were not activated in the dura during EAE. Several of our experiments seemed to support this hypothesis. First, i.t. administration of antigens showed that the leptomeninges were the primary site of antigen uptake and T cell reactivation, while the dura was largely spared. On the other hand, when we selectively activated T cells in the dura by transcranial addition of the cognate antigen, inflammation was mostly confined to the dura. Second, and perhaps most importantly, in contrast to the leptomeninges and CNS parenchyma, the dura did not display spontaneous presentation of CNS antigens. We tested the ability of the dura tissue to spontaneously activate autoreactive T_{bSYN} and/or T_{MBP} cells in steady state, acute CNS inflammation and chronic CNS inflammation induced by repeated EAE bouts. Even in those situations of increased CNS tissue destruction and neurodegeneration, which correlate with autoantigen release in the CSF, the dura did not display detectable autoantigen presentation.

These data suggested that, despite their proximity, leptomeninges and dura are functionally distinct compartments. It would be of interest to precisely understand what properties of the meningeal layers ensure this separation. It has been shown that the dura-arachnoid barrier is a relatively impermeable structure,[54] due to the presence of tight junctions.[47] Indeed, even in animal models of headache, which require dural activation by epidural application of inflammatory cocktails, no extravasation of 70KDa solutes in the underlying parenchyma has been reported.[171] On the other hand, the transcranial passage of solutes from the dura to the underlying brain meninges and parenchyma has been described for molecules up to 40KDa.[55]

The concept that the dura is largely separated from the CNS can be inferred also by clinical observations. In the dura, florid inflammatory processes can persist chronically, for decades, even without inducing overt changes in CSF compositions, as observed for tuberculous pachymeningitis[172,173] and IgG4 pachymeningitis.[96] While invasion of the underlying CNS parenchyma in the course of pachymeningitis is reported, it occurs by continuity and due to the aggressive invasiveness of the pathogenic agent.[97]

Conversely, the leptomeninges, despite their relative quiescent immune cell repertoire, can readily mount an overwhelming immune response, with massive immune cell recruitment and frequent dissemination to the underlying parenchyma (meningoencephalitis). Such over-reactivity is exemplified by infectious meningitis, when leptomeningeal inflammation is sudden (hence the term fulminant meningitis), widespread and potentially fatal due to the consequent intracranial hypertension.[57]

Besides structural factors, cells in the dura may functionally contribute to a dampened immune response. Regulatory T cells[174] and type 2 innate lymphocytes have been described in the

dura.[89] Type 2 innate lymphocytes secrete IL-13 which may limit Type-1 immune responses during CNS injury.[89] It is therefore possible that T_{bSYN} cells reaching the dura may well encounter CNS antigens, but be limited in their activation by the immunomodulatory milieu of the dura.

A more in-depth characterization of the immune cell composition of the dura and leptomeninges in the steady state and during T_{bSYN} cell EAE may help clarify this aspect.

Nevertheless, it is important to point out that our experiments do not support this scenario: exogenous antigen administration on the dura readily activated T cells in vivo within a few hours. Similarly, when the cognate antigen was provided, dural cells activated T cells *in vitro* to levels comparable to other peripheral organs. These observations argue against a possible constitutive immune quiescence of the dura.

On the other hand, recent publications suggest that the dura immune profile may share similarities with other peripheral barrier tissues, such as the gut or the skin, which are regularly challenged by exogenous microorganisms and therefore have an immune repertoire skewed towards type-2 responses. This interesting hypothesis is supported by reports of microbial pathogens disseminating and persisting in the dura, with a potential predilection for areas around the large sinuses of the dura.[92-94]

These peri-sinus areas have been studied in a recent publication.[32] T cells have been found around those large venous conduits, in proximity to APCs. Further, traces of CNS autoantigens have been detected in the dura. These observations led to the hypothesis that dural APCs may sample CNS antigens selectively and exclusively in these peri-sinus areas and therefore, similarly to leptomeningeal APCs, activate CNS-autoreactive T cells and initiate CNS immunity.

In our system, we indeed observed an increased accumulation of effector pathogenic T cells in these sinus adjacent dural areas compared to areas of the hemispheric dura. However, the numbers of effector T cells were still significantly lower compared to the ones of the leptomeninges and T_{bSYN} cells isolated from these sinus-adjacent areas did not display an activated phenotype. Accordingly, cells isolated from peri-sinusal areas, similarly to cells from the dura hemispheres, failed to spontaneously present autoantigens.

Assessment of secondary cell recruitment in the peri-sinus areas compared to the hemispheric dura and leptomeninges, as well as a better understanding of the ability of distinct subsets of APCs in the dura and leptomeninges to sample and present CNS antigens, may further clarify the potential involvement of these peri-sinusal areas in EAE.

5.3 The dura lymphatic system is not involved in transfer EAE

Another immunological component of the dura tissue that has been recently implicated in CNS autoimmunity is the dura lymphatic vasculature. These vessels follow the big venous conduits of the dura sinuses and, in the mouse, have been described as especially abundant in the cranial base and in the cervical spinal cord. It has been demonstrated that these structures contribute to the drainage of solutes from the subarachnoid space and their functionality may be relevant for a variety of pathologies, ranging from Alzheimer's disease to traumatic brain injury.

The recent re-discovery of these structures has led to the speculation that, unlike historically thought, the CNS in fact possesses a lymphatic drainage system, which may contribute to immune responses in the CNS. On that note, ablation of the dural lymphatic vasculature in a mouse model of active EAE has been reported to delay disease onset and reduce disease severity.[122] The ameliorated disease course was ascribed to a dampened activation of the pathogenic T cells in the deep cervical lymph nodes.

In our system, we did not detect any contribution of the dura lymphatics or the deep cervical lymph nodes to the EAE disease process. Effector T cells did not accumulate in substantial numbers in the dura lymphatics and in the dcLNs. Even when injected intrathecally, T cells distributed preferentially along the leptomeninges and reached the deep cervical lymph nodes only 2.5 days after i.t. injection. Further, CNS-reactive T cells isolated from the dcLNs were transcriptionally identical to T cells found in other, non-CNS-draining lymph nodes. We also were unable to detect any functional drainage of CNS autoantigens to the dcLNs in the steady state and EAE conditions. Even in the "extreme" set-up of chronic inflammation, when animals had undergone multiple bouts of EAE, no spontaneous activation of T cells in the deep cervical lymph nodes was detected. Accordingly, elimination of the dura lymphatic vessels had no effect on T cell migration to the CNS and on the clinical symptoms of the animals.

It is not immediately intuitive how the dura lymphatics and dcLNs may contribute to EAE pathology. In active EAE, priming and expansion of autoreactive T cells occurs in the periphery, in lymph nodes which drain the site of immunization. There, massive amounts of antigen and adjuvants are injected and enlargement of the draining lymph nodes is visible roughly one week after immunization. The draining lymph nodes contain competent encephalitogenic T cells, which can be isolated and transferred in animals to induce disease.[17] The fully activated T cells then enter the circulation and, after upregulation of migratory

genes, access the CNS, where they are re-activated. The timing of disease onset, roughly 9-10 days after immunization, is compatible with this kinetic.

Also in transfer EAE, it is not clear where precisely in this sequence of events the deep cervical lymph nodes would play a role: the effector T cells blasts upregulate migratory genes and rapidly reach the CNS, where they are re-activated and induce disease 2.5-3 days after i.v. injection.[23] A further re-activation in the deep cervical lymph nodes prior to T cell entry is not only unlikely from a timing perspective (T cell re-activation requires on average 48 hours), but also from an immunological point of view: upon antigen encounter, T cells are re-activated and stimulate the recruitment of cells at the site of re-activation. Indeed, peripheral infusion of CNS antigens prior to EAE induction traps autoreactive T cells in peripheral secondary lymphoid organs and prevents disease development.[175,176] In line with this is also the finding that, even in animals that lack secondary lymphoid tissue, passive transfer EAE develops normally.[45]

The proposition that CNS antigens may be drained to the deep cervical lymph nodes and stimulate CNS autoimmunity has experienced cyclical popularity in EAE research, starting from the first observations of myelin antigens in the cervical lymph nodes of MS patients[117] and that surgical removal of CNS-draining lymph nodes ameliorates EAE severity.[119,120] Indeed, in a spontaneous model of EAE, it has been speculated that priming occurs in the deep cervical lymph nodes.[119] More recently, it has been reported that in a model of demyelination, which implies widespread apoptosis of oligodendrocytes, the release of autoantigens may prime MOG-reactive T cells in the dcLNs.[177] However, a previous report had obtained diametrically opposite results, showing that, upon oligodendrocyte death no convincing autoimmune T cell response could be elicited.[178]

On that note, the evidence of a possible association between prior CNS lesions and MS has not been proven.[179]

Another possible mechanism for activation of autoreactive T cells is cross-recognition by CNS-reactive T cells of peptides of foreign origins by mechanisms of molecular mimicry. It has been demonstrated that viral peptides that share sequences with CNS proteins are capable of eliciting autoimmunity.[180] This is in line with the observation that autoreactive T cells are frequently cross-reactive, recognizing foreign peptides as well as autoantigens.[8,9,181,182]

In conclusion, at present there is no convincing evidence that antigens drained from the CNS to peripheral lymphoid stations may contribute to the priming and activation of autoreactive T cells. On the other hand, mechanisms of molecular mimicry, which involve the re-activation

of the CNS-reactive T cells in by exogenous antigens, e.g. by commensal bacteria in the gut or by viruses in the respiratory tract, seem to be involved in the onset and perpetuation of MS.

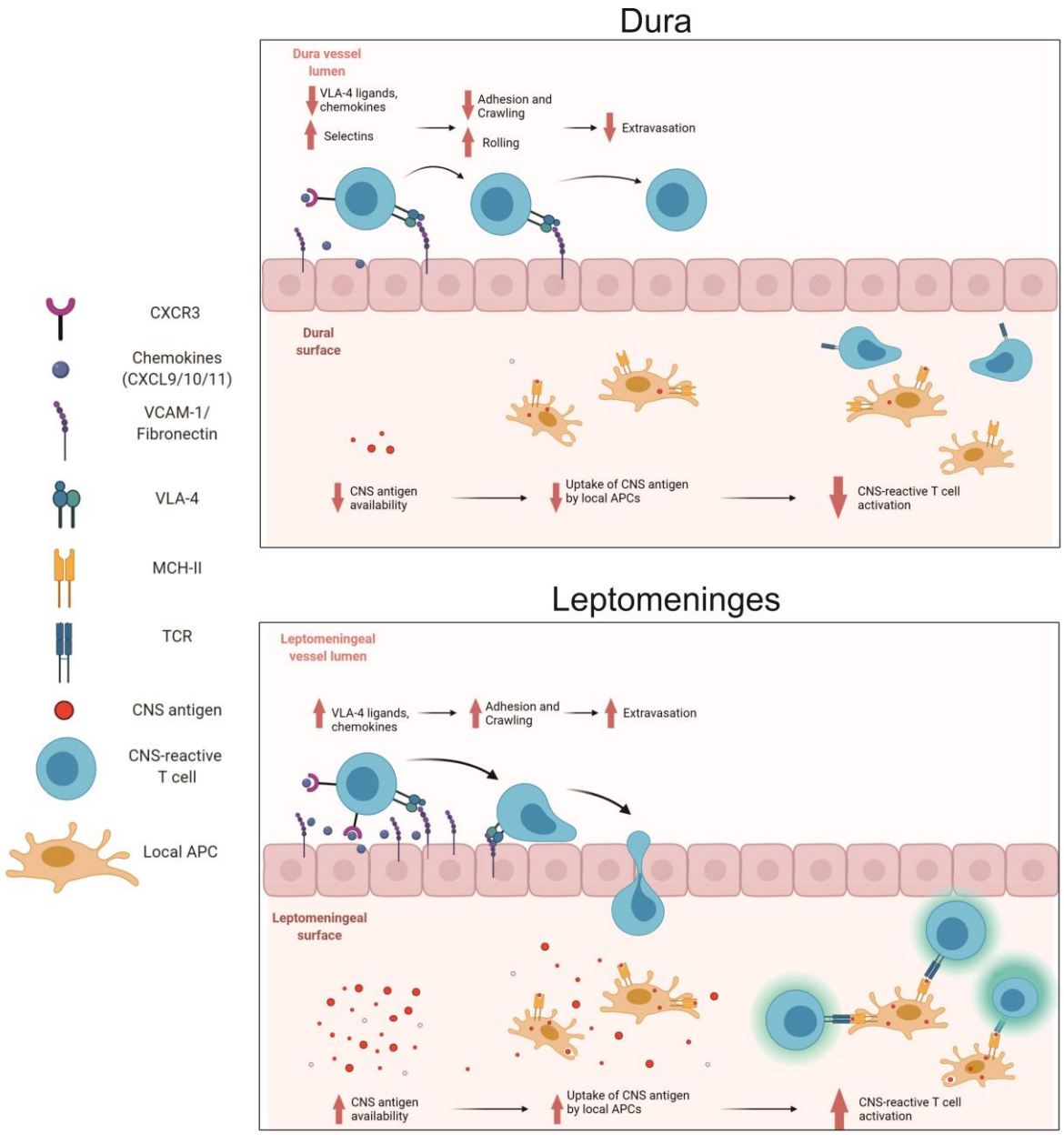

Figure 45: Differential contribution of the meningeal layers to the autoimmune process of EAE. In the dura, the reduced adhesiveness of the T cells to the vascular surface limits T cell adhesion. Further, the reduced antigen availability limits the reactivation of CNS-reactive T cells. In the leptomeninges, the vessels are permissive to T cell adhesion and extravasation. Local APCs sample CNS antigens from the underlying parenchyma and are capable of activating autoreactive T cells. Illustration created with Biorender (https://app.biorender.com).

6 CONCLUSIONS AND PERSPECTIVES

This work describes the contribution of the different meningeal layers to CNS autoimmunity (**Figure 45**). Due to its intrinsic vascular properties and reduced access to CNS autoantigens, the dura is largely shielded from the neuroinflammatory process. In contrast, the permissive nature of the leptomeningeal vessels to immune cell trafficking and the ability of local APCs to present CNS antigens, pose the leptomeninges as the crucial site for initiation of CNS inflammation.

These findings are substantiated by the observation that, in human MS, leptomeningeal inflammation is widespread and florid during every phase of the disease, from early diagnosis to chronic progression. Studies comparing the extent of inflammation in dural and leptomeningeal tissue from MS samples may indicate if this differential contribution of the meningeal layers is observed also in human disease.

Furthermore, investigation of the immune cell responses in the leptomeninges and dura in models of chronic neuroinflammation, where repeated bouts of EAE cause persistent CNS degeneration and therefore more closely resemble the human clinical course, will allow us to clarify if the anatomical and functional segregation of dura and leptomeninges is maintained or disrupted during chronic inflammation.

7 REFERENCES

1. Reich DS, Lucchinetti CF, Calabresi PA. Multiple Sclerosis. N Engl J Med 2018;378:169-80.

2. Frischer JM, Bramow S, Dal-Bianco A, et al. The relation between inflammation and neurodegeneration in multiple sclerosis brains. Brain 2009;132:1175-89.

3. Lucchinetti CF, Popescu BF, Bunyan RF, et al. Inflammatory cortical demyelination in early multiple sclerosis. N Engl J Med 2011;365:2188-97.

4. Howell OW, Reeves CA, Nicholas R, et al. Meningeal inflammation is widespread and linked to cortical pathology in multiple sclerosis. Brain 2011;134:2755-71.

5. Kidd D, Barkhof F, McConnell R, Algra PR, Allen IV, Revesz T. Cortical lesions in multiple sclerosis. Brain 1999;122 (Pt 1):17-26.

6. Sospedra M, Martin R. Immunology of Multiple Sclerosis. Semin Neurol 2016;36:115-27.

7. Hohlfeld R, Dornmair K, Meinl E, Wekerle H. The search for the target antigens of multiple sclerosis, part 1: autoreactive CD4+ T lymphocytes as pathogenic effectors and therapeutic targets. Lancet Neurol 2016;15:198-209.

8. Jelcic I, Al Nimer F, Wang J, et al. Memory B Cells Activate Brain-Homing, Autoreactive CD4(+) T Cells in Multiple Sclerosis. Cell 2018;175:85-100 e23.

9. Wang J, Jelcic I, Muhlenbruch L, et al. HLA-DR15 Molecules Jointly Shape an Autoreactive T Cell Repertoire in Multiple Sclerosis. Cell 2020;183:1264-81 e20.

10. Bahbouhi B, Pettre S, Berthelot L, et al. T cell recognition of self-antigen presenting cells by protein transfer assay reveals a high frequency of anti-myelin T cells in multiple sclerosis. Brain 2010;133:1622-36.

11. Zhang J, Markovic-Plese S, Lacet B, Raus J, Weiner HL, Hafler DA. Increased frequency of interleukin 2-responsive T cells specific for myelin basic protein and proteolipid protein in peripheral blood and cerebrospinal fluid of patients with multiple sclerosis. J Exp Med 1994;179:973-84.

12. Ellmerich S, Mycko M, Takacs K, et al. High incidence of spontaneous disease in an HLA-DR15 and TCR transgenic multiple sclerosis model. J Immunol 2005;174:1938-46.

13. International Multiple Sclerosis Genetics C, Hafler DA, Compston A, et al. Risk alleles for multiple sclerosis identified by a genomewide study. N Engl J Med 2007;357:851-62.

14. Haghikia A, Hohlfeld R, Gold R, Fugger L. Therapies for multiple sclerosis: translational achievements and outstanding needs. Trends Mol Med 2013;19:309-19.

15. Hoftberger R, Leisser M, Bauer J, Lassmann H. Autoimmune encephalitis in humans: how closely does it reflect multiple sclerosis ? Acta Neuropathol Commun 2015;3:80.

16. Ben-Nun A, Kaushansky N, Kawakami N, et al. From classic to spontaneous and humanized models of multiple sclerosis: impact on understanding pathogenesis and drug development. J Autoimmun 2014;54:33-50.

17. Ben-Nun A, Wekerle H, Cohen IR. The rapid isolation of clonable antigen-specific T lymphocyte lines capable of mediating autoimmune encephalomyelitis. Eur J Immunol 1981;11:195-9.

18. Flügel A, Willem M, Berkowicz T, Wekerle H. Gene transfer into CD4+ T lymphocytes: green fluorescent protein-engineered, encephalitogenic T cells illuminate brain autoimmune responses. Nat Med 1999;5:843-7.

19. Flügel A, Berkowicz T, Ritter T, et al. Migratory activity and functional changes of green fluorescent effector cells before and during experimental autoimmune encephalomyelitis. Immunity 2001;14:547-60.

20. Lodygin D, Hermann M, Schweingruber N, et al. beta-Synuclein-reactive T cells induce autoimmune CNS grey matter degeneration. Nature 2019;566:503-8.

21. Kawakami N, Lassmann S, Li Z, et al. The activation status of neuroantigen-specific T cells in the target organ determines the clinical outcome of autoimmune encephalomyelitis. J Exp Med 2004;199:185-97.

22. Kawakami N, Nagerl UV, Odoardi F, Bonhoeffer T, Wekerle H, Flugel A. Live imaging of effector cell trafficking and autoantigen recognition within the unfolding autoimmune encephalomyelitis lesion. J Exp Med 2005;201:1805-14.

23. Odoardi F, Sie C, Streyl K, et al. T cells become licensed in the lung to enter the central nervous system. Nature 2012;488:675-9.

24. Engelhardt B, Vajkoczy P, Weller RO. The movers and shapers in immune privilege of the CNS. Nat Immunol 2017;18:123-31.

25. Bartholomäus I, Kawakami N, Odoardi F, et al. Effector T cell interactions with meningeal vascular structures in nascent autoimmune CNS lesions. Nature 2009;462:94-8.

26. Kivisäkk P, Imitola J, Rasmussen S, et al. Localizing central nervous system immune surveillance: meningeal antigen-presenting cells activate T cells during experimental autoimmune encephalomyelitis. Ann Neurol 2009;65:457-69.

27. Lodygin D, Odoardi F, Schläger C, et al. A combination of fluorescent NFAT and H2B sensors uncovers dynamics of T cell activation in real time during CNS autoimmunity. NatMed 2013;19:784-90.

28. Schläger C, Körner H, Krueger M, et al. Effector T-cell trafficking between the leptomeninges and the cerebrospinal fluid. Nature 2016;530:349-53.

29. Magliozzi R, Howell O, Vora A, et al. Meningeal B-cell follicles in secondary progressive multiple sclerosis associate with early onset of disease and severe cortical pathology. Brain 2007;130:1089-104.

30. Vajkoczy P, Laschinger M, Engelhardt B. Alpha4-integrin-VCAM-1 binding mediates G protein-independent capture of encephalitogenic T cell blasts to CNS white matter microvessels. J Clin Invest 2001;108:557-65.

31. Reboldi A, Coisne C, Baumjohann D, et al. C-C chemokine receptor 6-regulated entry of TH-17 cells into the CNS through the choroid plexus is required for the initiation of EAE. Nat Immunol 2009;10:514-23.

32. Rustenhoven J, Drieu A, Mamuladze T, et al. Functional characterization of the dural sinuses as a neuroimmune interface. Cell 2021;184:1000-16 e27.

33. Vestweber D. How leukocytes cross the vascular endothelium. Nat Rev Immunol 2015;15:692-704.

34. Schmid-Schönbein GW, Usami S, Skalak R, Chien S. The interaction of leukocytes and erythrocytes in capillary and postcapillary vessels. Microvasc Res 1980;19:45-70.

35. McEver RP, Cummings RD. Role of PSGL-1 binding to selectins in leukocyte recruitment. J Clin Invest 1997;100:S97-103.

36. Campbell JJ, Hedrick J, Zlotnik A, Siani MA, Thompson DA, Butcher EC. Chemokines and the arrest of lymphocytes rolling under flow conditions. Science 1998;279:381-4.

37. Constantin G, Majeed M, Giagulli C, et al. Chemokines trigger immediate beta2 integrin affinity and mobility changes: differential regulation and roles in lymphocyte arrest under flow. Immunity 2000;13:759-69.

38. Mues M, Bartholomaus I, Thestrup T, et al. Real-time in vivo analysis of T cell activation in the central nervous system using a genetically encoded calcium indicator. Nat Med 2013;19:778-83.

39. Avasarala J. Leptomeningeal Enhancement for Multiple Sclerosis: Another Radiological Biomarker for a Relapse? JAMA Neurol 2017;74:745-6.

40. Choi SR, Howell OW, Carassiti D, et al. Meningeal inflammation plays a role in the pathology of primary progressive multiple sclerosis. Brain 2012;135:2925-37.

41. Weller RO. Microscopic morphology and histology of the human meninges. Morphologie 2005;89:22-34.

42. Kaplan GP, Hartman BK, Creveling CR. Localization of catechol-O-methyltransferase in the leptomeninges, choroid plexus and ciliary epithelium: implications for the separation of central and peripheral catechols. Brain Res 1981;204:353-60.

43. Feurer DJ, Weller RO. Barrier functions of the leptomeninges: a study of normal meninges and meningiomas in tissue culture. Neuropathol Appl Neurobiol 1991;17:391-405.

44. Mundt S, Mrdjen D, Utz SG, Greter M, Schreiner B, Becher B. Conventional DCs sample and present myelin antigens in the healthy CNS and allow parenchymal T cell entry to initiate neuroinflammation. Sci Immunol 2019;4.

45. Greter M, Heppner FL, Lemos MP, et al. Dendritic cells permit immune invasion of the CNS in an animal model of multiple sclerosis. Nat Med 2005;11:328-34.

46. Heppner FL, Greter M, Marino D, et al. Experimental autoimmune encephalomyelitis repressed by microglial paralysis. Nat Med 2005;11:146-52.

47. Schachenmayr W, Friede RL. The origin of subdural neomembranes. I. Fine structure of the dura-arachnoid interface in man. Am J Pathol 1978;92:53-68.

48. Anderson DR. Utrastructure of meningeal sheaths. Normal human and monkey optic nerves. Arch Ophthalmol 1969;82:659-74.

49. Pease DC, Schultz RL. Electron microscopy of rat cranial meninges. Am J Anat 1958;102:301-21.

50. Nabeshima S, Reese TS, Landis DM, Brightman MW. Junctions in the meninges and marginal glia. J Comp Neurol 1975;164:127-69.

51. Schwechheimer K, Kartenbeck J, Moll R, Franke WW. Vimentin filament-desmosome cytoskeleton of diverse types of human meningiomas. A distinctive diagnostic feature. Lab Invest 1984;51:584-91.

52. Kartenbeck J, Schwechheimer K, Moll R, Franke WW. Attachment of vimentin filaments to desmosomal plaques in human meningiomal cells and arachnoidal tissue. J Cell Biol 1984;98:1072-81.

53. Yasuda K, Cline C, Vogel P, et al. Drug transporters on arachnoid barrier cells contribute to the blood-cerebrospinal fluid barrier. Drug Metab Dispos 2013;41:923-31.

54. Balin BJ, Broadwell RD, Salcman M, el-Kalliny M. Avenues for entry of peripherally administered protein to the central nervous system in mouse, rat, and squirrel monkey. J Comp Neurol 1986;251:260-80.

55. Roth TL, Nayak D, Atanasijevic T, Koretsky AP, Latour LL, McGavern DB. Transcranial amelioration of inflammation and cell death after brain injury. Nature 2014;505:223-8.

56. Doran KS, Fulde M, Gratz N, et al. Host-pathogen interactions in bacterial meningitis. Acta Neuropathol 2016;131:185-209.

57. van de Beek D, de Gans J, Tunkel AR, Wijdicks EF. Community-acquired bacterial meningitis in adults. N Engl J Med 2006;354:44-53.

58. Rosenberg J, Galen BT. Recurrent Meningitis. Curr Pain Headache Rep 2017;21:33.

59. Rodriguez SC, Olguin AM, Miralles CP, Viladrich PF. Characteristics of meningitis caused by Ibuprofen: report of 2 cases with recurrent episodes and review of the literature. Medicine (Baltimore) 2006;85:214-20.

60. Jolles S, Sewell WA, Leighton C. Drug-induced aseptic meningitis: diagnosis and management. Drug Saf 2000;22:215-26.

61. Salvarani C, Pipitone N, Hunder GG. Management of primary and secondary central nervous system vasculitis. Curr Opin Rheumatol 2016;28:21-8.

62. Greco A, Fusconi M, Gallo A, et al. Vogt-Koyanagi-Harada syndrome. Autoimmun Rev 2013;12:1033-8.

63. Haddad N, Roussel B, Pelcovits A, Rizvi S. Optic neuritis, encephalitis and leptomeningeal enhancement in a patient with anti-MOG antibodies: A case study. Mult Scler Relat Disord 2019;34:14-6.

64. Xiang XM, Evans R, Lovera J, Rao R. Myelin Oligodendrocyte Glycoprotein Antibody-Associated Disease Presenting as Recurrent and Migrating Focal Cortical Encephalitis. Child Neurol Open 2020;7:2329048X20966172.

65. Nagabushana D, Shah R, Pendharkar H, et al. MOG antibody seropositive aseptic meningitis: A new clinical phenotype. J Neuroimmunol 2019;333:476960.

66. Shi B, Jiang W, He M, et al. Aseptic meningitis as an atypical manifestation of neuromyelitis optica spectrum disorder flare. Mult Scler Relat Disord 2020;41:102013.

67. Protasoni M, Sangiorgi S, Cividini A, et al. The collagenic architecture of human dura mater. J Neurosurg 2011;114:1723-30.

68. Roland J, Bernard C, Bracard S, et al. Microvascularization of the intracranial dura mater. Surg Radiol Anat 1987;9:43-9.

69. Adeeb N, Mortazavi MM, Tubbs RS, Cohen-Gadol AA. The cranial dura mater: a review of its history, embryology, and anatomy. Childs Nerv Syst 2012;28:827-37.

70. Kida S, Yamashima T, Kubota T, Ito H, Yamamoto S. A light and electron microscopic and immunohistochemical study of human arachnoid villi. J Neurosurg 1988;69:429-35.

71. Weis S, Sonnberger M, Dunzinger A, et al. Venous Drainage of the Brain. Imaging Brain Diseases. Vienna: Springer; 2019:211-24.

72. Rua R, McGavern DB. Advances in Meningeal Immunity. Trends Mol Med 2018;24:542-59.

73. Markowitz S, Saito K, Moskowitz MA. Neurogenically mediated leakage of plasma protein occurs from blood vessels in dura mater but not brain. J Neurosci 1987;7:4129-36.

74. Wang X, Fang Y, Liang J, Yan M, Hu R, Pan X. 5-HT7 receptors are involved in neurogenic dural vasodilatation in an experimental model of migraine. J Mol Neurosci 2014;54:164-70.

75. Edvinsson JCA, Vigano A, Alekseeva A, et al. The fifth cranial nerve in headaches. J Headache Pain 2020;21:65.

76. Keller JT, Marfurt CF, Dimlich RV, Tierney BE. Sympathetic innervation of the supratentorial dura mater of the rat. J Comp Neurol 1989;290:310-21.

77. Schueler M, Neuhuber WL, De Col R, Messlinger K. Innervation of rat and human dura mater and pericranial tissues in the parieto-temporal region by meningeal afferents. Headache 2014;54:996-1009.

78. Keller JT, Marfurt CF. Peptidergic and serotoninergic innervation of the rat dura mater. J Comp Neurol 1991;309:515-34.

79. Lv X, Wu Z, Li Y. Innervation of the cerebral dura mater. Neuroradiol J 2014;27:293-8.

80. Bolay H, Reuter U, Dunn AK, Huang Z, Boas DA, Moskowitz MA. Intrinsic brain activity triggers trigeminal meningeal afferents in a migraine model. Nat Med 2002;8:136-42.

81. Van Hove H, Martens L, Scheyltjens I, et al. A single-cell atlas of mouse brain macrophages reveals unique transcriptional identities shaped by ontogeny and tissue environment. Nat Neurosci 2019;22:1021-35.

82. Xu T, Lu S, Zhang H. Transmission electron microscope evidence of telocytes in canine dura mater. J Cell Mol Med 2016;20:188-92.

83. Peptan IA, Hong L, Evans CA. Multiple differentiation potentials of neonatal dura mater-derived cells. Neurosurgery 2007;60:346-52; discussion 52.

84. McMenamin PG. Distribution and phenotype of dendritic cells and resident tissue macrophages in the dura mater, leptomeninges, and choroid plexus of the rat brain as demonstrated in wholemount preparations. J Comp Neurol 1999;405:553-62.

85. McMenamin PG, Wealthall RJ, Deverall M, Cooper SJ, Griffin B. Macrophages and dendritic cells in the rat meninges and choroid plexus: three-dimensional localisation by environmental scanning electron microscopy and confocal microscopy. Cell Tissue Res 2003;313:259-69.

86. Artico M, De Santis S, Cavallotti C. Cerebral dura mater and cephalalgia: relationships between mast cells and catecholaminergic nerve fibers in the rat. Cephalalgia 1998;18:183-91.

87. Baun M, Pedersen MH, Olesen J, Jansen-Olesen I. Dural mast cell degranulation is a putative mechanism for headache induced by PACAP-38. Cephalalgia 2012;32:337-45.

88. Sayed BA, Christy AL, Walker ME, Brown MA. Meningeal mast cells affect early T cell central nervous system infiltration and blood-brain barrier integrity through TNF: a role for neutrophil recruitment? J Immunol 2010;184:6891-900.

89. Gadani SP, Smirnov I, Smith AT, Overall CC, Kipnis J. Characterization of meningeal type 2 innate lymphocytes and their response to CNS injury. J Exp Med 2017;214:285-96.

90. Louveau A, Smirnov I, Keyes TJ, et al. Structural and functional features of central nervous system lymphatic vessels. Nature 2015;523:337-41.

91. Alves de Lima K, Rustenhoven J, Da Mesquita S, et al. Meningeal gammadelta T cells regulate anxiety-like behavior via IL-17a signaling in neurons. Nat Immunol 2020;21:1421-9.

92. Fitzpatrick Z, Frazer G, Ferro A, et al. Gut-educated IgA plasma cells defend the meningeal venous sinuses. Nature 2020;587:472-6.

93. Coles JA, Myburgh E, Ritchie R, et al. Intravital imaging of a massive lymphocyte response in the cortical dura of mice after peripheral infection by trypanosomes. PLoS Negl Trop Dis 2015;9:e0003714.

94. Casselli T, Divan A, Vomhof-DeKrey EE, Tourand Y, Pecoraro HL, Brissette CA. A murine model of Lyme disease demonstrates that Borrelia burgdorferi colonizes the dura mater and induces inflammation in the central nervous system. PLoS Pathog 2021;17:e1009256.

95. Dziedzic T, Wojciechowski J, Nowak A, Marchel A. Hypertrophic pachymeningitis. Childs Nerv Syst 2015;31:1025-31.

96. Lu LX, Della-Torre E, Stone JH, Clark SW. IgG4-related hypertrophic pachymeningitis: clinical features, diagnostic criteria, and treatment. JAMA Neurol 2014;71:785-93.

97. Kupersmith MJ, Martin V, Heller G, Shah A, Mitnick HJ. Idiopathic hypertrophic pachymeningitis. Neurology 2004;62:686-94.

98. Hildesheim FE, Ramasamy DP, Bergsland N, et al. Leptomeningeal, dura mater and meningeal vessel wall enhancements in multiple sclerosis. Mult Scler Relat Disord 2021;47:102653.

99. Mascagni P, Sanctius C. Vasorum lymphaticorum corporis humani historia et ichnographia: Ex typographia Pazzini Carli; 1787.

100. Bucchieri F, Farina F, Zummo G, Cappello F. Lymphatic vessels of the dura mater: a new discovery? J Anat 2015;227:702-3.

101. His W. Über ein perivăsculares canalsystem in den nervösen centralorganen. Z Wiss Zool 1865;15:127-41.

102. Schwalbe G. Der Arachnoidalraum, ein Lymphraum und sein Zusammenhang mit dem Perichorioidalraum. Zentralbl Med Wiss 1869;7:465-7.

103. Földi M, Gellért A, Kozma M, Poberai M, Zoltán OT, Csanda E. New contributions to the anatomical connections of the brain and the lymphatic system. Acta Anat (Basel) 1966;64:498-505.

104. Li J, Zhou J, Shi Y. Scanning electron microscopy of human cerebral meningeal stomata. Ann Anat 1996;178:259-61.

105. Andres KH, von Düring M, Muszynski K, Schmidt RF. Nerve fibres and their terminals of the dura mater encephali of the rat. Anat Embryol (Berl) 1987;175:289-301.

106. Koh L, Zakharov A, Johnston M. Integration of the subarachnoid space and lymphatics: is it time to embrace a new concept of cerebrospinal fluid absorption? Cerebrospinal Fluid Res 2005;2:6.

107. Aspelund A, Antila S, Proulx ST, et al. A dural lymphatic vascular system that drains brain interstitial fluid and macromolecules. J Exp Med 2015;212:991-9.

108. Ahn JH, Cho H, Kim JH, et al. Meningeal lymphatic vessels at the skull base drain cerebrospinal fluid. Nature 2019;572:62-6.

109. Antila S, Karaman S, Nurmi H, et al. Development and plasticity of meningeal lymphatic vessels. J Exp Med 2017;214:3645-67.

110. Mrdjen D, Hartmann FJ, Becher B. High Dimensional Cytometry of Central Nervous System Leukocytes During Neuroinflammation. Methods Mol Biol 2017;1559:321-32.

111. Galea I, Bechmann I, Perry VH. What is immune privilege (not)? Trends Immunol 2007;28:12-8.

112. Shirai Y. On the transplantation of the rat sarcoma in adult heterogenous animals. Jap Med World 1921;1:14-5.

113. Murphy JB, Sturm E. Conditions Determining the Transplantability of Tissues in the Brain. J Exp Med 1923;38:183-97.

114. Medawar PB. Immunity to homologous grafted skin. III. The fate of skin homographs transplanted to the brain, to subcutaneous tissue, and to the anterior chamber of the eye. British journal of experimental pathology 1948;29:58.

115. Stevenson PG, Hawke S, Sloan DJ, Bangham CR. The immunogenicity of intracerebral virus infection depends on anatomical site. J Virol 1997;71:145-51.

116. Mason D, Charlton H, Jones A, Lavy C, Puklavec M, Simmonds S. The fate of allogeneic and xenogeneic neuronal tissue transplanted into the third ventricle of rodents. Neuroscience 1986;19:685-94.

117. de Vos AF, van Meurs M, Brok HP, et al. Transfer of central nervous system autoantigens and presentation in secondary lymphoid organs. J Immunol 2002;169:5415-23.

118. Phillips MJ, Needham M, Weller RO. Role of cervical lymph nodes in autoimmune encephalomyelitis in the Lewis rat. J Pathol 1997;182:457-64.

119. Furtado GC, Marcondes MC, Latkowski JA, Tsai J, Wensky A, Lafaille JJ. Swift entry of myelin-specific T lymphocytes into the central nervous system in spontaneous autoimmune encephalomyelitis. J Immunol 2008;181:4648-55.

120. van Zwam M, Huizinga R, Heijmans N, et al. Surgical excision of CNS-draining lymph nodes reduces relapse severity in chronic-relapsing experimental autoimmune encephalomyelitis. J Pathol 2009;217:543-51.

121. Hatterer E, Davoust N, Didier-Bazes M, et al. How to drain without lymphatics? Dendritic cells migrate from the cerebrospinal fluid to the B-cell follicles of cervical lymph nodes. Blood 2006;107:806-12.

122. Louveau A, Herz J, Alme MN, et al. CNS lymphatic drainage and neuroinflammation are regulated by meningeal lymphatic vasculature. Nat Neurosci 2018;21:1380-91.

123. Goldmann J, Kwidzinski E, Brandt C, Mahlo J, Richter D, Bechmann I. T cells traffic from brain to cervical lymph nodes via the cribroid plate and the nasal mucosa. J Leukoc Biol 2006;80:797-801.

124. Louveau A, Nerriere-Daguin V, Vanhove B, et al. Targeting the CD80/CD86 costimulatory pathway with CTLA4-Ig directs microglia toward a repair phenotype and promotes axonal outgrowth. Glia 2015;63:2298-312.

125. Upton ML, Weller RO. The morphology of cerebrospinal fluid drainage pathways in human arachnoid granulations. J Neurosurg 1985;63:867-75.

126. Johnston M, Zakharov A, Papaiconomou C, Salmasi G, Armstrong D. Evidence of connections between cerebrospinal fluid and nasal lymphatic vessels in humans, non-human primates and other mammalian species. Cerebrospinal Fluid Res 2004;1:2.

127. Caversaccio M, Peschel O, Arnold W. The drainage of cerebrospinal fluid into the lymphatic system of the neck in humans. ORL J Otorhinolaryngol Relat Spec 1996;58:164-6.

128. Planas AM, Gomez-Choco M, Urra X, Gorina R, Caballero M, Chamorro A. Brain-derived antigens in lymphoid tissue of patients with acute stroke. J Immunol 2012;188:2156-63.

129. Cserr HF, Knopf PM. Cervical lymphatics, the blood-brain barrier and the immunoreactivity of the brain: a new view. Immunol Today 1992;13:507-12.

130. Engelhardt B, Carare RO, Bechmann I, Flugel A, Laman JD, Weller RO. Vascular, glial, and lymphatic immune gateways of the central nervous system. Acta Neuropathol 2016;132:317-38.

131. Iliff JJ, Wang M, Liao Y, et al. A paravascular pathway facilitates CSF flow through the brain parenchyma and the clearance of interstitial solutes, including amyloid beta. Sci Transl Med 2012;4:147ra11.

132. Iliff JJ, Wang M, Zeppenfeld DM, et al. Cerebral arterial pulsation drives paravascular CSF-interstitial fluid exchange in the murine brain. J Neurosci 2013;33:18190-9.

133. Jessen NA, Munk AS, Lundgaard I, Nedergaard M. The Glymphatic System: A Beginner's Guide. Neurochem Res 2015;40:2583-99.

134. Carare RO, Bernardes-Silva M, Newman TA, et al. Solutes, but not cells, drain from the brain parenchyma along basement membranes of capillaries and arteries: significance for

cerebral amyloid angiopathy and neuroimmunology. Neuropathol Appl Neurobiol 2008;34:131-44.

135. Carare RO, Hawkes CA, Weller RO. Afferent and efferent immunological pathways of the brain. Anatomy, function and failure. Brain Behav Immun 2014;36:9-14.

136. Schley D, Carare-Nnadi R, Please CP, Perry VH, Weller RO. Mechanisms to explain the reverse perivascular transport of solutes out of the brain. J Theor Biol 2006;238:962-74.

137. Sharp MK, Diem AK, Weller RO, Carare RO. Peristalsis with Oscillating Flow Resistance: A Mechanism for Periarterial Clearance of Amyloid Beta from the Brain. Ann Biomed Eng 2016;44:1553-65.

138. Mestre H, Du T, Sweeney AM, et al. Cerebrospinal fluid influx drives acute ischemic tissue swelling. Science 2020;367.

139. Esposito E, Ahn BJ, Shi J, et al. Brain-to-cervical lymph node signaling after stroke. Nat Commun 2019;10:5306.

140. Sun BL, Xia ZL, Yan ZW, Chen YS, Yang MF. Effects of blockade of cerebral lymphatic drainage on cerebral ischemia after middle cerebral artery occlusion in rats. Clin Hemorheol Microcirc 2000;23:321-5.

141. Yanev P, Poinsatte K, Hominick D, et al. Impaired meningeal lymphatic vessel development worsens stroke outcome. J Cereb Blood Flow Metab 2020;40:263-75.

142. Bolte AC, Dutta AB, Hurt ME, et al. Meningeal lymphatic dysfunction exacerbates traumatic brain injury pathogenesis. Nat Commun 2020;11:4524.

143. Sun BL, Xia ZL, Wang JR, et al. Effects of blockade of cerebral lymphatic drainage on regional cerebral blood flow and brain edema after subarachnoid hemorrhage. Clin Hemorheol Microcirc 2006;34:227-32.

144. Sun BL, Xie FM, Yang MF, et al. Blocking cerebral lymphatic drainage deteriorates cerebral oxidative injury in rats with subarachnoid hemorrhage. Acta Neurochir Suppl 2011;110:49-53.

145. Chen J, Wang L, Xu H, et al. Meningeal lymphatics clear erythrocytes that arise from subarachnoid hemorrhage. Nat Commun 2020;11:3159.

146. Reeves BC, Karimy JK, Kundishora AJ, et al. Glymphatic System Impairment in Alzheimer's Disease and Idiopathic Normal Pressure Hydrocephalus. Trends Mol Med 2020;26:285-95.

147. Da Mesquita S, Louveau A, Vaccari A, et al. Functional aspects of meningeal lymphatics in ageing and Alzheimer's disease. Nature 2018;560:185-91.

148. Ding XB, Wang XX, Xia DH, et al. Impaired meningeal lymphatic drainage in patients with idiopathic Parkinson's disease. Nat Med 2021;27:411-8.

149. Jung E, Gardner D, Choi D, et al. Development and Characterization of A Novel Prox1-EGFP Lymphatic and Schlemm's Canal Reporter Rat. Sci Rep 2017;7:5577.

150. Dobin A, Davis CA, Schlesinger F, et al. STAR: ultrafast universal RNA-seq aligner. Bioinformatics 2013;29:15-21.

151. Li H, Handsaker B, Wysoker A, et al. The Sequence Alignment/Map format and SAMtools. Bioinformatics 2009;25:2078-9.

152. Anders S, Pyl PT, Huber W. HTSeq--a Python framework to work with high-throughput sequencing data. Bioinformatics 2015;31:166-9.

153. Anders S, Huber W. Differential expression analysis for sequence count data. Genome Biol 2010;11:R106.

154. Durinck S, Moreau Y, Kasprzyk A, et al. BioMart and Bioconductor: a powerful link between biological databases and microarray data analysis. Bioinformatics 2005;21:3439-40.

155. Schläger C, Litke T, Flügel A, Odoardi F. In Vivo Visualization of (Auto)Immune Processes in the Central Nervous System of Rodents. Methods MolBiol 2016;1304:117-29.

156. Shih AY, Driscoll JD, Drew PJ, Nishimura N, Schaffer CB, Kleinfeld D. Two-photon microscopy as a tool to study blood flow and neurovascular coupling in the rodent brain. J Cereb Blood Flow Metab 2012;32:1277-309.

157. Akerman S, Holland PR, Hoffmann J. Pearls and pitfalls in experimental in vivo models of migraine: dural trigeminovascular nociception. Cephalalgia 2013;33:577-92.

158. Hojo M, Maghni K, Issekutz TB, Martin JG. Involvement of alpha-4 integrins in allergic airway responses and mast cell degranulation in vivo. Am J Respir Crit Care Med 1998;158:1127-33.

159. Song E, Mao T, Dong H, et al. VEGF-C-driven lymphatic drainage enables immunosurveillance of brain tumours. Nature 2020;577:689-94.

160. Rosenling T, Stoop MP, Attali A, et al. Profiling and identification of cerebrospinal fluid proteins in a rat EAE model of multiple sclerosis. J Proteome Res 2012;11:2048-60.

161. Querol L, Clark PL, Bailey MA, et al. Protein array-based profiling of CSF identifies RBPJ as an autoantigen in multiple sclerosis. Neurology 2013;81:956-63.

162. Berlin C, Bargatze RF, Campbell JJ, et al. alpha 4 integrins mediate lymphocyte attachment and rolling under physiologic flow. Cell 1995;80:413-22.

163. Makarem R, Newham P, Askari JA, et al. Competitive binding of vascular cell adhesion molecule-1 and the HepII/IIICS domain of fibronectin to the integrin alpha 4 beta 1. J Biol Chem 1994;269:4005-11.

164. Vonderheide RH, Springer TA. Lymphocyte adhesion through very late antigen 4: evidence for a novel binding site in the alternatively spliced domain of vascular cell adhesion molecule 1 and an additional alpha 4 integrin counter-receptor on stimulated endothelium. J Exp Med 1992;175:1433-42.

165. Moyano JV, Carnemolla B, Domínguez-Jiménez C, et al. Fibronectin type III5 repeat contains a novel cell adhesion sequence, KLDAPT, which binds activated α4β1 and α4β7 integrins. Journal of Biological Chemistry 1997;272:24832-6.

166. Liao YF, Gotwals PJ, Koteliansky VE, Sheppard D, Van De Water L. The EIIIA segment of fibronectin is a ligand for integrins alpha 9beta 1 and alpha 4beta 1 providing a novel mechanism for regulating cell adhesion by alternative splicing. J Biol Chem 2002;277:14467-74.

167. Woodside DG, Kram RM, Mitchell JS, et al. Contrasting roles for domain 4 of VCAM-1 in the regulation of cell adhesion and soluble VCAM-1 binding to integrin alpha4beta1. J Immunol 2006;176:5041-9.

168. Cinamon G, Shinder V, Alon R. Shear forces promote lymphocyte migration across vascular endothelium bearing apical chemokines. Nat Immunol 2001;2:515-22.

169. Abadier M, Pramod AB, McArdle S, et al. Effector and Regulatory T Cells Roll at High Shear Stress by Inducible Tether and Sling Formation. Cell Rep 2017;21:3885-99.

170. SenGupta S, Parent CA, Bear JE. The principles of directed cell migration. Nat Rev Mol Cell Biol 2021.

171. Lundblad C, Haanes KA, Grände G, Edvinsson L. Experimental inflammation following dural application of complete Freund's adjuvant or inflammatory soup does not alter brain and trigeminal microvascular passage. The Journal of Headache and Pain 2015;16:91.

172. Fonseka CL, Kanakkahewa TE, Singhapura S, et al. Tuberculous Pachymeningitis Presenting as a Diffused Dural Thickening in a Patient with Chronic Headache and Recurrent Neurological Abnormalities for More than a Decade: A Case Report and a Review of the Literature. Case Rep Infect Dis 2018;2018:3012034.

173. Thurtell MJ, Keed AB, Yan M, Gottlieb T, Spies JM, Halmagyi GM. Tuberculous cranial pachymeningitis. Neurology 2007;68:298-300.

174. Da Mesquita S, Herz J, Wall M, et al. Aging-associated deficit in CCR7 is linked to worsened glymphatic function, cognition, neuroinflammation, and beta-amyloid pathology. Sci Adv 2021;7.

175. Odoardi F, Kawakami N, Li Z, et al. Instant effect of soluble antigen on effector T cells in peripheral immune organs during immunotherapy of autoimmune encephalomyelitis. Proc Natl Acad Sci U S A 2007;104:920-5.

176. Zheng P, Fu H, Wei G, et al. Antigen-oriented T cell migration contributes to myelin peptide induced-EAE and immune tolerance. Clin Immunol 2016;169:36-46.

177. Traka M, Podojil JR, McCarthy DP, Miller SD, Popko B. Oligodendrocyte death results in immune-mediated CNS demyelination. Nat Neurosci 2016;19:65-74.

178. Locatelli G, Wörtge S, Buch T, et al. Primary oligodendrocyte death does not elicit anti-CNS immunity. Nature Neuroscience 2012;15:543-50.

179. Warren SA, Olivo SA, Contreras JF, et al. Traumatic injury and multiple sclerosis: a systematic review and meta-analysis. Can J Neurol Sci 2013;40:168-76.

180. Fujinami RS, Oldstone MB. Amino acid homology between the encephalitogenic site of myelin basic protein and virus: mechanism for autoimmunity. Science 1985;230:1043-5.

181. Lang HL, Jacobsen H, Ikemizu S, et al. A functional and structural basis for TCR cross-reactivity in multiple sclerosis. Nat Immunol 2002;3:940-3.

182. Planas R, Santos R, Tomas-Ojer P, et al. GDP-l-fucose synthase is a CD4(+) T cell-specific autoantigen in DRB3*02:02 patients with multiple sclerosis. Sci Transl Med 2018;10.

ACKNOWLEDGEMENTS

First, I would like to thank Prof. Alexander Flügel for his support, advice and guidance during my doctoral studies and for giving me the opportunity to work at his institute, which has provided a stimulating working environment that has widened my scientific interests.

My extreme gratitude goes to Prof. Francesca Odoardi for her outstanding mentorship and invaluable practical, theoretical and mental assistance. Her knowing and resourceful inputs have been fundamental in the development of the project and her dedication and enthusiasm have been a constant encouragement.

I would like to thank Prof. Jochen Staiger and Prof. Wolfgang Brück for being part of my thesis advisory committee and for the valuable discussions during the committee meetings.

Thanks also to Prof. Hannelore Ehrenreich, Prof. Holger Reichardt, Prof. Martin Weber for being part of my examination board.

Thanks to Prof. Kari Alitalo and Dr. Dmitri Chilov at the University of Helsinki for providing the Prox-1-eGFP rats and AAVs for the studies on the dura lymphatics.

I am also very grateful to my colleagues and friends at the IMSF:
Michael Haberl, for helping with endothelial cell sorting and performing most of the NGS analysis. I am also grateful for his friendly support, patience in troubleshooting 2-photon problems and constructive discussions.
Luisa Hildebrand for her reliable technical assistance and for uncountable hours of help and support during several extensive experiments.
Dr. Judith Strauß for her collaboration with mouse experiments and especially for her mental and personal support.
Roger Cugota Canals, Pari Kargaran and Dr. Leon Hosang for being exceptional co-workers and friends, always ready to help with any lab (or non-lab) related emergency.
Simone Hamann and Simon Mole for technical assistance.
Dr. Fred Lühder and Dr. Henrike Körner for helping with any issues concerning transgenic animals.
Dr. Dmitri Lodygin for help and troubleshooting with T cell culture.
Cathy Ludwig for the help in countless organizational matters.
Omar Diaz for IT support.
All other past and present colleagues and friends at the IMSF for the great atmosphere and working environment.

Finally, I want to thank my family for their unconditional love and support that has sustained and guided me throughout these years.

CURRICULUM VITAE

Personal Data

Full name	Arianna Merlini
Date of birth	25th July 1986
Place of birth	New York (U.S.A.)
Nationality	Italian
Address	Institute for Multiple Sclerosis Research and Neuroimmunology (IMSF), Von-Siebold-Str. 3a, 37075 Göttingen, Germany
Phone	0049 (0)551 3961143
Email	arianna.merlini@med.uni-goettingen.de

Education

2005–2011	Medical School, Università Vita-Salute San Raffaele, Milan, Italy *Graduated with honors (110/110 cum laude) and merit distinction*
2012–2017	Neurology Residency, Neurology Department, San Raffaele Hospital and Università Vita-Salute San Raffaele, Milan, Italy *Graduated with honors (70/70 cum laude)*
2017-present	PhD, Institute of Neuroimmunology and Multiple Sclerosis Research (IMSF), Göttingen, Germany

Publications

Merlini A, Haberl M, Strauß S, Hildebrand L, Genc N, Chilov D, Alitalo K, Flügel-Koch C, Stadelmann C, Flügel A, Odoardi F. The role of the meningeal layers in CNS autoimmunity. *Under revision*

Li Z, Korhonen EA, **Merlini A**, Strauss J, Wihuri E, Nurmi H, Antila S, Paech J, Deutsch U, Engelhardt B, Chintharlapalli S, Koh GY, Flügel A, Alitalo K. Angiopoietin-2 blockade ameliorates autoimmune neuroinflammation by inhibiting leukocyte recruitment into the CNS. *J Clin Invest.* 2020 Apr 1;130(4):1977-1990.

Lodygin D, Hermann M, Schweingruber N, Flügel-Koch C, Watanabe T, Schlosser C, **Merlini A**, Körner H, Chang HF, Fischer HJ, Reichardt HM, Zagrebelsky M, Mollenhauer B, Kügler S, Fitzner D, Frahm J, Stadelmann C, Haberl M, Odoardi F, Flügel A. β-Synuclein-reactive T cells induce autoimmune CNS grey matter degeneration. *Nature.* 2019 Feb;566(7745):503-508.

Romeo MAL, Martinelli V, Dalla Costa G, Colombo B, De Feo D, Esposito F, Ferrè L, Guaschino C, Guerrieri S, Liberatore G, Martinelli Boneschi F, **Merlini A**, Messina M, Messina R, Nuara A, Preziosa P, Radaelli M, Rocca MA, Rodegher M, Sangalli F, Strambo D,

Moiola L, Comi G. Assessing the role of innovative therapeutic paradigm on multiple sclerosis treatment response. *Acta Neurol Scand*. 2018 Nov;138(5):447-453.

De Feo D, **Merlini A**, Brambilla E, Ottoboni L, Laterza C, Menon R, Srinivasan S, Farina C, Garcia Manteiga JM, Butti E, Bacigaluppi M, Comi G, Greter M, Martino G. Neural precursor cell-secreted TGF-β2 redirects inflammatory monocyte-derived cells in CNS autoimmunity. *J Clin Invest*. 2017 Nov 1;127(11):3937-3953.

Ottoboni L*, **Merlini A***, Martino G. Neural Stem Cell Plasticity: Advantages in Therapy for the Injured Central Nervous System. *Front Cell Dev Biol*. Review. 2017 May 12;5:52.

Zecca C*, **Merlini A***, Disanto G, Rodegher M, Panicari L, Romeo MAL, Candrian U, Messina MJ, Pravatà E, Moiola L, Stefanin C, Ghezzi A, Perrone P, Patti F, Comi G, Gobbi C, Martinelli V. Half-dose fingolimod for treating relapsing-remitting multiple sclerosis: Observational study. *Mult Scler*. 2018 Feb;24(2):167-174.

Ottoboni L*, De Feo D*, **Merlini A***, Martino G. Commonalities in immune modulation between mesenchymal stem cells (MSCs) and neural stem/precursor cells (NPCs). *Immunol Lett*. Review. 2015 Dec;168(2):228-39.

Radaelli M, **Merlini A**, Greco R, Sangalli F, Comi G, Ciceri F, Martino G. Autologous bone marrow transplantation for the treatment of multiple sclerosis. *Curr Neurol Neurosci Rep*. Review. 2014 Sep;14(9):478.

Pengo N, Scolari M, Oliva L, Milan E, Mainoldi F, Raimondi A, Fagioli C, **Merlini A**, Mariani E, Pasqualetto E, Orfanelli U, Ponzoni M, Sitia R, Casola S, Cenci S. Plasma cells require autophagy for sustainable immunoglobulin production. *Nat Immunol*. 2013 Mar;14(3):298-305.

Laterza C, **Merlini A**, De Feo D, Ruffini F, Menon R, Onorati M, Fredrickx E, Muzio L, Lombardo A, Comi G, Quattrini A, Taveggia C, Farina C, Cattaneo E, Martino G. iPSC-derived neural precursors exert a neuroprotective role in immune-mediated demyelination via the secretion of LIF. *Nat Commun*. 2013;4:2597.

De Feo D, **Merlini A**, Laterza C, Martino G. Neural stem cell transplantation in central nervous system disorders: from cell replacement to neuroprotection. *Curr Opin Neurol*. Review. 2012 Jun;25(3):322-33.

Merlini A, Peruzzotti-Jametti L, Bacigaluppi M, Mantovani G, Spada A, Rodegher M, Comi G. Falling too Fahr. *J Neurol*. Case Report. 2012 Jul;259(7):1483-4.

*= equal contribution